- I don't mind if you don't mind
Cause I don't shine if you don't shine
Before you go can you read my mind?
(The Killers - Read my mind)

- ***Nothing shocks me I'm a scientist*** *(Indiana Jones in The temple of doom)* -

Acknowledgments

The work on this master-thesis has been carried out at the Department of Chemistry at the Norwegian University of Science and technology (NTNU), Trondheim Norway. I would like to thank NTNU and the Norwegian Research Council for the funding of the two different beam times at MAX-lab (Spring-2008) and ESRF (Summer-2008).

I would like to thank Prof. David G. Nicholson for some guidance in the world of titanium and questions you have answered through this master period.
Dr. Karina Mathisen thanks to you for all answered questions and guidance at the laboratory, MAX-lab, ESRF and the different pubs. Thank you for all the different music, movies and tv-shows I have borrowed, and all the conversations about science-fiction/fantasy (E. Cullen) ☺.

In addition I would like to thank Dr. Camilla Nordhei for help with XAS analyses, Syverin Lierhagen for ICP-MS measurements, Dr. Nina Hammer for showing me the TGA (in the early beginning of this master), the staff at SNBL in Grenoble at ESRF, and the staff at MAX-lab / beamline I811.

I would like to thank all the other master students at "nanokatalysegruppa" which will finish the same time as me. "Lesesalen" has been a very fun place to be, and for all the long evenings and days at the school, where a lot of crazy things have happened. This master period would not have been so much fun, if there hadn't been 6 others (Beate, Asmira, Mari N, Tina, Katrine and Anlaug).

Katrine, Tina and Christina I will truly miss all the hours at "Sito", "Kantina" and all the other places in "Realfagsbygget" we have explored during the five year period we have spent here, plus all the partying during this study period in Trondheim. I really treasure our friendship and as we say "We will always have Paris".

I would like to thank my family for their support, my mother and father for saying that I only have to do my best, and my two sisters for just helping me when needed.

I am especially grateful for my boyfriend Geir for saying that I can do this, and his understanding and patience when all I have talked about is this thesis.

Contents

1 Introduction

The goal for this thesis was to successfully incorporate titanium in the framework of $AlPO_4$-5 and SAPO-5, and to use different characterisation methods to find out if that has happened. Why the metal titanium was chosen to be incorporated in the structure is that few people have done studies on TAPO-5 and TAPSO-5. In this thesis it has been a focus on the redox properties of the TAPO-5 and TAPSO-5.

The TAPO-5 and TAPSO-5 has been synthesised with different templates, titanium source and crystallisation times to see what gave the best results. The samples were analysed with different characterisation methods such as X-Ray Diffraction (XRD), ICP-MS, BET and SEM in Trondheim at NTNU which is described in this thesis. X-ray Absorption Spectroscopy (XAS) data were collected at MAX-lab and at the European Synchrotron Radiation Facility (ESRF) at the Swiss-Norwegian Beam Lines (SNBL).

Analyses of as-synthesised and calcined samples of TAPO-5's and a TAPSO-5 have been done. Also analysis of the models anatase and rutile has been done. The analyses have been executed in Athena from the IFEFFIT package and *EXCURV98*.

Two in-situs has been done on a TAPO-5 and TAPSO-5. These have then been analysed to see what happens during heating in propene/O_2 and cooling in NO/O_2. There was another insitu of an ion-exchanged Ti-SAPO-5 but that had very noisy data, so it was not chosen to write about in this thesis.

To my knowledge, no insitu has been carried out on a TAPO-5 or TAPSO-5, and there is very few studies containing XANES and EXAFS analyses of TAPO-5 and TAPSO-5.

Analytical methods:

The two main methods used are XRD and XAS (XANES / EXAFS)

Powder X-ray Diffraction (P-XRD or just XRD) is a technique used to characterise crystallographic structures. It is a fingerprint method where unknown samples and substances are compared to known crystalline structures in a database [1].

EXAFS is an experimental method used to determine the local bonding environments of metals by analysing the oscillations that occur in the X-ray absorption versus photon energy, and these oscillations are caused by interference [2].

2 Theory

2.1 Microporous material

Molecular sieves are a material with small pores that are uniform in size and are used as an adsorbent for gases and liquids [3]. Zeolites go under the definition of microporous material and are also a molecular sieve. Microporous material contains pores less than 2nm and a mesoporous material have pore diameter between 2 and 50 nm [4].

A Zeolite consists of aluminosilicate minerals, both natural and synthetic. They have three dimensional structure, with a framework of $[SiO_4]^{4-}$ and $[AlO_4]^{5-}$ coordination polyhedra. The frameworks are generally very open and contain channels and cavities where cation and water molecules are located [5]. The word zeolite means "boiling stones" from the Greek words *zein*, to boil and *lithos*, stone and that name was given by a Swedish mineralogist A. F. Chrönstedt [6].

Stephen T. Wilson published an article in 1982 where he described a new type of inorganic microcrystalline solid, which were aluminophosphates [7]. Aluminophosphates is a zeotypic material which is similar to zeolites. Figure 1 shows the different types of materials molecular sieves consists of. This is just a partial overview that shows where the zeolites and the aluminophosphates are situated. In this thesis the focus is on titanium substituted aluminophosphates, a type of $MeAPO_4$.

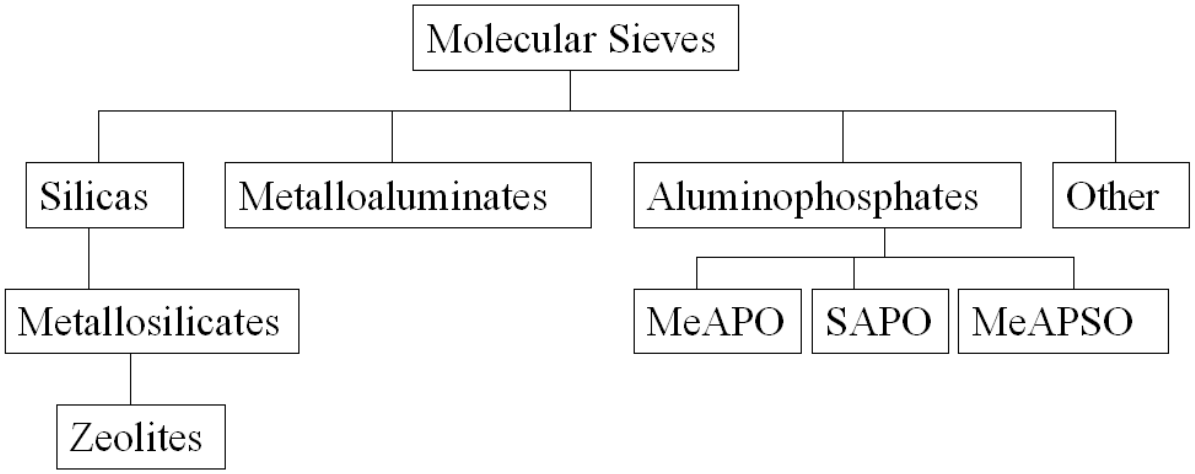

Figure 1: *A partial classification of molecular sieve materials. Zeolites occupy a subcategory of the metallosilicates. A more extensive classification exists in the book to R. Szostak [8].*

The $AlPO_4$-5 has an AFI structure and the largest pores of this material are 0.73 nm. The microporous materials such as zeolites and aluminophosphates can be used in different areas. They can be used in catalysis as support materials or as a catalyst itself with active sites. Titanium substituted aluminophosphates can be used as a catalyst. Aluminophoshate ($AlPO_4$) MeAPO-5, Figure 2 shows how the structure of TAPO-5 looks like.

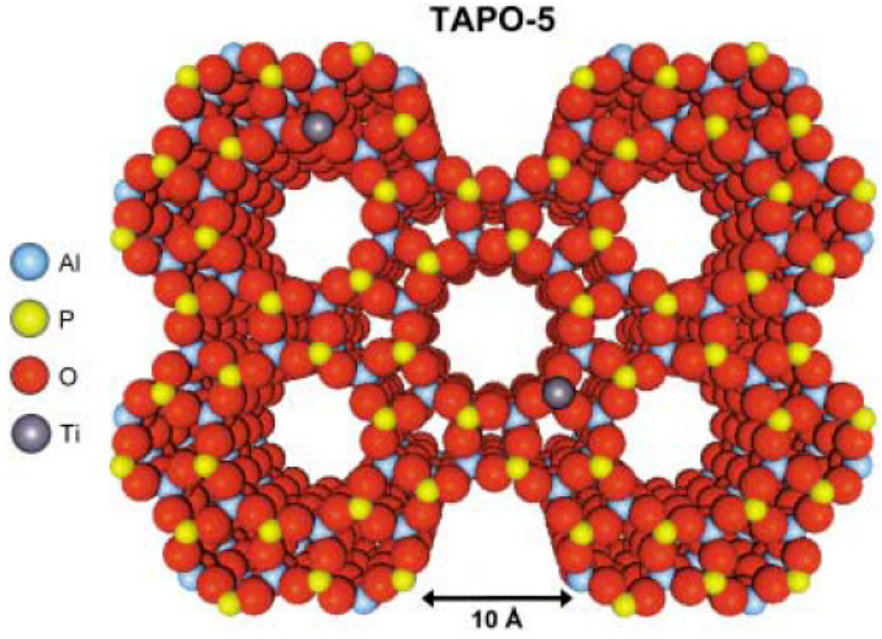

Figure 2: *The structure of TAPO-5 [9]*

Incorporation of titanium

When the titanium is incorporated in the framework of the $AlPO_4$-5 it can either replace aluminium or phosphorus. According to the Löwenstein rule the zeolite has strong alternating Al, P bonds. The oxygen cannot bond Al-O-Al it has to be Al-O-P-O-Al. This has something to say when the titanium is going to be incorporated in to the framework, which place it will take, aluminium or phosphorus [5].

If the titanium has an oxidation state of 4 (Ti^{4+}), it can be seen from the charge that if it replaces phosphorus it will potentially create a Brønsted site as shown in Figure 3. If it replaces aluminium it will probably create a Lewis site. Either way there will be a distortion in the framework where the titanium gets incorporated. From a simplified figure below shows an incorporation of Ti^{4+} when it replaces phosphorus. If the Ti^{4+} also has a six-coordination it will then have six neighbours and then the framework will not look like this at all. This shows the titanium with 4 neighbours. There is not a lot of research with how the titanium will behave in the framework of the $AlPO_4$-5 so this is just a suggestion on how it may be. It is

more likely that titanium replaces phosphorus and creates a Brønsted site, this is because then there will be a negative charge in the framework.

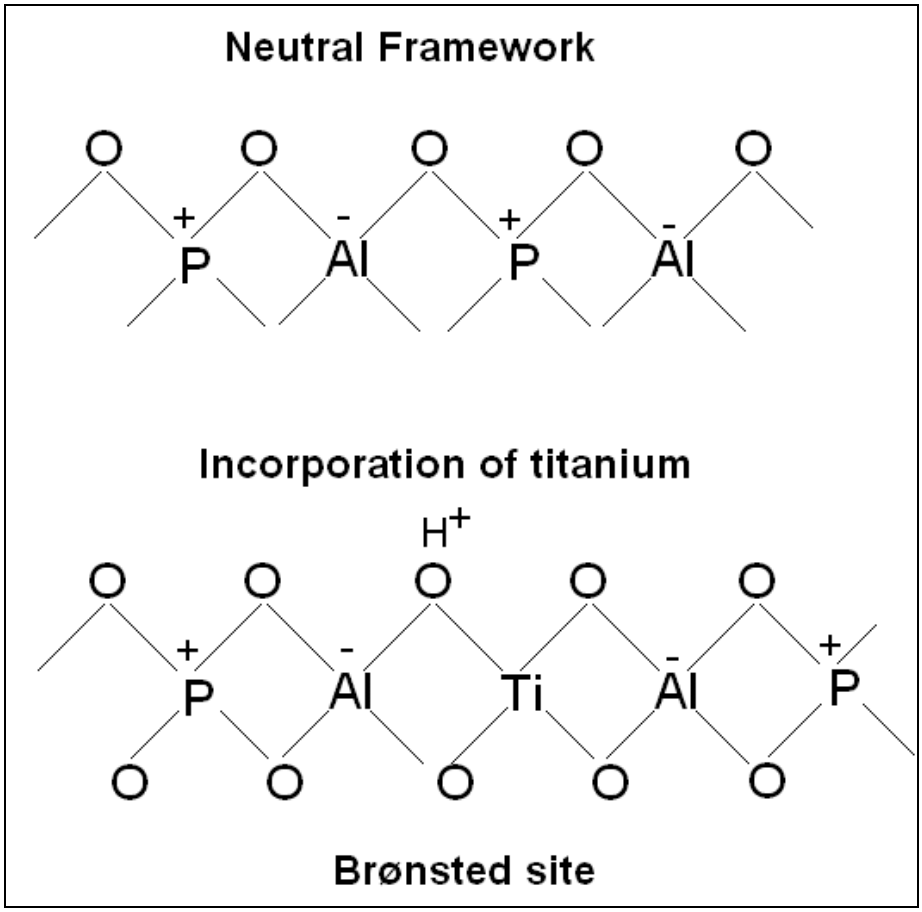

Figure 3: *possible incorporation with titanium, a very simplified sketch of the mechanism, since it creates distortion in the lattice around the Ti, which is not shown here.*

2.1.1 Zeolites as catalysts [5]

The first use of zeolites as catalysts occurred in 1959 when zeolite Y was used as an isomerisation catalyst by Union Carbide. Zeolite X was used as a cracking catalyst in 1962, in the petroleum industry. The catalytic functionality of zeolites consists of variable pore size, ion exchange, framework modification and crystal voidage and channels. The zeolites and zeotypes as aluminophopshates have a large inner surface, with variable pore size. These can be used in catalysis. The characteristics of ion exchange are used to place cations into very specific framework sites, to create active sites.

Zeolite active sites:

Acid sites

Most of the industrial applications of zeolites are based upon technology adapted from the acid silica/alumina catalysts originally developed for the cracking reaction. This means that the activity required is based upon the production of Brønsted active sites which arises from the creation of "hydroxyls" within the zeolite pore structure. These hydroxyls are usually formed either by ammonium or polyvalent cation exchange followed by a calcination step.

Ammonium ion exchange:

$$NaZ_{(s)} + NH_4^+{}_{(aq)} \leftrightarrow NH_4Z_{(s)} + Na^+{}_{(aq)}$$

Calcine step: $NH_4Z_{(s)} \rightarrow NH_3{}_{(g)} + HZ_{(s)}$

Polyvalent ion exchange:

$$NaZ_{(s)} + M\,(H_2O)^{n+}{}_{(aq)} \leftrightarrow M(H_2O)^{n+}\,Z_{(s)} + nNa^+{}_{(aq)}$$

Calcine step: $M\,(H_2O^{n+}Z_{(s)} \rightarrow MOH^{(n-1)}{}_{(s)} + HZ_{(s)}$

In high – silica zeolites the protonated zeolites can be made by direct exchange with mineral acid. Ideally the "protonated" form contains hydroxyls which are protons associated with negatively charged framework oxygens linked to alumina tetrahedral. This will mean that Brønsted sites are created as shown in Figure 4. The Lewis sites are unstable and will eventually create "true" Lewis sites by ejecting Al species from the framework.

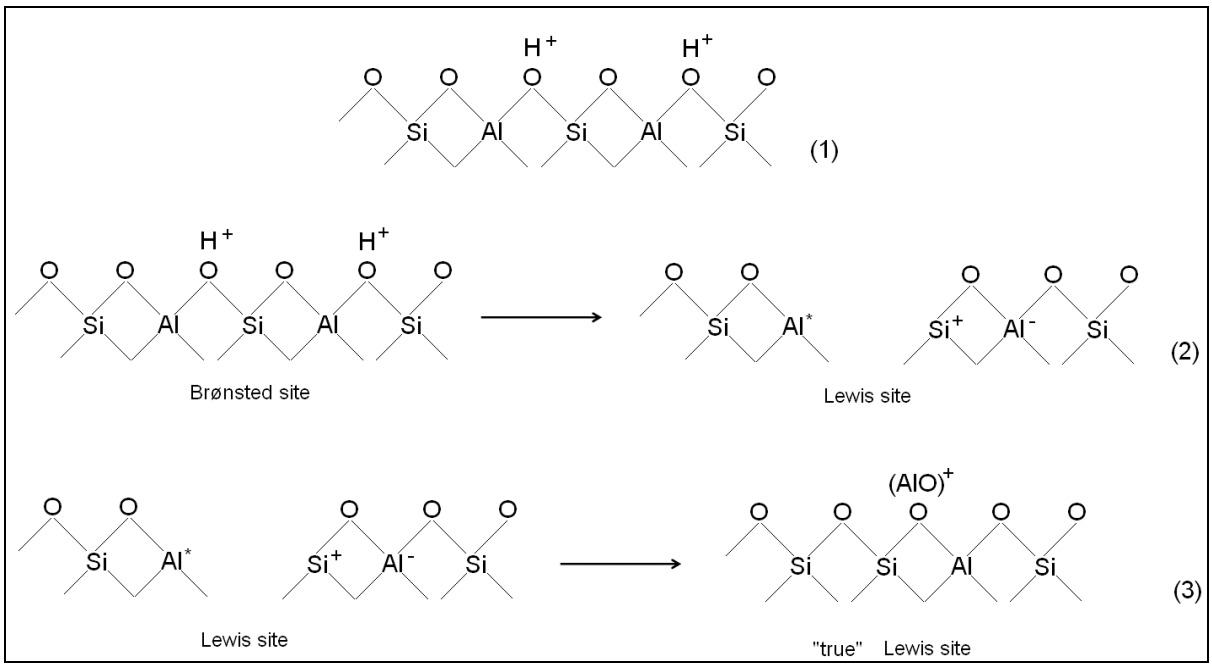

Figure 4: *Acid sites in zeolites, the Lewis and Brønsted sites (recreation after the figure in A.Dyer [5]).*

The zeolites have shape selectivity where it can allow certain shapes and formes of different compounds in the channels. A figure of the shape selectivity of zeolites is illustrated in Figure 5.

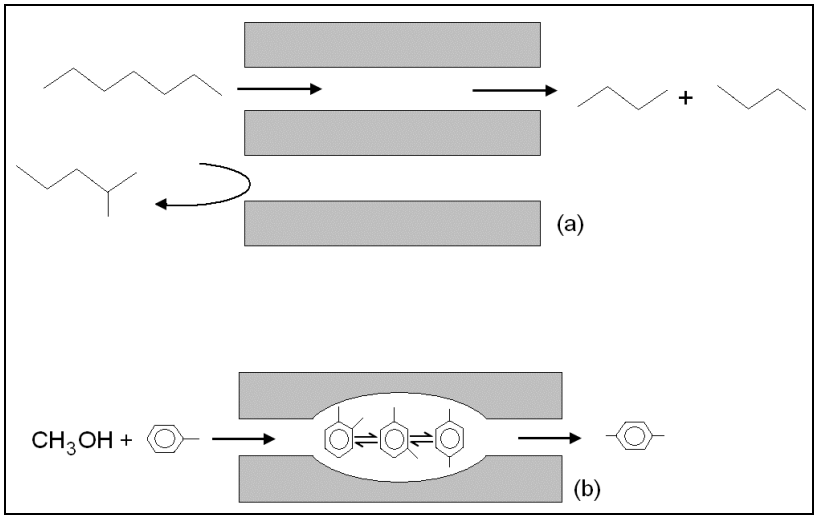

Figure 5: *Shape selectivity in zeolites (recreation after the figure in A. Dyer [5]).*

Zeolite – like materials are called zeotypes. The zeotypes contains elements other than Si or Al in tetrahedral frameworks sites, one example of zeotypes are the aluminophosphates. $AlPO_4$ was discovered and created by Union carbide in 1982. Most of these $AlPO_4$'s have three dimensional structures but some are layered compounds. $AlPO_4$-5 has been made from many templates. After the discovery of $AlPO_4$'s, the Union Carbide researchers discovered $SAPO_4$'s which is the same as $AlPO_4$-5, except for that they have silicon as well in the structure.

2.2 Why Titanium?

Titanium is a relatively common element, it's the ninth most abundant element in the earth's crust, and is widely distributed. The two major titanium-containing ores are ilmenite ($FeTiO_3$) and rutile (TiO_2) [10]. Titanium is number 22 in the periodic system and is a transition metal. The molar mass is 47.87 g/mole.

Some of the titanium compounds are hydrides (TiH_2), fluorides (TiF_2, TiF_3, TiF_4), chlorides ($TiCl_2$, $TiCl_3$, $TiCl_4$), bromides ($TiBr_3$, TiBr4), iodides (TiI_2, TiI_3, TiI_4), oxides (TiO, TiO_2, Ti_2O_3, Ti_3O_5), sulfides (TiS, TiS_2, Ti_2S_3) and nitrides (TiN) [11].

Titanium occurs primarily in the minerals anatase (TiO_2), brookite (TiO_2), rutile (TiO_2), ilmenite ($TiFeO_3$), leucoxene (mineraloid derived from weathered ilmenite), perovskite ($CaTiO_3$) and sphene ($CaTiSiO_5$). Approximatley 95% of titanium is consumed in

the form of titanium dioxide (TiO_2). One of the usages of TiO_2 is as a whitening pigment in paint, paper and plastics [12].

Titanium oxide has also been of focus for a long time in catalytic research. This is because it shows a high catalytic activity. Titanium compounds can be applied on various support materials, or it can be used as a support material. Zeolites, mesoporous materials, platinum or carbon nanofibres are examples of support materials for TiO_2 and other forms for titanium. The research of titanium as a catalyst, branches off into different fields in the catalytic science.

Photocatalysis and photocatalytic systems are one of those areas. The TiO_2 is very interesting because it is a stable and non-toxic material. A photocatalyst is conversion of light energy into applicable and non-polluting clean energy, where an artificial photosynthesis is created with conversion and storage of solar energy [13]. M. Anpo et.al has looked at various applications for the TiO_2 powdered catalyst for photocatalytic reduction as an example to reduce toxic agents in the atmosphere and water to improve the environment. They have also seen at decomposition of NO_x by photocatalysis [14].

Other areas of research are CO removal reactions, as Nina Hammer did in her doctoral thesis. In her thesis she used gold as a catalyst and TiO_2 as support material (Au-TiO_2) which was deposited on carbon nanostructures and then tested for CO removal [15].

Haldor Topsøe has looked at $DeNO_x$ catalysts and the most common of those catalysts is the selective catalytic reduction (SCR) by ammonia over vanadia-titania catalyst. Where the catalyst was V_2O_5/TiO_2 and the titanium oxide was the support material and vanadium was the catalytic active material which was examined with FTIR [16]. Mostly of the $DeNO_x$ catalysts that exists today with titanium, use titanium oxide as support and vanadium oxide as the reductive material [17, 18, 19].

In this master thesis there is a focus on titanium substituted $AlPO_4$-5 (TAPO-5) for redox insitu XAS studies.

2.3 Redox properties of titanium

Redox properties of metal oxides [20]

Metal oxides are used for both their acid-base and redox properties and constitute the largest family of catalysts in heterogeneous catalysis. Metal oxides are mainly made up of metallic cations and oxygen anions. The application of metaloxides in catalysis is dependent of; 1) the

coordination environment of the surface atoms, 2) redox properties of the oxide→ largely a matter of choice of the oxide, 3) oxidation state of the surface.

Redox catalysts

The characteristic for a redox catalyst is that it undergoes reduction and reoxidation simultaneously. For metal oxides such as TiO_2, the catalytic redox processes are often described in a general redox mechanism:

cat-O + Red → cat + red-O

cat + O Ox-O → cat-O + Ox

Cat-O (oxide catalyst surface) is reduced by a reductant (red) and re-oxidised by an oxidant (Ox-O) to its initial state. This mechanism is called the Mars-van Krevelen mechanism. According to this mechanism the substrate is oxidised by the catalyst and not directly by molecular oxygen of the gaseous phase. The mechanism involves the presence of two types of distinct active sites: 1) An active cationic state which oxidises the substrate and 2) Another site active for dioxygen reduction (the role of dioxygen is to regenerate or maintain the oxidised state of the catalyst).

Such a mechanism necessitates a catalyst that contains a red-ox couple as for instance transition metal ions which exhibit high electrical conductivity to favour electron transfer and which has high lattice oxygen anion mobility within the material to ensure the re-oxidation of the reduced catalyst.

2.4 X-ray diffraction

2.4.1 Generation of X-rays [1, 21, 22]

X-rays are electromagnetic radiation and lies between ultraviolet light and gamma rays in the electromagnetic spectrum. X-rays are generated when high speed electrons are suddenly stopped by a solid object. The common way to generate X-rays is with an X-ray tube. In an X-ray tube, electrons are created by a hot filament which is made by tungsten or similar heavy metal. This filament is heated by a great potential difference (e.g. 60 kV) and creates electrons. These electrons accelerate and hit the target, and then they decelerate and radiate intense electromagnetic radiation. X-rays has relative short wavelengths of 0.01 Å–100 Å, hard x-rays lies in the shorter wavelengths, and the softer in the other. This kind of radiation is called Brehmsstrahlung. Common targets used in X-ray tubes include copper (Cu) and molybdenum (Mo), which emit 8 keV and 14 keV X-rays. This is wavelengths of 1.54Å and 0.8Å respectively. The X-rays escapes through a window in the X-ray tube, how a tube looks like is shown in Figure 6.

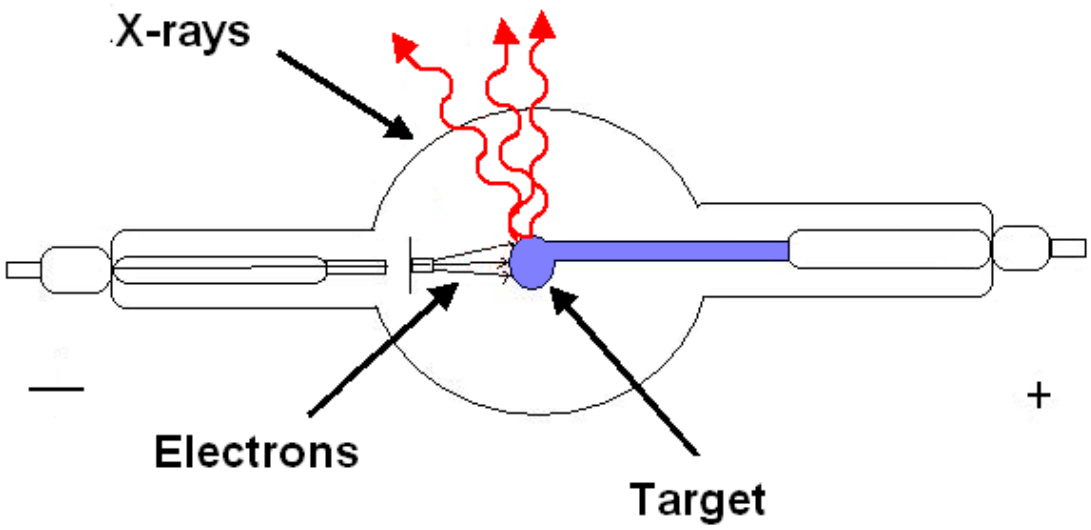

Figure 6: *X-ray tube which heats up the filament and emits X-rays.*

2.4.2 X-ray diffraction [1, 21, 23]

XRD is a technique used to characterise crystallographic structures, it can either be of a crystalline powder, or one-crystal diffraction. The one used in this thesis is powder XRD (p-XRD) which will be described further. XRD is a fingerprint method where unknown crystalline samples and substances are compared to known crystalline structures in a database.

The typical photon energies for X-rays are in the range of 100 eV-100 keV. For diffraction applications, only short wavelength X-rays (hard X-rays) in the range of a few angstroms to 0.1 angstrom (1 keV - 120 keV) are used.

The advantage of using X-rays is that the wavelength for X-rays is comparable to the size of atoms and molecules in a very wide range of materials. The X-rays provides information of the bulk structure because they penetrate deep into the material. Powder diffraction is a useful method to find the composition in a crystalline material. The crystals are randomly distributed in the powder and when the X-rays hit the crystalline powder it will diffract in a ring pattern. It will create front and back reflections as shown in Figure 7.

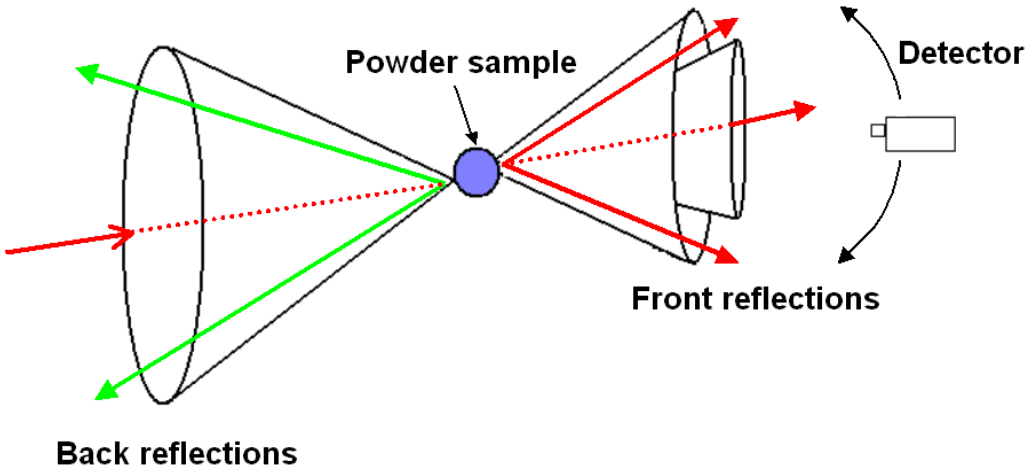

Figure 7: *Front and back reflection from a powder sample*

The powder sample will scatter in a cone shape as shown in figure 6. In a powder diffractometer there is a detector that detects and measure a cross section of the front reflections. This means that the detector cuts through the different maxima and minima and creates a powder diffraction pattern. A diffraction pattern of a titanium substituted $AlPO_4$-5, (TAPO-5) is shown in Figure 8. There are well defined peaks in this pattern, which makes it easier to determine what kind of structure this is. The analysis of the diffraction patterns are done with the use of powder diffraction databases. The International Centre for Diffraction Data gathers and sells these databases to universities and companies [24].

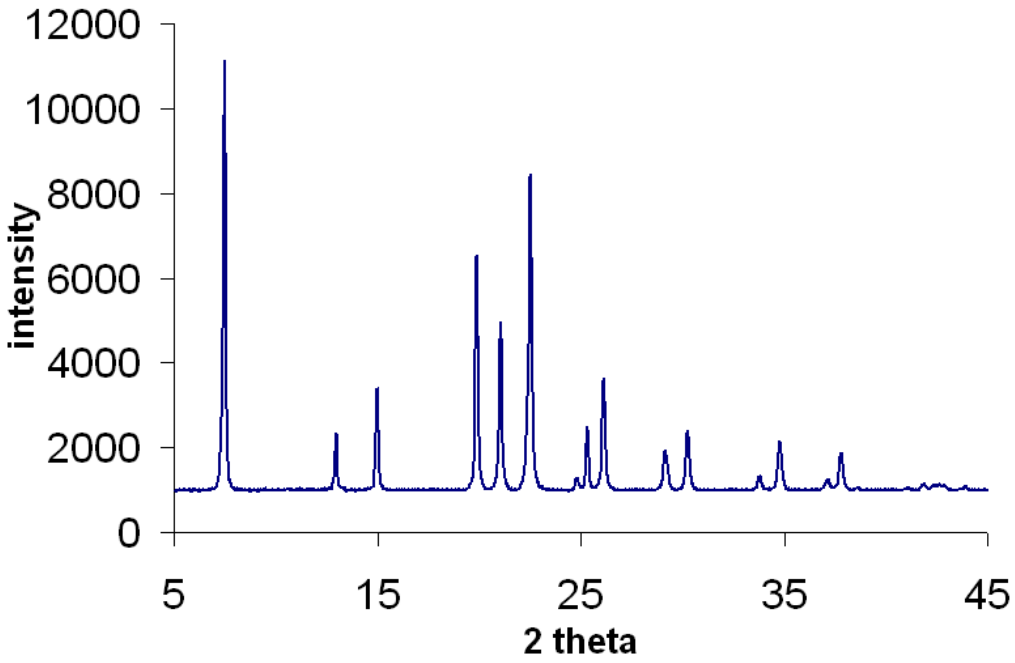

Figure 8: *A powder diffraction pattern of a titanium substituted $AlPO_4$-5*

2.5 X-ray Absorption Spectroscopy (XAS)

2.5.1 Introduction

The X-ray spectroscopy history started with Maurice de Broglie (1875-1960). In his work he invented the X-ray spectroscopy, and he was the first to observe the K-edge to silver and bromide in 1913, even though he did not probably know what it was. The correct interpretation of this observation did not happen after two decades with Ralph Kronig [25]. Nowadays X-ray absorption spectroscopy uses a synchrotron for X-rays and not X-ray tubes. The invention and further development of the synchrotron helped the progress of XAS. The spectroscopy data could be gathered in less time, from days and down to minutes. Interpretation of XAS data was very hard, and Ralph Kronig was the first person who wrote about the theory of EXAFS at the start of the 1930s [25], but it was not until Sayers, Lytle and Stern in the 1970s that the correct interpretation of the spectra happened, and the development of the Extended X-ray Absorption Fine Structure (EXAFS) equation [26].

The XAS spectrum is divided into two different main areas. These are Extended X-ray Absorption Fine Structure (EXAFS) and X-ray Absorption Near Edge Spectroscopy (XANES). Further division reveals also the pre-edge area and the edge which is in the XANES area, and a figure of an XAS spectrum of anatase is shown in Figure 9 [27].

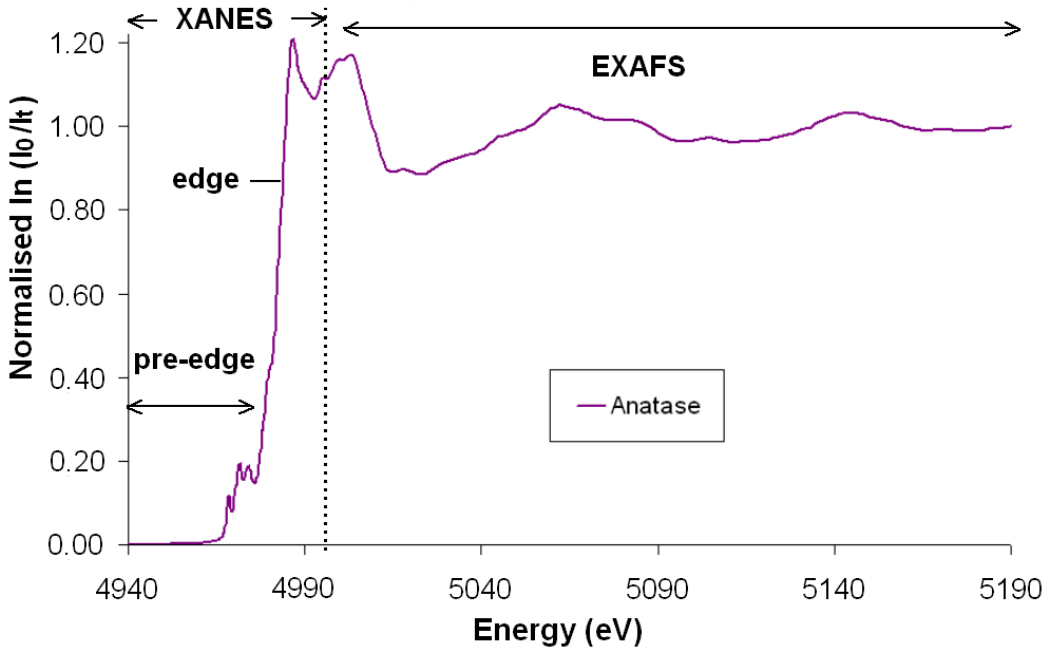

Figure 9: *A K-edge XAS spectrum of anatase (TiO_2), which shows the different parts of it.*

2.5.2 Synchrotron radiation [27, 28, 29, 30]

Synchrotron radiation covers all the wavelengths of the electromagnetic spectrum with an intensity of more than 1000 times higher than the conventional X-ray tubes used for XRD instruments and provides polychromatic X-rays (white light) from the storage ring.

The synchrotron consists of a linear accelerator, a booster ring and a storage ring, which is shown in Figure 10(a). To create the synchrotron radiation, charged particles like electrons are accelerated in the linear accelerator, and then they get sent to the booster ring where they are accelerated into a higher speed, and then finally sent to the storage ring. In the storage ring the electrons are kept in this high tempo with help from magnets that keep them in their trajectory. The storage ring consists of curved sections that are joined with straight parts. Strong magnets called bending magnets are placed around the ring and the magnetic field force the electrons to follow the ring in curved sections as shown in Figure 10(b).

The wavelength of the synchrotron radiation can be tuned by changing the magnetic field. This can be done with wigglers or undulators which consist of an array of dipole magnets, and gives a continuous energy range from infrared to hard X-rays. Wigglers are like undulators, but have stronger magnetic field and give radiation with a more uniform distribution [28]. Wigglers and undulators are insertion devices created to make a brighter beam than using only ordinary bending magnets. It is the third generation of synchrotrons that has these insertion devices. First generation synchrotrons were built parasitically on particle accelerators, beam-lines were built on the storage ring to particle accelerators and "stole" synchrotron light. Second generation synchrotron, were built as the only purpose to produce synchrotron light the difference form third generation was that there were none insertion devices.

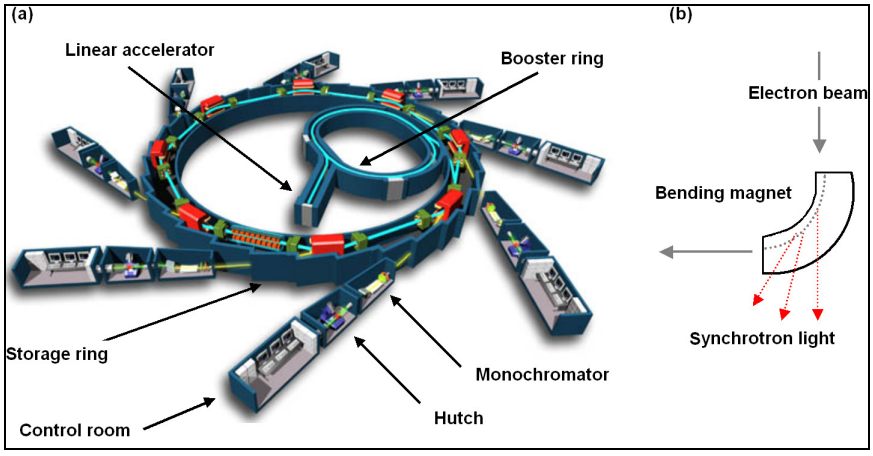

Figure 10:*(a) A synchrotron with the storage ring and hutches [31], and (b) a bending magnet which shows how synchrotron light is created.*

2.5.3 The information from EXAFS and XANES [27, 32]

EXAFS provides structural information of neighbouring atoms in the local 3D environments surrounding the central atom. EXAFS spectra are sensitive to the distances and species of the atoms in the short – range order of the central atom of its selected element. XANES spectra are sensitive to the formal oxidation state and coordination chemistry. This means that a XAS spectrum provides a practical way to determine the chemical state and local atomic structure for its selected atomic species. The sample does not need to be crystalline as required for XRD; it can also be a liquid. The X-rays penetrates the sample for transmission, and for fluorescence the X-rays hits the sample at a 45° angle, and then a detector obtain the signal.

2.5.4 XANES

XANES gives information of the coordination chemistry and formal oxidation state. In the XANES area exist the pre-edges and they arises when there is electronic transitions to half-filled orbitals. And the edge arises when the electron is photoejected out of the orbitals.

Pre-edge Transitions [33, 34, 35]

The XAS spectrum can be divided into EXAFS and XANES as mentioned previously. The XANES can also be divided into two different regions, before and after the pre-edges. The pre-edges come from electronic transitions and some of these transitions are not allowed and follows selection rules. The most important rule is the Laporte selection rule.

Laporte selection rule: Transitions between d-orbitals are forbidden in octahedral complexes. The only allowed transitions in a centrosymmetric molecule or ion are those who have a change in parity. Centrosymmetry means a centre of inversion. This means that transitions between *g* and *u* terms are allowed, but not between *g*-*g* or *u*-*u*. For a centrosymmeatric complex with no change in quantum number l, there is no change in parity and thus *s*-*s*, *p*-*p*,*d*-*d* and *f*-*f* is not allowed but *s*-*p*, *p*-*d* and *d*-*f* transitions are allowed [35].

In a centrosymmetric complex, the *d*-*d* ligand field transitions are *g*-*g* and therefore forbidden. The forbidden character accounts for the relative weakness of these transitions in octahedral complexes. For tetrahedral complexes the Laporte rule is silent because its noncentrosymmetric and have no *u* or *g* as subscript. The Laporte selection rule can be relaxed in two ways, the complex can depart slightly from perfect centrosymmetry in the ground state or the complex can undergo an asymmetrical vibration. This will destroy the

centre for inversion. The Laporte forbidden *d-d* ligand field band tends to be much more intense than a spin-forbidden transition [35].

Titanium

The pre-edge peaks are electronic transitions and for K-edge absorption spectra exists the 1s→d and 1s→p transitions, where 1s→d has been most studied. 1s to d transitions are forbidden in the dipole approximation for centrosymmetric systems and allowed in the remaining ones by d/p orbital mixing.

Titanium is the earliest studied transition row element. Series of Ti^{4+} minerals, Ti-Si xerogels or mixed oxides and zeolite containing Ti have been explored [34, 36]. The K-edge for titanium is divided in to parts, above and below approximately 4980 eV. The peaks above comes from dipole allowed 1s→*n*p ($n \geq 4$) transitions and the pre-edge peaks is located below.

Titanium dioxide (TiO_2)

Anatase and rutile are six coordinated materials and have the valence state of four (Ti^{4+}). The electronic transitions of pre-edge peaks have been widely discussed [34, 37, 38, 39]. Rutile has three pre-edges and anatase has four. Both of the compounds have low intensity pre-edges. The naming of the peaks has also varied slightly in the literature, From Antonioli et.al the peaks of anatase are named A_1-A_3 and B, and rutile is named A_1, A_3 and B [37]. And from Pickup et.al the rutile peaks are named A_1-A_3 where the A_2 peak corresponds to A_3 in other literature and A_3 corresponds to peak B [40]. In this thesis the naming of the peaks of anatase and rutile follow Antonioli et.al as seen in Figure 11 below.

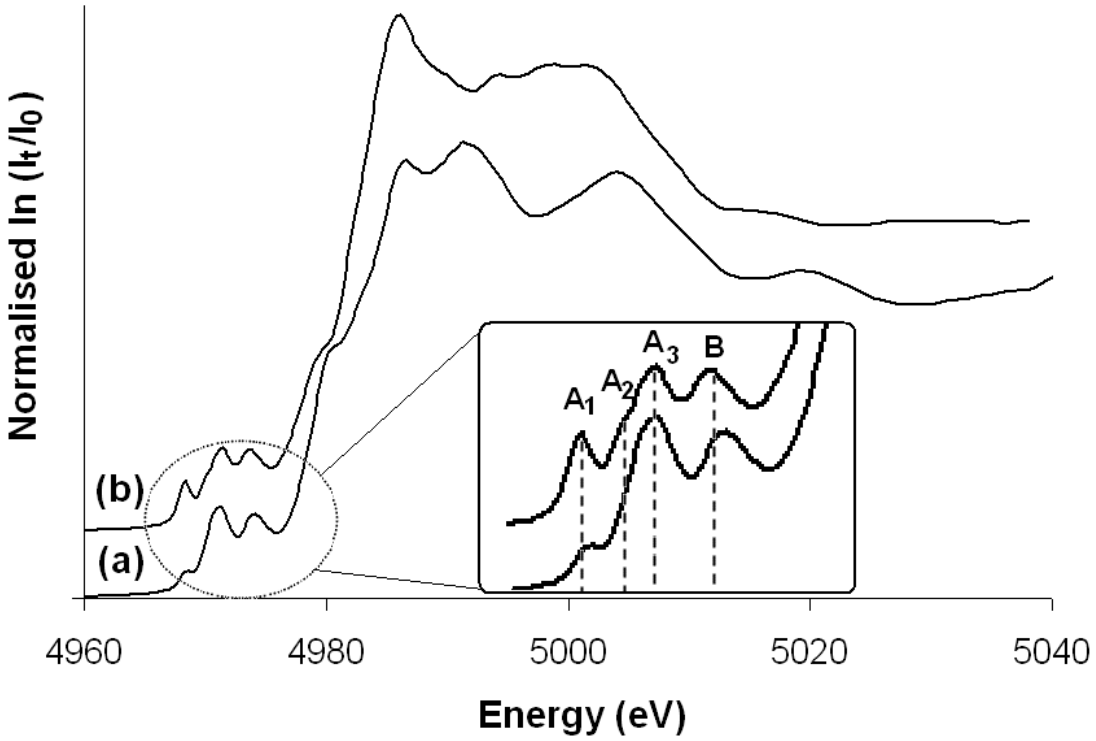

Figure 11: *The pre-edge peaks of anatase and rutile, and the naming of these peaks*

The pre-edge peaks are transitions of electrons to bound excited electronic states. The electronic state is strongly modulated by the surrounding atoms from short to medium range (<100 absorbing atoms). That means the pre-edge region of the K-edge gives valuable information about the structural and electronic state [33]. From band structure calculations have A_3 and B been assigned to the transition of the 1s electron to the t_{2g} and e_g bands due to orbital mixing of Ti 3d and 4p orbital's [41, 42].

There has been different opinion of what transitions the A_1 and A_2 peaks comes from. Parleabas et.al have suggested that A_1 should be attributed to the quadrapolar transition on the basis of its angular dependence [43]. From multiple scattering calculations have Wu et.al concluded that the peaks A_1, A_2 and A_3 comes from the hybridisation of Ti-3d-4p orbitals, and due to the different distances in the two Ti shells there is a different degree of hybridisation with the central Ti 4p orbitals [38].

Coordination number in titanium [44, 45]

The dependence of intensity and coordination number in the oxidation state 4 is significant. Farges et.al [45] did a study on the coordination number versus the intensity of the peaks of Ti^{4+}. From his study it is seen that the pre-edge peak intensity decreases with increasing coordination number of titanium. This can be seen in a Figure 12 where 4-, 5- and 6-

coordinated Ti^{4+} titanium is displayed. From this Figure it can also be seen that most of the six-coordinated material has weak triplets and the 4-, and 5-coordinated has sharp high intensity pre-edges.

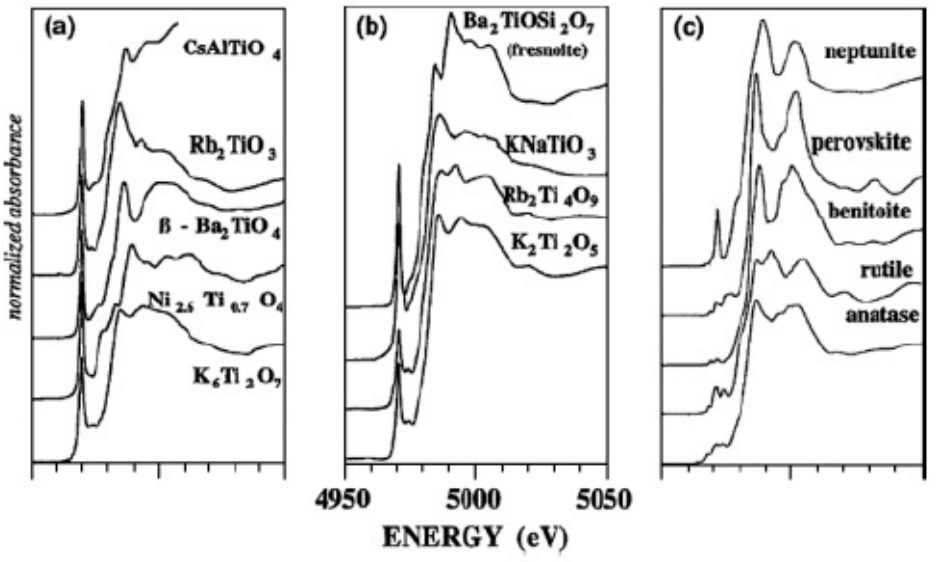

Figure 12: *Ti K-edge XANES spectra of titanium oxides containing four-(a), five-(b) and six-coordinated titanium compounds (c) reprinted from Geochim. Cosmochim. Acta, 60, Farges F, Brown GE, Rehr JJ, p 3023-3038, © (1996), with permission from Elsevier [45]*

Figure 13 below shows how the coordination number of Ti^{4+} varies in intensity and energy, the data for this plot is taken from Farges et.al [45].

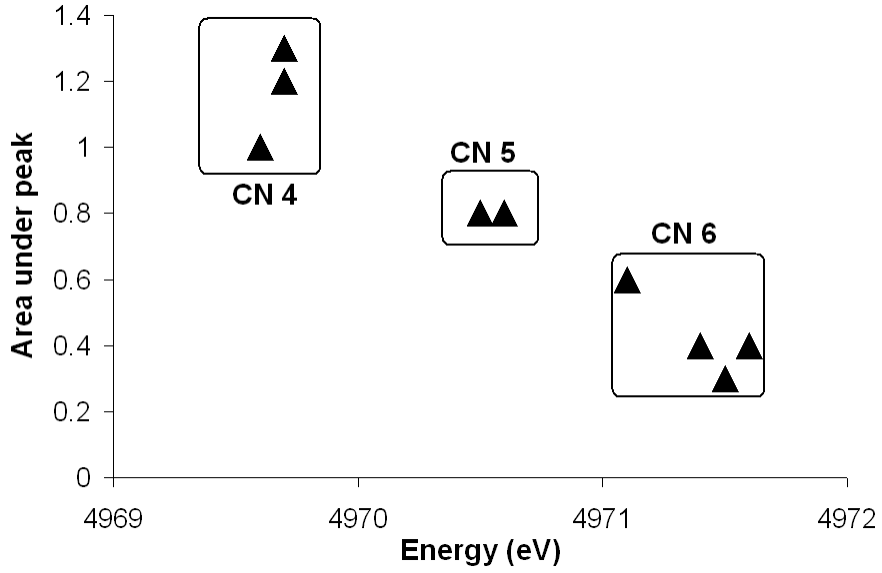

Figure 13: *Dependencies of the coordination number versus energy and intensity in Ti^{4+}*

There is a large difference in the energy of Ti^{3+} and Ti^{4+} as well; Figure 14 below shows the difference in the compounds at different oxidation state.

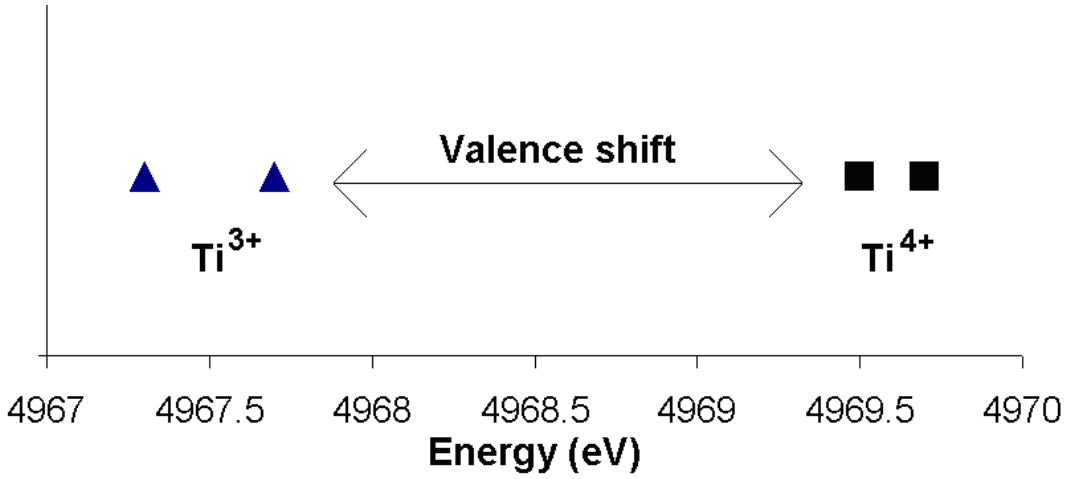

Figure 14: *The difference in energy at different oxidation states, the values for these different compounds are taken from an article from G. Waychunas [46]*

Geometry of titanium

The pre-edges are also dependent on the geometry of the titanium compound. Materials with 6 ligands are octahedral coordinated and materials with 4 ligands are tetrahedral as shown in Figure 15.

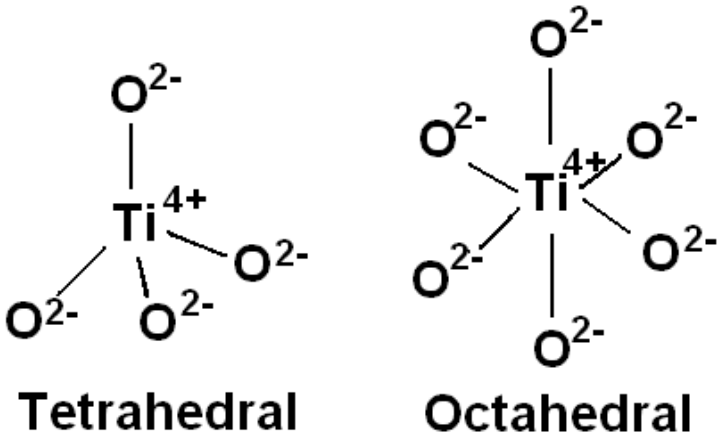

Figure 15: *Difference in geometry of different coordination number, tetrahedral has CN 4 and the octahedral has CN 6*

It can then be seen from the figure with different coordination number of the pre-edges of titanium (Fig.12) that 6-coordinated compounds has much smaller peak due to the fact that this is a Laporte forbidden transition. The octahedral has a centre of inversion and therefore this transition is not allowed. The tetrahedral with CN 4 has no centre of inversion and therefore it is allowed, thus the high intensity peaks.

Short Summary

The intensity of the pre-edge peaks of titanium is largely dependent on the coordination number. The intensity of the A_3 pre-edge of Ti^{4+} decreases with increasing coordination number. The shape is also very different, the 4- and 5- coordinated has a sharp high intensity peak and the 6-coordinated has lower intensity ad multiple peaks. The valence state of titanium is also different for the pre-edge, the Ti^{3+} is lower and Ti^{4+} has higher energy as shown in Figure 14.

2.5.5 Theory of EXAFS [2, 27, 32, 47]

EXAFS spectroscopy refers to the measurement of the X-ray absorption coefficient μ as a function of photon energy E above the threshold of an absorption edge. The information can be obtained with analysing the oscillating fine structure that occurs after the edge of the XAS-spectrum of the central atom.

Obtainment of an XAS spectrum: The synchrotron light passes a monochromator to select the correct energy for the experiment. After the monochromator the monoenergetic X-rays pass through a detector that measure their incident intensity (I_0). Then the X-rays hits the sample and the intensity of the transmitted (I_t) or the fluorescent (I_f) flux is measured as shown in Figure 16.

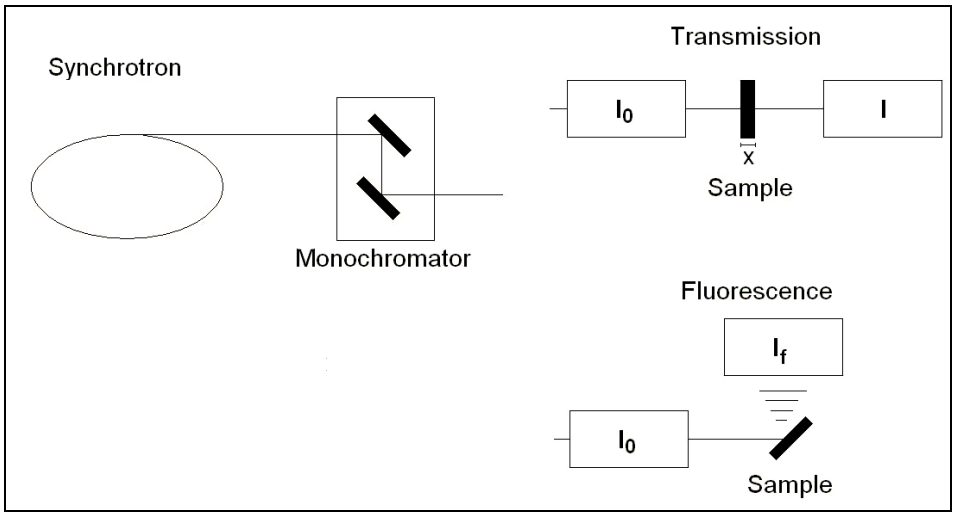

Figure 16: *The experimental set-up for transmission and fluorescence spectroscopy*

Ionisation chambers are the most common form of detector, and for fluorescence a scintillation or solid-state detector are used. In a transmission experiment, μ_t or $\mu_t x$ (x is the sample thickness) is calculated by

$$\mu_t x = \ln \frac{I_0}{I_t} \quad , \qquad (1)$$

where I_0 and I_t are the intensities of the incident and the transmitted beam. And for fluorescence $\mu_f x$ is calculated by

$$\mu_f x = \frac{I_f}{I_0} \ . \qquad (2)$$

The edge and the EXAFS

The edge which is shown in Figure 9 comes from a large increase in absorption. This increase occurs when the energy of the incident X-rays (E_{hv}) is equal to the threshold energy (E_0) which is necessary to photoeject the 1s electron of the central atom. At energies larger then E_0 the resultant photoelectrons are ejected with kinetic energy, E. This E is approximately equal to ($E_{hv} - E_0$), and these photo-emitted electrons are considered as waves.

EXAFS is a final state interference effect, which involves the scattering of the outgoing photoelectron from the neighbouring atoms. The oscillations in an EXAFS spectrum come from backscattering of the emitted photoelectron waves from atom (*a)* off neighbouring atoms (*b)*. The neighbouring atoms are hit by an outgoing wave, and produce an incoming electronic wave. The backscattered waves can interfere with the outgoing electron waves either constructive or deconstructive, this depends on the photoelectron wavelength λ_e and the nearest neighbour distance between (*a)* and (*b)*. This backscattering process is shown in Figure 17, where (*a)* is the central atom and (*b)* is the neighbouring atoms.

The probability that an X-ray photon will be absorbed by a core electron depends both on the initial and the final electronic state. The initial state is the core level which corresponds to the absorption edge, and the final state is the ejected photoelectron which can be represented as an outgoing spherical wave that originates from the X-ray absorbing atom. The final state is the sum of the outgoing and all the incoming waves that gives the sinusoidal variation of μ versus E that is known as EXAFS.

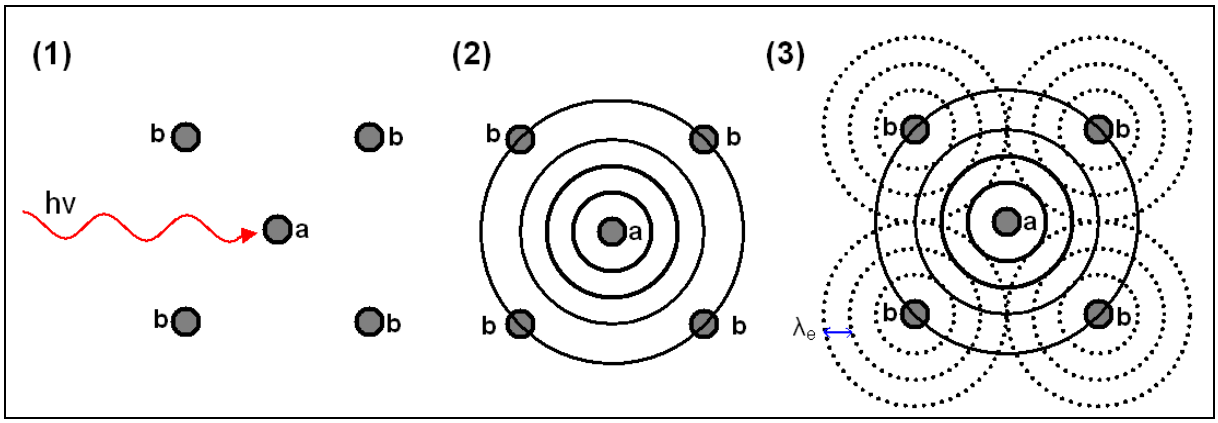

Figure 17: *Schematic diagram of the backscattering process where* a *is the central atom, and* b *is the neighbouring atoms. (1) A photon hits the central atom, (2) The central atom a produces outgoing electronic waves which hits the neighbouring atoms, (3) The neighbouring atoms b, produces electronic waves that goes back to the central atom.*

For a monoatomic gas there is no neighbouring atoms. A photoelectron ejected by absorption of an X-ray photon will travel as a spherical wave with a wavelength $\lambda = \frac{2\pi}{k}$ (eq. 3) where,

$$k = \sqrt{\frac{2m}{\hbar^2}(E_{hv} - E_0)} \qquad \text{(eq.4)}$$

$$\text{and, } \hbar = \frac{h}{2\pi} \qquad \text{(eq.5)}$$

E_{hv} is the incident energy and E_0 is the threshold energy of that particular absorption edge. For reasonably high energy (>60 eV) and moderate thermal or static disorders, the modulation of the absorption rate in EXAFS, normalised to the "background" absorption (μ_0) is given by

$$\chi = \frac{\mu(E) - \mu_0(E)}{\Delta\mu_0(E)} \qquad \text{(eq.6)}$$

In order to relate $\chi(E)$ to structural parameters, it is necessary to convert the energy scale (eV) into the photoelectron wave vector scale *k*-scale ($Å^{-1}$). *k* is related to the photoelectron kinetic energy, and is transformed by using eq.4.

This transformation of $\chi(E)$ in E space gives rise to $\chi(k)$ in *k* space and gives the EXAFS equation which is shown in equation 6a and b. The derivation of the EXAFS equation is based on a plane wave single scattering approximation which was formulated in the 1970s [26]. The plane wave theory which also is called the small atom approximation assumes that the atomic radii are much smaller than the interatomic distance. The single scattering approximation assumes that the outgoing wave function is backscattered only from the surrounding atoms before interfering with the unscattered wave.

The EXAFS equation [2, 27, 47]

Is a theoretical expression that describes χ(k) in terms of structural parameters, and from that allows structural information to be derived from the experimental χ(k). This EXAFS equation is strictly valid for K-edges which is shown in equation 7a and b.

$$\chi(k) = \sum_{j}^{shells} Aj(k)\sin(2kr_j + \phi_{ij}(k)) \qquad \text{(eq.7a)}$$

$$\chi(k) = \sum_{j}^{shells} N_j \times S_i(k) \times F_j(k) \times e^{-2\sigma_j^2 k^2} \times e^{\frac{-2r_j}{\lambda_j(k)}} \times \frac{\sin(2kr_j + \phi_{ij}(k))}{kr_j^2} \qquad \text{(eq.7b)}$$

Where:

- i refers to the absorber and j refers to the backscatterer
- $A_j(k)$ is the total amplitude
- $\text{Sin}(2kr_j + \varphi_{ij}(k))$ is the total phase
- N_j is the number of backscattering atoms in the j^{th} coordination shell (i.e multiplicity)
- r_j is the distance from the absorber to the atoms in the j^{th} coordination shell
- $F_j(k)$ the backscattering amplitude from an atom in the j^{th} coordination shell
- σ_j is the Debye-Waller factor
- $S_i(k)$ is the amplitude reduction factor due to many-body effects such as shake up/off processes at the central atom.
- The inelastic loss $e^{\frac{-2r_j}{\lambda_j(k)}}$ is due to scattering process of neighbour atoms or the medium between, this exponential term accounts for the finite lifetime of the excited state.
- λ_j is the photoelectron mean free path

Amplitude [2, 27, 47]

The backscattering amplitude ($F_j(k)$), is purely a function of the scatterer atom type and not the absorber atom. The $F_j(k)$ amplitude comes from each of the N_j neighbouring atoms of the jth type. The amplitude is reduced by the Debye-Waller factor σ_j , $S_i(k)$ which is the amplitude reduction factor and inelastic losses in the scattering process. Each EXAFS is determined by the backscattering amplitude (N_j $F_j(k)$), and is modified by the reduction factor $S_i(k)$, $e^{-2\sigma_j^2 k^2}$,

and $e^{\frac{-2r_j}{\lambda_j(k)}}$,and the $\frac{1}{kr_j^2}$ distance dependence, and the sinusoidal oscillation which is a function of interatomic distances ($2kr_j$) and the phase shift ($\varphi_{ij}(k)$) [2].

Trends of $F_j(k)$ as a function of atomic number (Z). The amplitude of $F_j(k)$ at high k generally increases with increasing atomic number, and the position of the amplitude maximum moves to higher k as the atomic number of the backscatterer increases [27].

Debye-Waller [2, 27]

The Debye-Waller (σ) takes account for the thermal vibration and static disorder for the jth backscatterer and it contains structural and chemical information. The Debye-Waller has two components $\sigma = \sigma_{stat} + \sigma_{vib}$, this is due to static disorder (assuming Gaussian pair distribution) and thermal vibrations (assuming harmonic vibration). These factors can in principal only be separated by a temperature dependent study of $\sigma(T)$[2]. These assumptions are valid for systems with low disorder. For systems with a high degree of static disorder or nonharmonic vibration will these approximation break down and lead to incorrect structural results [27].

Phase [2, 47]

The sine function which describes the phase can be divided into two parts; $2kr_j$ and $\varphi_{ij}(k)$. The phase can be thought of as being related the time for the electron to travel to the neighbouring atom and return. $2kr_j$ would then represent the time for the kinetic electron to travel from the absorber to the backscatterer and then back again [47]. The $\varphi_{ij}(k)$ can be divided into;

$$\phi_{ij}(k) = 2\phi_i(k) + \phi_j(k) \qquad \text{(eq.8)}$$

It will be a phase shift with the absorbing and the backscatterer. The time for the electron to move to i, j and back again is not constant which is represented by the $2kr_j$. The electron will have a higher speed when it reaches the scattering atom, and then slow down again. And when it comes back to the absorber it will also increase in speed. So this $\varphi_{ij}(k)$ represent that the electron will not have a constant speed .

2.5.6 Data reduction of XAS [27, 47]

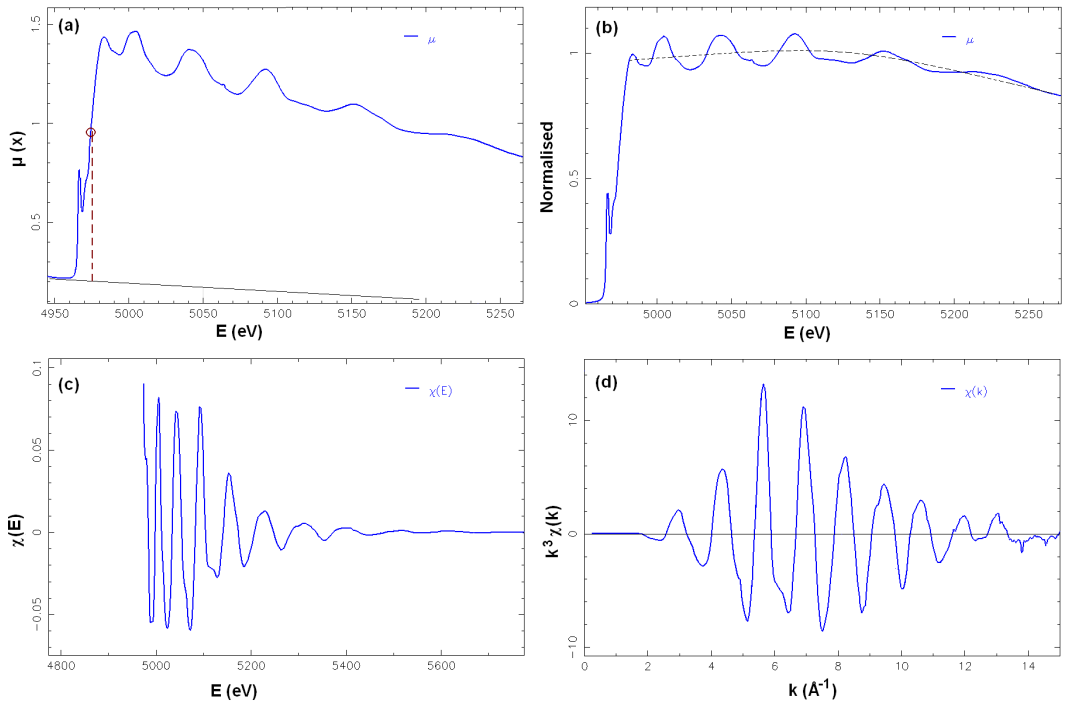

Figure 18: *Data reduction step by step of Ti-foil. (a) pre-edge background removal and determination of the edge position, (b) post-edge removal and normalisation, (c) the extracted χ(E) and (d) conversion into k-space χ(k)*

The EXAFS spectrum needs a lot of data treatment before any information can be extracted out of it. In this thesis the ATHENA program from the IFEFFIT package is used [48, 49].

The main steps of data treatment:

- Removing the absorption background from the XAS spectrum and determine the edge position (Fig. 18a)
- Extract χ(E) from the raw data μ(E) (Fig. 18b)
- Convert the χ(E) to k-space χ(*k*) (Fig. 18c,d)

The extraction of χ(E) from μ(E) is done with fitting a curve of the pre-edge region and extrapolating it to the end of the spectrum. The extrapolated curve is then subtracted from the spectrum as shown in Fig. 18c. The χ(E) is converted in to k-space as shown in Fig. 18d by equation 4. The E_0 (threshold energy), is measured experimentally from the energy position of the absorption edge. It is not very important to choose the E_0 exactly as long as it is consistent with the other samples. In this thesis it was measured as the first infliction point in the derivative spectrum or as the half of the edge jump [2, 27, 47].

The IFEFFITT package uses the Autobk algorithm where the background is determined by optimising the low frequency components of the Fourier transform data.

Athena uses edge-step normalisation, that means that the difference between μ(E) and μ_0(E) is divided by an estimation of μ_0(E) as shown in equation 4. This edge step value is determined by using a quadratic polynomial and extrapolation as explained above. In Athena further data-reduction is deglitching which is a method where the data group is plotted and points can be chosen to be removed. The data if it's very noisy can be truncated where a defined energy is chosen and the data point is removed. If there is more EXAFS scans of the same sample (this is done to get a better signal), the data is merged in Athena. The merging works by computing the mean and standard deviation of the samples chosen [49].

EXCURV98 [50] is another data processing program which is used to data analysis of the EXAFS spectrum. *EXCURV98* is based on the EXAFS equation and the theoretical model, which is based on the plane wave or small atom theory. To extract structural information of the different spectra, the other parameters in the theoretical EXAFS model need to be known. Figure 19 below shows how an analysis is done; this Figure shows what to do with the χ-curve. The χ-curve is weighted to get a better signal. The most normal is k^3 weighting, but for noisy data k^2 can be preferred. Fourier transformation of k^2 χ(k) will produce a frequency spectrum called a Pseudo Radial Distribution Function (PRDF). The peaks in this spectrum correspond to the different coordination shells in the sample. To get specific structural information an individual peak (or coordination shell) is back transformed into k-space producing a single shell, this is called Fourier filtering.

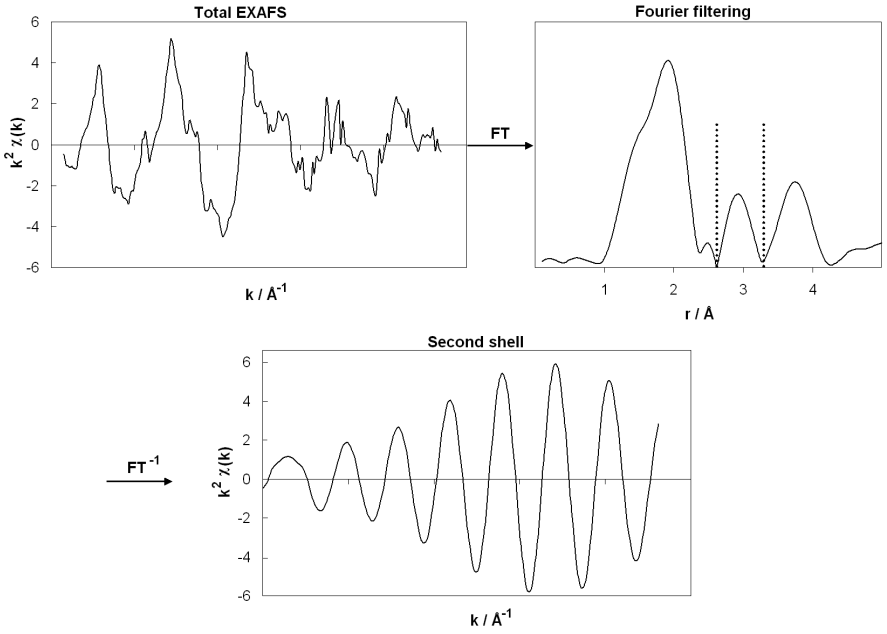

Figure 19: *EXAFS analysis: The total chi curve is Fourier transformed, then a Fourier filtering is done and a backwards Fourier filtering to a single shell*

2.5.7 Limitations to EXAFS concerning titanium

The K-edge of titanium is considered to be in a low energy range, and most beamlines delivers a spectral range that starts at around 4 keV and then goes upwards in energy. The K-edge of titanium is at 4966 eV. SNBL (BM01) sits on a bending magnet delivering photons in a spectral range between 4-70 keV [51]. Therefore titanium is at the lower limit of what can be achieved during XAS experiments. The data is not very good since the flux is very low, and a lot of the photons are absorbed by air and windows before it reaches the sample. Therefore vacuum tubes must be used between the source and the sample. Transmission gives very bad data for titanium at SNBL, and one way to solve this problem is to press the powder to pellets so it is compressed. Another way is to use fluorescence because that does not penetrate through the sample, but scans the surface of the compound.

At MAX-lab, beamline I811 the spectral range lays from 2.3 – 20 keV [52], so better data is obtained there. This is because there is a higher photon flux at a lower energy range. Figure 20 below illustrates how the beam is absorbed by air and beryllium windows before it reaches the sample when it comes from the storage ring. It can be seen that the line is getting thinner, which illustrates the photon flux. For a transmission experiment nearly no photons reaches to the other side of the sample, but for a fluorescence obtainment, one can get a better data as the photons penetrates a very thin layer of the surface.

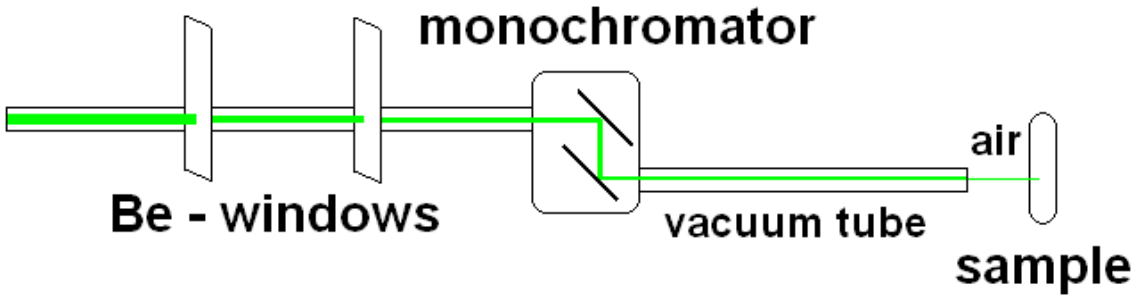

Figure 20: *An overview of the synchrotron beam before it hits the sample*

XAS does not provide information on long range order in a crystalline solid, such as XRD. XAS has also limited resolution; this will mean that it is difficult to separate bonds with similar lengths [2].

2.6 Other characterisation techniques

The other characterisation techniques which were used in this master thesis was Thermal Gravimetrical Analysis (TGA), BET - to measure the specific surface area of the TAPO-5 and TAPSO-5, Scanning Electron Microscopy (SEM) and Inductively coupled plasma – mass spectrometry (ICP-MS).

2.6.1 Inductively Coupled Plasma – Mass Spectrometry [53, 54]

ICP-MS is an analytical technique used for elemental determinations. This technique was commercially introduced in 1983, and the advantages for ICP-MS are that it has good detection limits and has an ability to obtain isotopic information [53].

An ICP-MS instrument consists of two parts, inductively coupled plasma and a mass spectrometer. Figure 21 below illustrates an ICP-MS instrument with the plasma, mass analyser, detector and the computer system the data is processed.

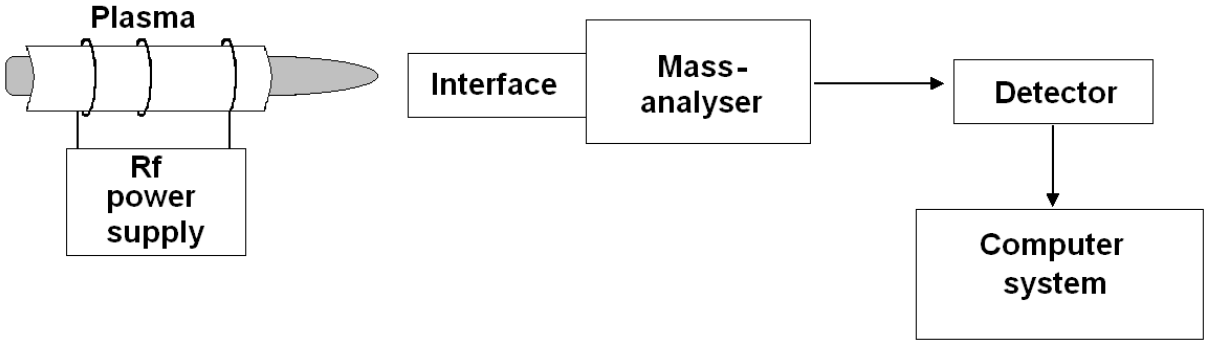

Figure 21: *Block diagram of an ICP-MS system (recreated from Ref.54)*

The ICP consists of three concentric quartz tubes where argon gas flows through. The top of the tube has a water cooled induction coil which is powered by a radio frequency generator. Ionisation of the flowing argon is initiated by a spark from a Tesla coil. The resulting ions and their associated electrons then interact with the fluctuating magnetic field produced by the induction coil [54].

The temperature of the ICP is very high and must be thermally isolated from the quartz cylinder. The isolation is achieved with argon gas which cools the inside walls. Samples can be introduced into the ICP by argon flowing at about 1 L/min through the central quartz tube. The sample can be an aerosol, a thermally generated vapour, or a fine powder. The other part of an ICP-MS is the mass spectrometer [54].

Mass analysers [54]

The most popular mass analyser for ICP-MS has been a quadrapole, magnetic-sector, and double focusing analysers. These analysers vary in resolution, throughput and scanning time. The resolution of a mass analyser is defined as R = m / Δm, where m is the nominal mass and Δm is the mass difference that can be just resolved.

A ***quadrapole mass analyser*** is basically mass filters that allow only ions of a certain mass-to charge (*m/z*) ratio to pass. ***A magnetic sector instrument*** uses a magnetic field to separate the different ions with (*m/z*) ratio. Typically, the magnetic field is scanned to bring ions of different *m/z* value to a detector. ***Double-focusing instruments*** have an electric sector before the magnetic sector. The electrostatic field focuses a beam of ions and the beam travels to the magnetic sector via a slit. These instruments can have resolution as high as 10,000. Some instruments allow operation in a low resolution mode (R~ 300), medium resolution mode (R~4,000) and high resolution (R~10,000). High resolution instruments are significantly more expensive than quadrapole instruments. They usually allow much better separation of the ions of interest from background ions.

2.6.2 BET – Theory [55]

BET is a rule for the physical adsorption of gas molecules on a solid surface, and is a technique to measure the specific surface area of a material. The name of BET comes from the persons Stephen **B**runauer, Paul Hugh **E**mmett and Edward **T**eller (**BET**), who published an article about the BET- theory in 1938.

The concept of this theory is an extension of the Langmuir theory, which is a theory for monolayer molecular adsorption to multilayer adsorption. The following hypotheses are:

- Gas molecules physically adsorb on a solid layer infinitely
- There is no interaction between each adsorption layer
- The Langmuir theory can be applied to each layer

The resulting BET equation is:

$$\frac{1}{\upsilon\left[(P_0 / P)-1\right]} = \frac{c-1}{\upsilon_m c}\left(\frac{P_0}{P}\right) + \frac{1}{\upsilon_m c} \qquad \text{(eq. 9)}$$

where:

- P and P_0; the equilibrium and the saturation pressure of adsorbates at the temperature of adsorption

- υ; the adsorbed gas quantity
- υ_m; the monolayer adsorbed gas quantity
- c; the BET constant

$$c = \exp\left(\frac{E_1 - E_L}{RT}\right) \quad \text{(eq.10)}$$

where:

- E_1; heat of adsorption for the first layer
- E_L; the second and higher layers and is equal to the heat of liquefaction

The BET equation is an adsorption isotherm and can be plotted as a straight line with $1/\upsilon[P_0/P-1]$ on the y-axis and $\varphi = P / P_0$ on the x-axis according to the experimental results, and this plot is called a BET plot.

The BET method is used in surface science for the calculation of surface areas of solids by physical adsorption of gas molecules. A total surface area S_{total} and a specific surface area S are calculated from the following equations.

$$S_{BET,\,total} = \frac{\upsilon_m N_S}{V} \quad \text{(eq.11)}$$

$$S_{BET} = \frac{S_{total}}{a} \quad \text{(eq.12)}$$

where:

- *N*; Avogadro's number
- *s*; adsorption cross section
- *V*; molar volume of adsorbent gas
- *a*; molar weight of adsorbed species

2.6.3 Thermal Gravimetric Analysis (TGA) [56 ch.4]

TGA is a simple analytical technique that measures the weight loss or weight gain of a material as a function of temperature. In this thesis TGA were used to see what happens in the calcination of the TAPO-5 and TAPSO-5, when the template were burned off. The TGA can also be coupled with a mass spectrometer to see which compounds is either lost or gained.

When a material is heated they can loose weight from a something simple as drying (water losses) or from chemical reactions that liberates gases. Some materials can gain weight by reacting with the atmosphere in the testing environment.

2.6.4 Temperature Programmed Reduction (TPR) [57]

Temperature – programmed experiments are applied in heterogeneous catalysis to characterise the activation and the reactivity of catalysts. TPR is a good tool to analyse the reduction kinetics of oxidic catalyst precursors. This technique consists of heating the catalyst with a linear ramp in a flow of hydrogen while monitoring the hydrogen consumption. TPR experiments are some time complemented with temperature programmed oxidation (TPO) where it measures the uptake of oxygen. TPR/TPO can be done to study the reversibility of reduction /reoxidation cycles.

In this thesis TPR were done with the TGA and a mass spectrometer. To see if any masses were obtained or lost with heating in hydrogen.

2.6.5 Scanning Electron Microscope [56 ch.7]

It is a large electronic microscope that images the sample surface by scanning it with a high energy beam. The types of signal the SEM microscope produce is secondary electrons, backscattered electrons, x-rays. Any sample can be examined with the SEM as long it is electrically conductive, if not it can be sputter coated with gold or carbon to make it conductive.

When a beam of primary electrons strikes a bulk solid, the electrons are either reflected (scattered) or absorbed. This will produce varying signals. The most frequent mode in the SEM involve the capture of secondary and backscattered electrons, while the most commonly used micro analytical techniques based on the detection of x-rays are energy dispersive x-ray (EDX) analysis and wavelength dispersive (WD) analysis. Modern SEM is usually equipped with the EDX detector. The SEM can produce very high resolution images of a sample surface and can reveal details down to 1-5 nm.

3 Experimental

The samples that have been synthesised and analysed are shown in table 1, this gives an overview of the molar ratio, crystallisation time and temperature of the syntheses. The characterisation methods used are XRD, BET, ICP-MS, SEM, TGA with TPR and XAS.

Table 1: *An overview of the synthesised samples which has been analysed in this master thesis with molar ratio, crystallisation time and temperature, (a) is the samples which also has been obtained XAS spectra of, the other samples has been analysed with other characterisation methods.*

Sample	Molar ratio	Crystallisation Time (hours)	Temperature (°C)	Titanium Source
TAPO-5/1	Al:P:0.1Ti:0.5TEA:15H_2O	48[a]	200	TiO_2
TAPO-5/2	Al:P:0.05Ti:0.5TEA:20H_2O	4[a]	200	Titanum-isopropoxide
		48	200	
TAPO-5/3	Al:P:0.05Ti:0.5TEA:20H_2O	48	180	Titanium-tetrabutoxide
TAPO-5/4	Al:P:0.01Ti:0.5TEA:15H2O	48	200	$TiOSO_4$
TAPO-5/ Ti^{3+}	Al:P:0.05Ti:0.5TEA:20H_2O	4	200	Ti_2O_3
		48	200	
TAPSO-5/1	Al:P:0.2Si:0.15Ti:0.5TEA:15H_2O	48[a]	200	Titanium-isopropoxide
T APSO-5/2	Al:P:0.2Si:0.05Ti:0.5TEA:20H_2O	48	180	Titanium-tetrabutoxide
TAPSO-5/Ti^{3+}	Al:P:0.2Si:0.05Ti:0.5TEA:20H_2O	4	200	Ti_2O_3
		48	200	

3.1 Synthesis

In this thesis there were used two different for the TAPO-5 and TAPSO-5 syntheses. The molar ratio and methods of preparation came from Bo-Ya Hsu et.al and Ulagappan et.al [58, 59], and there were done some alterations regarding the crystallisation time and the titanium sources. Bo-Ya Hsu et.al had a one step method and Ulagappan et.al had a two step method which lasted over two days. The syntheses of the different samples are gathered in two different tables where one is the method from Bo-Ya Hsu et.al (Table 2) and the other from Ulagappan et.al (Table 3). All the syntheses in this thesis used triethylamine (TEA) as the template, there were some syntheses which used different template, such as dicyclohexylamine (DCHA) but the result was not very good. And the samples were less crystalline when it was characterised with XRD. All the samples were also calcined with a calcination program where the sample was heated to 550°C for 34 hours using a ramp rate at 1K/minute as shown in Figure 22.

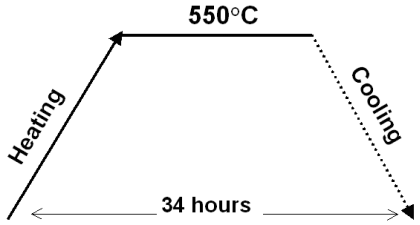

Figure 22: *The calcination program: 1 is the heating from room temperature to 550°C, 2 is the stable temperature at 550°C for 16 hours, 3 is the cooling from 550° to room temp. The ramp rate was 1K/minute and the total calcination process was approximately 34 hours.*

Table 2: *Method of preparation according to Bo-Ya Hsu et.al [58] and what added for the different synthesised samples.*

Chemicals	Quantity (g)	TAPO-5/1 (g)	TAPO-5/4 (g)	TAPSO-5/1 (g)
H_3PO_4	11.5	11.53	11.61	11.52
Al_2O_3 (pseudoboehmite)	7.065	7.07	7.052	7.06
TEA	5.0595	5.05	5.08	5.05
H_2O	27.024	27.4	28.14	27.11
TiO_2	0.799	0.809	-	-
$TiOSO_4$	0.1656	-	0.1656	-
Titanium(IV)isopropoxide	2.84	-	-	3.0
LUDOX As-40	3.00	-	-	2.99

In Table 2 above shows three samples which were synthesised with the modification according to Bo-Ya Hsu et.al.

TAPO-5/1: The ortho-phosphoric acid (85%, Fluka) was mixed and stirred with distilled water before adding the titanium source (TiO_2, unknown producer). This was mixed until the titaniumsalt was dissolved. When dissolved the pseudoboehmite (72, 2% Catapal B alumina, Sasol) was added and stirred until this made a homogenous mixture. The template TEA (99%, Aldrich) was added at the end and the resulting gel was stirred for 1, 5 hours. The final mixture was poured into a Teflon coated beaker, and put in an autoclave with a crystallisation time for 48 hours at 200°C. The crystallised product was then filtered and dried at 100°C. After drying, a part of the TAPO-5/1 was calcined at 550°C for 34 hours using a ramp rate at 1K/minute as shown in Figure 22.

TAPO-5/4: This synthesis had the same procedure as TAPO-5/1 with a molar ratio displayed in table 2. The titanium source used was titanium sulphate ($TiOSO_4$, Riedel DE Haen AG). The phosphoric acid (85%, Fluka), distilled water and $TiOSO_4$ was mixed and stirred until it was dissolved. The pseudoboehmite (72, 2% Catapal B alumina, Sasol) was added and stirred until a homogenous mixture was obtained. The template TEA (99% Aldrich) was added at the end and the resulting gel was stirred for approximately 1 hour. The final mixture was poured into a Teflon coated autoclave and crystallised at 200°C for 48 hours, it also had the same calcination program as described above.

TAPSO-5/1: The silicon source was LUDOX As-40 (E.I. du Pont de Nemours & Co, 40 wt% susp. in H_2O). Distilled water and ortho-phosphoric acid (85%, Fluka) was added and stirred, then the titanium source was added which was titanium(IV)isopropoxide (97%, Aldrich). This was stirred until a homogenous mixture was obtained. CATAPAL B, Pseudoboehmite (72.2%, Sasol) was added and again stirred until homogenous. The template TEA (99%, Aldrich) and silicon source was added in the end. This mixture was put in an autoclave at 200°C for 48 hours. Afterwards the TAPSO-5/1 was calcined at the same ramp rate as the other synthesis.

Table 3: *Method of preparation according to Ulagappan et.al [59], and what added for the different synthesised samples.*

Chemicals	Quantity (g)	TAPO-5/2 (g)	TAPSO-5/2 (g)	TAPO-5/3 (g)	TAPO-5/Ti^{3+} (g)	TAPSO-5/Ti^{3+} (g)
Gel A						
Aluminium isopropoxide	28.6	28.57	28.76	28.57	28.61	28.68
Water	35	35	34.95	34.96	35.09	35.55
Solvent B						
Water	10	10	10.00	10.09	10.03	10.03
H_3PO_4	15	15.04	14.98	15.00	15.22	15.22
Titanium(IV)butoxide	2.39	-	2.57	2.42	-	-
Titanium(IV)isopropoxide	2.12	2.13	-	-	-	-
Ti_2O_3	0.536	-	-	-	0.53	0.53
H_2O_2	3.36	3.36	3.37	3.38	3.35	3.38
TEA	7.60	7.58	7.58	7.54	7.58	7.58
As-40	3.0	-	3.04	-	-	3.0

The table 3 above shows 5 samples which were synthesised with modification according to Ulagappan et.al.

TAPO-5/2: The gel A consisted of distilled water and aluminiumisopropoxide (Fluka, purum) which was mixed and stirred overnight, with a pH 5. The solvent B was made with mixing distilled water, ortho-phosphoric acid (85%, Fluka) and adding of titanium(IV)isopropoxide (97%, Aldrich). This was stirred for 2h it was still a bit lumpy. The hydrogen peroxide (Normapur AR, 30 wt% susp. in H_2O, VWR) was added and the solvent became dark yellow in colour, this was stirred until homogenous mixture. The solvent was added into the gel and the TEA (99%, Aldrich) was added and stirred til the mixture became homogenous. The pH was 5-6 before it was put into different autoclaves and crystallised at 200°C. One sample was in the oven for 4 hours and the other for 48 hours. The pH for the 4 hours was 8 and for the 48 hours was 10-11. the reason for the 4 hours crystallisation time was that from an article written by L. Montes et.al [60] they had a crystallisation time on a VAPO-5 (vanadium substituted AlPO4-5) 4 hours. Since titanium and vanadium shares a lot of similarities with one another it would be interesting to see what happened with this shorter crystallisation time.

TAPO-5/3 had the same procedure as TAPO-5/2. This synthesis had another titaniumsource which was titaniumtetrabutoxide (Aldrich, 97%). The pH for this sample was 4-5 before it was put into an autoclave. The crystallisation time was 48 hours at 180°C.
TAPSO-5/2 had the same procedure as TAPO-5/2 and TAPO-5/3 and the titaniumsource was titaniumtetrabutoxide(Aldrich,97%). The pH for this sample was 5 before it was put into an autoclave with a 48 hours crystallisation time at 180°C. The TAPO-5/3 and TAPSO-5/2 was made simultaneously, the only difference was the addition of silicon which then made one a TAPO-5 and the other a TAPSO-5.

The synthesis for TAPO-5/Ti^{3+} and TAPSO-5/Ti^{3+} is showed in table 3. It has not been taken XAS of these samples, but TPR – data has been obtained at NTNU to check any reducibility of the samples in hydrogen. The titanium source was Titanium(III)oxide powder (100 mesh, 99.9% metals basis, Sigma-Aldrich). The gel A was made the day before as the TAPO-5/2 synthesis. When the solvent B was made the Ti_2O_3 did not dissolve properly in the ortho-phosphoric acid, some were dissolved but a lot was left at the bottom of the beaker. Hydrogen peroxide was then added to the solvent B, the pH dropped to 2. The solvent B was added in the gel A, then the TEA was added in the mixture. The titanium was still stubborn and did not really dissolve properly. It was made two parallel syntheses, one of them was added LUDOX As-40 in so it became a TAPSO-5. The TAPSO-5/Ti^{3+} and TAPO-5/Ti^{3+} was then poured into four autoclaves where one TAPO-5/Ti^3 and TAPSO-5/Ti^3 was in for four hours and the two others for 48 hours at 200°C. It had the same calcination procedure as before.

3.2 Data collection and characterisation

The different characterisation methods for analysing the different TAPO-5's and TAPSO-5 were XRD, TGA, TPR, SEM, ICP-MS ,BET and XAS.

XRD

The XRD data were obtained at NTNU at two different XRD machines. TAPO-5/1 diffraction data were collected on a Siemens D-5005 diffractometer unit B. The diffractometer uses a Cu tube as X-ray source and is equipped with a scintillation detector. The diffractometer operates at 40 kV and 50 mA. The step size was set to 0.03 with a step time of 5 seconds per step, and the angular range covered was 5-45° 2θ. The other samples were obtained on a Bruker D8 focus diffractometer. The diffractometer uses a Cu Ka X-ray tube as X-ray source and is equipped with a LynxEye detector and the angular range covered was 5-50° 2θ. The step size was set to 0.02° . The diffractometer operates at 40 kV and 40 mA.

TGA and TPR

The Thermogravimetric analysis (TGA) and Temperature Programmed Reduction (TPR) were done at NTNU. The TGA and TPR analyses were carried out using a Perkin-Elmer Thermo gravimetric Analyzer (TGA7); a Jupiter STA 449C connected to a QMS Aëolos Mass Spectrometer from Netzsch was used in the TGA and TPR. The air flow for the TGA was 80mL/min air/20mL/min argon (protective gas for the weighing house, was fed through the sample compartment). The sample was heated from room temperature with a ramp rate of 2°C/minute to 550°C, and then it was held at this temperature for and cooled down with a ramp rate of 10°C/min, the whole process took 17 hours approximately. The TPR had a gas flow of 31 mL/min total where 11mL/min was H_2(7%)/Ar(93%), and 20 mL/min Ar (protective gas), the sample was heated from room temperature with a ramp rate of 5°C /minute to 600°C, then it was held at 600°C for 20 minutes before it cooled down.

SEM

The SEM pictures of TAPO-5/2 were taken at NTNU; the machine was an S-3004N Hitachi.

ICP-MS

The equipment used for ICP-MS analysis was an Ultraclave from Milestone, with 18ml vessels of Teflon, for pre-treatment and a High Resolution Element 2, a double focusing magnetic sector field ICP-MS.

Pre-treatment for Ultraclave: The aluminophosphates were digested with aqua regia and the titanium substituted SAPO-5's was digested with hydrofluoric acid.

The vessels were flushed twice with MQ-water (milli-q) and 10-20 mg of the sample was weighed in. The samples was either digested with 18% HF (45% v/v) + 42% HNO_3 (67% v/v) or Aqua regia. The samples were diluted so the final digestion gave approximately 43 mg Si/l and 0.1 HNO_3 for HF, and for aqua regia 20 mg/l P and Al and 0.1 M HNO_3. Then the samples were ready for the ICP-MS analysis.

BET

The samples were degassed for 24 hours at liquid nitrogen temperature; the instrument used for degassing was a VacPrep 061 from Micromeritics. The samples were heated to 250ºC at 0.12 mbar. Instruments used for pore measurement was a Micromeretics TriStar-3000 Porosity Analyzer.

X-ray absorption data collection

The XAS data were collected both at ESRF in Grenoble and at MAX-lab in Sweden. The data was collected at the Swiss-Norwegian Beamline (SNBL) BM1B at the European Synchrotron Radiation Facility (ESRF) in Grenoble. The TAPO-5/1 and the models anatase and rutile were obtained in transmission mode. The beamline is equipped with a channel cut Si (111) monochromator. The ion chamber detectors were filled with the following detector gases: I_0, 13 % N_2 + 87 % He, I_1/I_2, 100 % N_2. The ESRF is a 6 GeV synchrotron and provides those energies and a 200mA current. The EXAFS scan were measured with 5 eV steps below the edge, 0.3 eV steps in the edge region, and steps equivalent to 0.04 $Å^{-1}$ increments above the edge (region borders were 4900, 4960 and 4990.9 eV). The XANES scan had the same steps and region borders. The scan stopped for EXAFS at 5900 eV and for XANES the scan stopped at 5000 eV

The data was collected at beamline I811 at MAX-II in Lund, Sweden. The data for samples TAPO-5/2 and TAPSO-5/1 was obtained in fluorescence mode. This beamline has an energy range of 2.3-20 keV, and is based on a superconducting multi pole wiggler. It is equipped with a double crystal monochromator Si(111). The EXAFS scan started at 4866.4 eV with 10 eV step below the edge, 0.5 eV steps in the edge region, and steps equivalent to 0.05 $Å^{-1}$ increments above the edge (region borders were 4866.4, 4936.4 and 4996.4 eV) the scan stopped at 5466.4 eV. The XANES scan started at 4816.4 eV with 10 eV steps below the

edge, 0.5 eV steps in the edge region, and steps equivalent to 0.05$Å^{-1}$ increments above the edge (region borders were 4816.4, 4936.4 and 4996.4 eV) the scan stopped at 5166.4 eV.

At MAX-lab there was done two in-situ's one of a TAPO-5/2 and the other of TAPSO-5/1. The TAPO-5/2 were heated to approximately 330°C in a mixture of propene and oxygen, and then cooled down to room temperature in NO/O_2. The gas mixture for the heating was 60% propene and 24 % O_2 and the gas mixture for the cooling was 60% NO and 29% O_2 the total flow for both was 15mL/min. The samples were prepared with putting the powder in sample holders and kapton tape secured the powder inside.

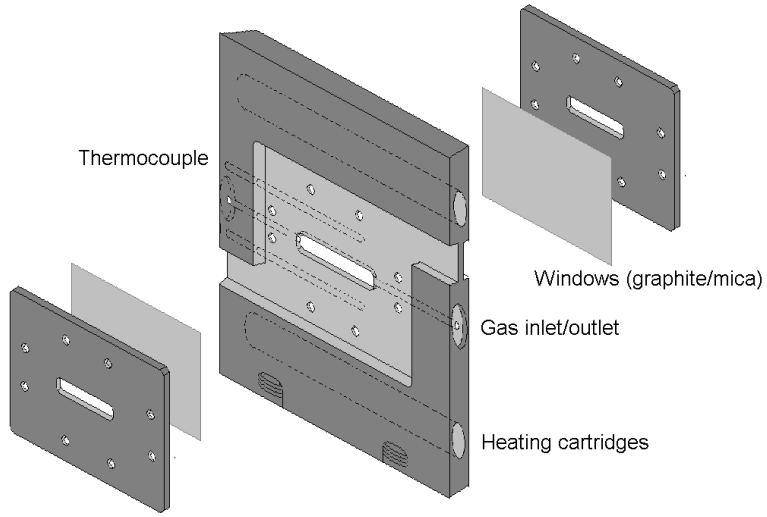

Figure 23: *In situ cell for XAS experiments, (illustration by Karina Mathisen)*

In those two in situ experiments, the samples were sealed in place between graphite or mica windows. In this cell which is illustrated in Figure 23 the reaction gases flow directly through the sample with the flow rate being regulated by flow controllers. The exhaust can be connected to a mass spectrometer if wanted. The heating cartridges are inserted above and below the cell window to obtain uniform temperature gradient of the whole sample. The temperature is measured by a thermocouple inserted in the cell. The advantage for this cell is it can be used for combined XAS, XRD and Raman measurements. EXAFS and XANES were obtained on the different TAPO-5 and TAPSO-5. Figure 24 displays a chart of the insitu setup.

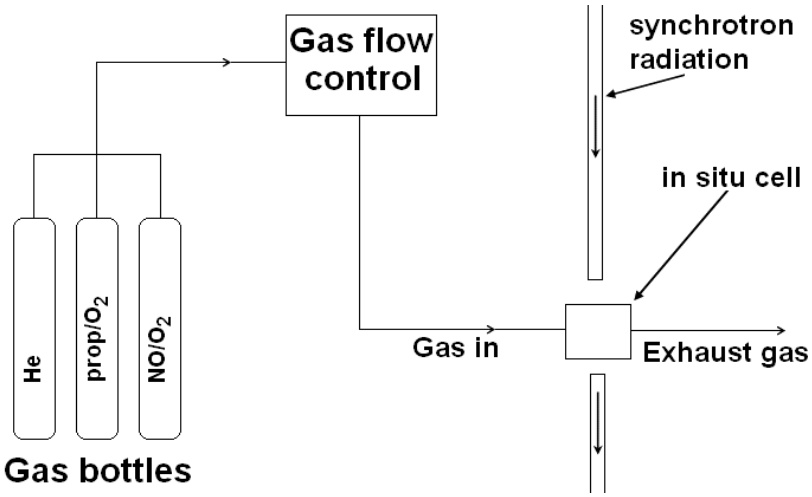

Figure 24: *Insitu setup for XAS experiments*

Results and discussion

3.3 XRD

There were done XRD on different synthesised samples, both as-prepared and calcined of TAPO-5's and TAPSO-5's. This was done to see if the samples were crystalline, and had the same crystal structure as an $AlPO_4$-5. This method helped to sift out the samples that should be further investigated with other characterisation methods such as XAS.

3.3.1 The difference of template

Different syntheses were done with the use of different templates. The most successful template was TEA. Two other templates were used in this thesis for making TAPO-5. These were N,N-Dicyclohexylmethylamine (Fluka ≥97%), and Tetraethylammoniumhydroxide (Aldrich 35wt% in H_2O). these are called DCHA and TEAOH for short. Two syntheses were done using DCHA and TEAOH, but neither of them gave a proper and crystalline sample of TAPO-5. The method of preparation is given for these samples in appendix 1.

Figure 25 and 26 below displays to non-crystalline XRD, where Figure 26 is more non-crystalline than Figure 25. These were synthesised with different templates than TEA which gave very crystalline material. So from these results, the further syntheses used TEA as source of template.

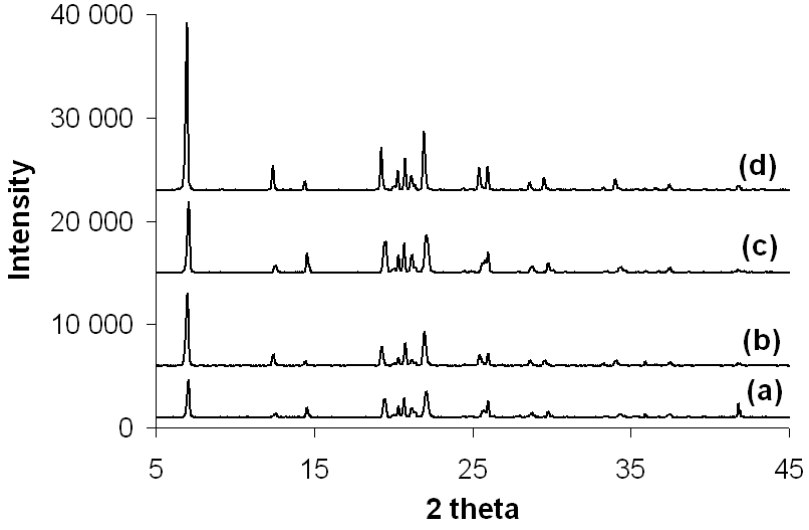

Figure 25: *Diffractogram with TEAOH as template, where (a) and (b) is as-synthesised and calcined with crystallisation time of 24 hours. (c) and (d) is as-synthesised and calcined with crystallisation time of 48 hours.*

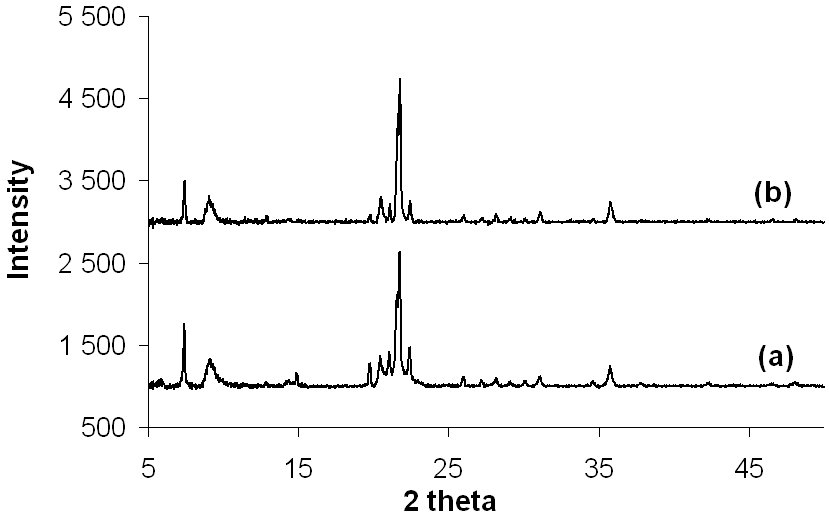

Figure 26: *A XRD with DCHA as template were (a) is the as-synthesised sample and (b) is the calcined sample*

3.3.2 Successful syntheses

Figure 27 below shows the diffractogram of TAPO-5/1, the dot over the two peaks is the anatase phase of this sample. This TAPO-5/1 was prepared with TiO_2 as the source of titanium. From the diffractogram it can be seen that the sample is crystalline but also has an anatase peak, which indicates anatase particles in the sample.

A noticeable thing for nearly all the diffractograms is peak number two and three, for the as-synthesised sample peak number two is smaller then peak three and the other way around for the calcined. Why this is I am not certain, but it is a fine way to see the difference of which is calcined and which is as-synthesised.

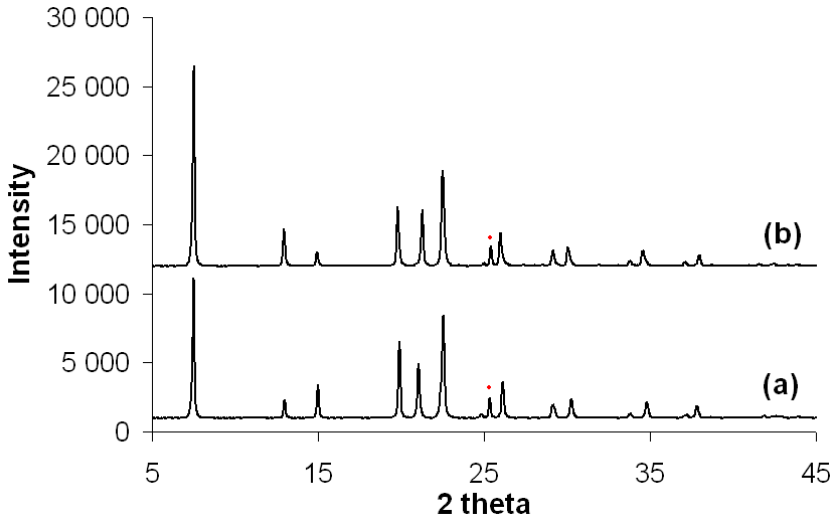

Figure 27: *XRD of calcined and as-synthesised TAPO-5/1 with anatase particles, (a) is the as-synthesised and (b) is the calcined sample. The red dot shows the anatase peak of the diffractogram.*

Figure 28 below shows the diffractogram of TAPO-5/2 which had crystallisation time of 4 and 48 hours in the autoclave. This was done to see if there was any difference for the crystallisation time. From the Figure it can be seen that both of the samples are crystalline, both he as-prepared and calcined of the two different crystallisation times. The 4 hours sample was chosen for XAS in-situ at MAX-lab in Sweden.

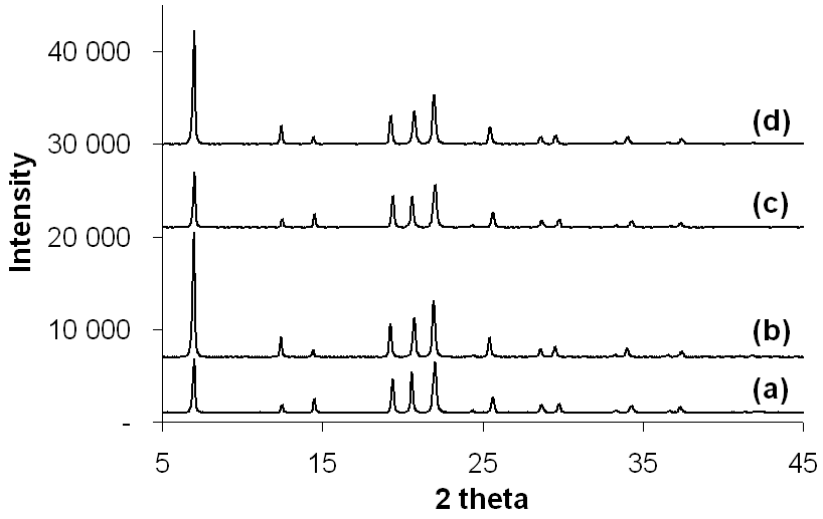

Figure 28: *XRD of calcined and as-synthesised TAPO-5/2 which has been in an autoclave for 4 hours and 48 hours. Where (a) is as-synthesised 48 hours, (b) is calcined 48 hours, (c) is as-synthesised 4 hours, and (d) is calcined 4 hours.*

Figure 29 shows the diffractogram of TAPSO-5/1. This sample was obtained an XAS insitu for at MAX-lab in Sweden. The TAPSO-5/1 is a bit more messy and has some peaks which should not be there, but it is crystalline and the best TAPSO-5 candidate for an XAS obtainment. The other TAPSO-5, TAPSO-5/2 was more untidy than this one.

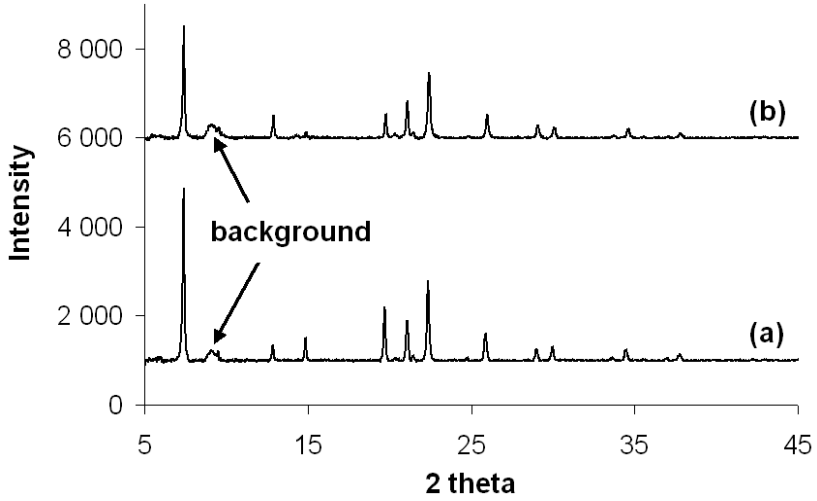

Figure 29: *XRD of TAPSO-5/1 where (a) is the as-synthesised sample and (b) is the calcined sample, it shows a background from the machine which probably is from the sample holder.*

Since there was already done a crystallisation time of 4 hours and 48 hour for a sample, it was interesting to try the same crystallisation times for other syntheses. Previous all the titanium sources for synthesis purpose was Ti^{4+}, but a Ti^{3+} source was ordered and there was made a TAPO-5 and TAPSO-5 with Ti^{3+}. The diffractograms of these TAPO-5/Ti^{3+}, and TAPSO-5/Ti^{3+} is displayed in Figure 30 and 31 respectively. From these XRD's it can be seen that the diffractograms are very clean with no extra peaks, and this indicates that they are crystalline. No XAS was obtained of these, because the set-up in Grenoble did not detect any titanium in the samples. But it would have been very interesting to see if the titanium was still Ti^{3+} or if it has oxidated to Ti^{4+} during the crystallisation in the autoclave.

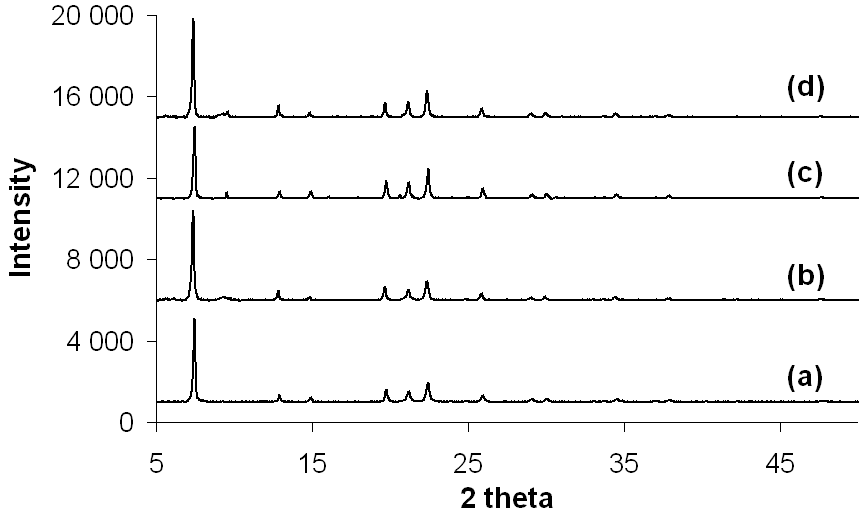

Figure 30: *XRD of TAPSO-5/ Ti^{3+} where (a) is as-synth 4h, (b) is calcined 4h, (c) is as-synth 48 h and (d) is calcined 48h.*

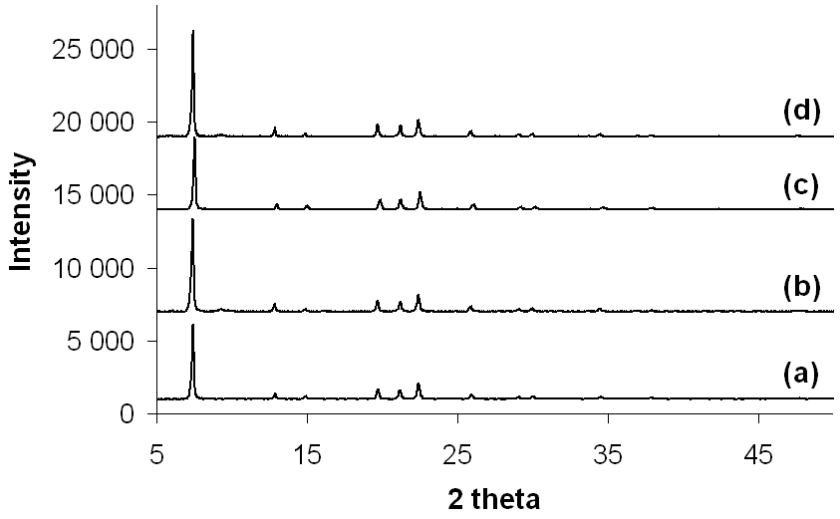

Figure 31: *XRD of TAPO-5/ Ti^{3+} where (a) is as-synth 4h, (b) is calcined 4h, (c) is as-synth 48 h and (d) is calcined 48h.*

There were also done different syntheses with different titanium source and molar composition, Figures 32, 33 and 34 below show the diffractograms of TAPO-5/3, TAPO-5/4 and TAPSO-5/2. These were not chosen to do XAS of, because there were other and better candidates for this. The reason for this was because there was not a lot of time to do XAS, and therefore the most crystalline samples should be chosen. These samples has been characterised with ICP-MS to see the elemental analysis.

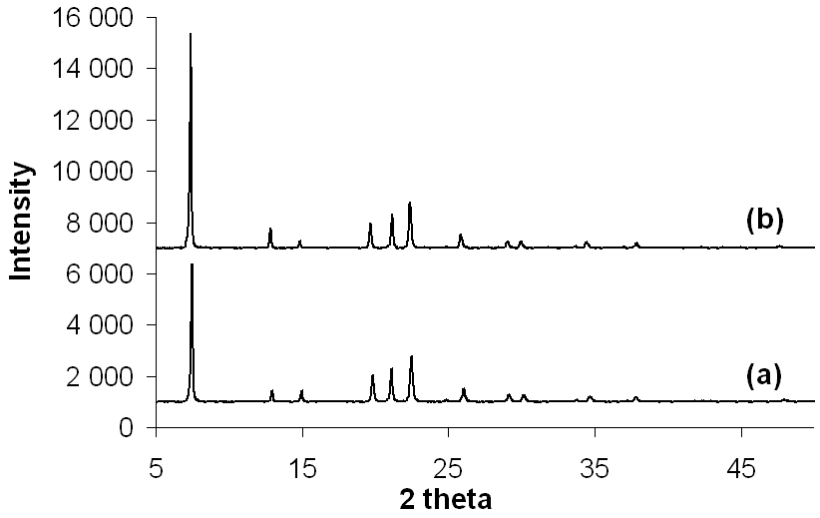

Figure 32: *XRD of TAPO-5/3, where (a) is as-synthesised and (b) is calcined*

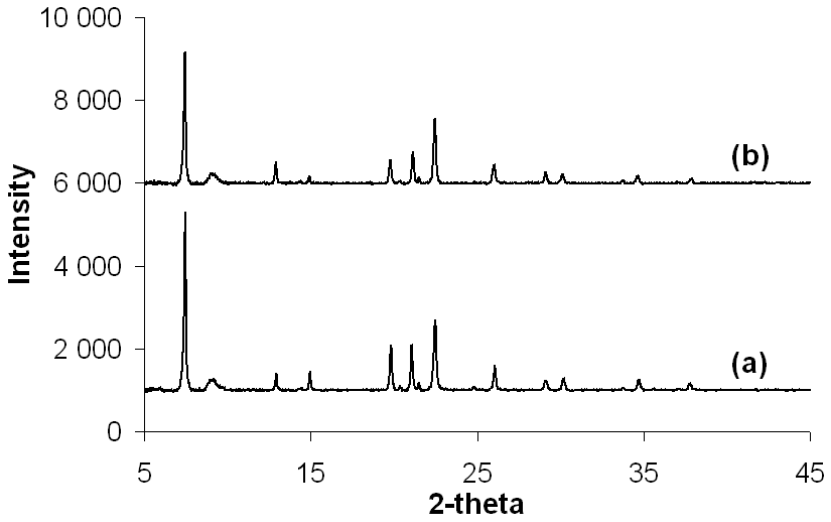

Figure 33: *XRD of TAPO-5/4, where (a) is as-synthesised and (b) is calcined*

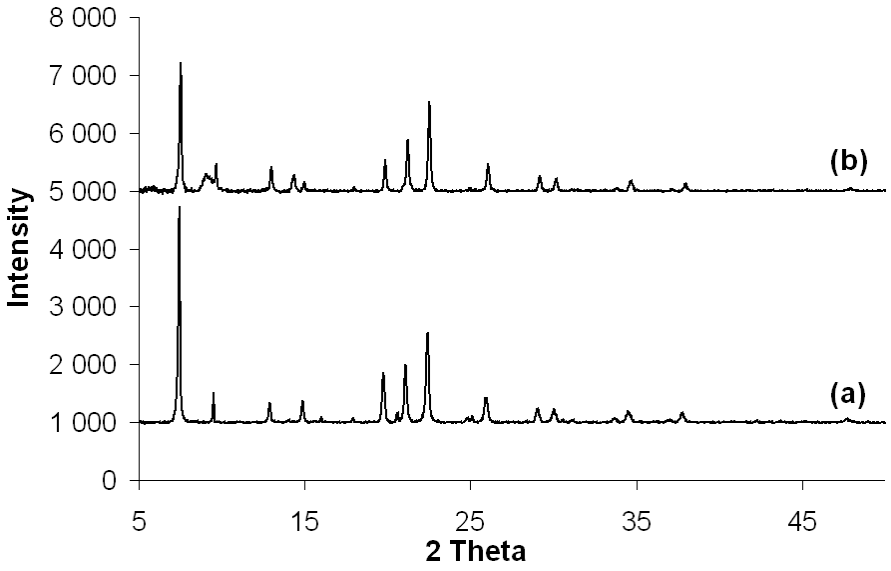

Figure 34: *XRD of TAPSO-5/2, where (a) is as-synthesised and (b) is calcined*

3.4 Thermogravimetric Analysis (TGA)

TGA-data were obtained at NTNU of the TAPSO-5/1 and TAPO-5/2 with mass-spec data. The TGA were done to see if and when the template was burned off.

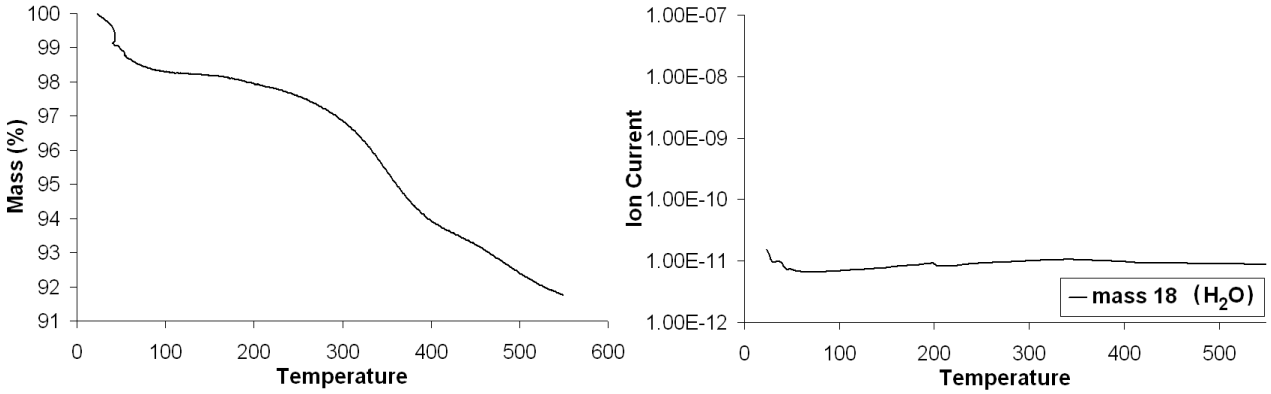

Figure 35: *TGA spectra with mass-spec data of TAPSO-5/1, where the ion current is plotted logarithmically.*

Figure 35 shows the TGA spectra of TAPSO-5/1. The mass-spec data didn't show that water evaporates at 100°C as expected, and the masses for the template do not show on the TGA. One explanation can be that the parameter file for the mass-spectrometer did not have the fragment masses for the template. So if the template was burned off no masses were registered, because the masses were not in the parameter file. The other explanation can be that the template disappeared at drying at 100°C, that will mean that it desorbs and not burns off. In the synthesis method of the TAPSO-5/1 which was taken from Bo-Ya Hsu et.al did they calcine their TAPSO-5 sample at 550°C to remove the template. So the most reasonable to think is that the mass-spec parameter file did not have the correct masses, since the TGA spectra in Figure 36 for TAPO-5/2 4h shows different masses burned off.

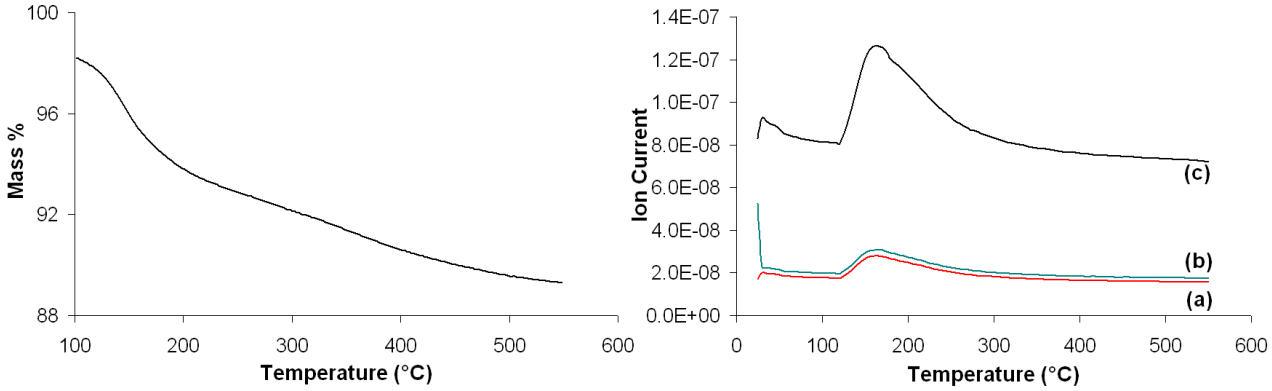

Figure 36: *TGA spectra with mass-spec data of TAPO-5/2 with crystallisation time of 4 hours, where (a) is mass 32, (b) is mass 40 and (c) is mass 28.*

Figure 36 shows the TGA spectrum of TAPO-5/2, with mass-spec data. Mass 32 can be O_2, H_2NO, CH_4O; mass 40 can be C_2O, C_2H_2N. Mass 28 can be CO, CH_2N. The mass-spec data shows that the template disappears at around 200°C, and it is decomposed to different compounds. The TAPO5/2 was synthesised with TEA as template. TEA has a molecular formula of $(C_2H_5)_3N$, which shows that one of the masses most likely contains nitrogen.

3.5 BET results

BET were done on three samples; TAPO-5/1, TAPO-5/2 4h and TAPSO-5/1. This was done to measure the specific surface area (m^2/g). Table 4 displays the result and the specific surface area was calculated using the BET equation.

Table 4: *The specific surface area of three TAPO-5 and TAPSO-5*

Sample	Specific surface area
TAPO-5/1	9.8 m^2/g
TAPO-5/2	241.7 m^2/g
TAPSO-5/1	252.5 m^2/g

The surface area of the TAPO-5/2 and TAPSO-5/1 can be reckoned as "normal". The result of 241.7m^2/g and 252.5m^2/g indicates that the material has a high surface area, and it is a porous material. The TAPSO-5/1 used the method of preparation from Bo-Ya Hsu et.al [58], and from those results in that article, shows that surface area of theirs TAPSO-5's lie between 198-254m^2/g. This means that the surface areas of the TAPO-5/2 and TAPSO-5/1 are in the same range.

The TAPO-5/1 had a completely different result at 9.8m^2/g. The surface area of this sample is not large at all. From the diffractogram of the TAPO-5/1 it can be seen an anatase peak. This indicates from the low surface area, that something clogs the pores of this microporous material. It can be seen from the diffractogram, that the sample is crystalline and has an $AlPO_4$-5 structure with an anatase peak. The explanation can be that there are anatase particles that clog the pores, and there are anatase particles in the sample. The TiO_2 did not dissolve properly in the synthesis.

3.6 SEM pictures

Three SEM micrographs were obtained of the calcined TAPO-5/2 4h. These pictures are displayed in Figure 37, and from these it can be seen that the shape and size of varies for the different particles.

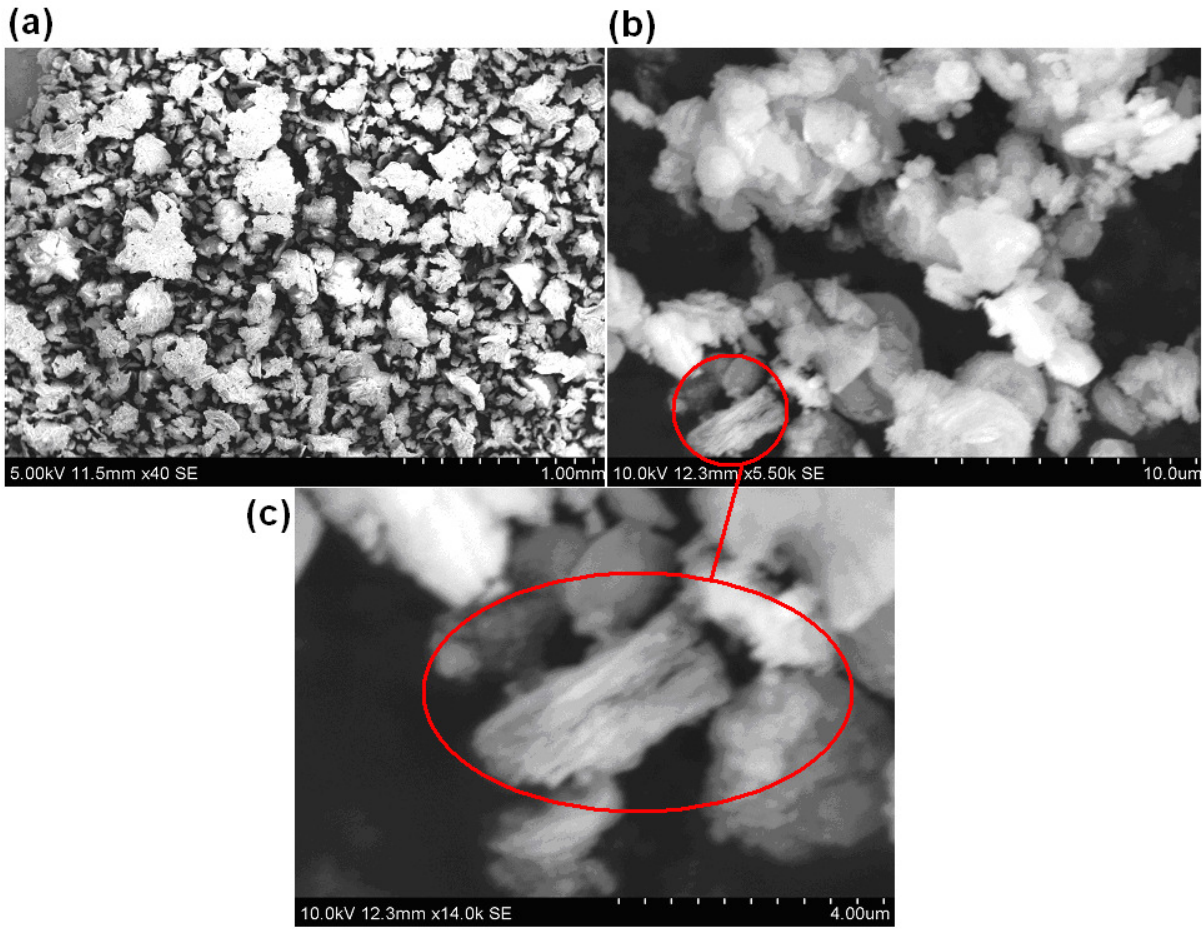

Figure 37: *SEM picture of TAPO-5/2, (a) is a overview of the sample, (b)is magnified down to 10µm, (c) Is a magnification of one particle in (b) at 4 µm scale.*

These pictures which were obtained are a bit fuzzy, but show clearly that the particle distribution is not homogenous. The particle size for some of the particles is around 4µm. (a) is an overview which shows the agglomerates of the sample powder. (b) is a bit more magnified picture and (c) is a magnified particle from (b), which is encircled with red. One reason for the fuzzy pictures are that the kV are too high, if that would be a bit reduced, the samples would be seen more clearly. There was no time to take new SEM or on other samples, because the SEM broke down when it was scheduled to do new micrographs.

3.7 ICP-MS results

ICP-MS on 6 different samples were done; 4 TAPO-5's and 2 TAPSO-5's. The results of these are displayed in table 5. The TAPO-5's were dissolved in aqua regia, and the TAPSO-5's were dissolved in hydrofluoric acid (HF).

Some problems occurred with the hydrofluoric acid. It reacted with the aluminium in the samples and made AlF. This problem caused a faulty elemental analysis of the samples dissolved in HF, and there was no time to re-analyse the samples in aqua regia. The elemental analyses are only correct for the TAPO-5's, but the weight percent for all the samples are correct.

Table 5: *Molar composition and wt% of some of the synthesised TAPO-5 and TAPSO-5*

Sample	Molar composition	Elemental analysis	Ti wt%
TAPO-5/2 4h	$Al:P:0.05Ti:0.5TEA:20H_2O$	$Al:P_{0.95}:Ti_{0.0057}:O_4$	0.2
TAPO-5/2 48h	$Al:P:0.05Ti:0.5TEA:20H_2O$	$Al:P_{0.93}:Ti_{0.012}:O_4$	0.45
TAPO-5/3	$Al:P:0.05Ti:0.5TEA:20H_2O$	$Al_{0.97}:P:Ti_{0.01}:O_4$	0.29
TAPO-5/4	$Al:P:0.01Ti:0.5TEA:15H_2O$	$Al:P_{0.95}:Ti_{0.0053}:O_4$	0.19
TAPSO-5/1	$Al:P:0.2Si:0.15Ti:0.5TEA:15H_2O$	-	0.67
TAPSO-5/2	$Al:P:0.2Si:0.05Ti:0.5TEA:20H_2O$	-	0.33

From the ICP-MS results a clear difference can be seen of the molar composition from the synthesis and from the element analysis, which shows the molar composition of the samples. The aluminium and phosphorus have roughly a ratio of 1:1 this is similar for the synthesis composition. The molar ratio of titanium was less in the samples then what was added from the syntheses. One explanation of the disappearance of titanium can be when it was taken out from the autoclave. After it was taken out from the oven, the sample was washed and dried. The washing process was used to remove any excess template; some of the titanium can have disappeared down the drain with the excess template.

3.8 XANES analyses

The samples that have been analysed and synthesised are shown in table 6. This table gives an overview of where these samples have been taken XAS of and which type of XAS it is.

Table 6: *Overview of the samples that has been synthesised and analysed in this master thesis*

Sample names	Place	Type	Transmission/fluorescence
TAPO-5/1 as-synthesised	Grenoble-07 SNBL	Ex-situ	Transmission
TAPO-5/1 calcined	Grenoble-07 SNBL	Ex-situ	Transmission
TAPO-5/2 as-synthesised	MAX-lab-08	Ex-situ	Fluorescence
TAPO-5/2 calcined	MAX-lab-08	In-situ	Fluorescence
TAPSO-5/1 as-synthesised	MAX-lab-08	Ex-situ	Fluorescence
TAPSO-5/1 calcined	MAX-lab-08	In-situ	Fluorescence

The XANES spectra were analysed using the Athena program [48]. XAS data was also collected on the models Ti-foil, anatase (TiO_2) and rutile (TiO_2). Initially, the edge energy E_0 was determined for all samples, and all the spectra was energy corrected against the Ti-foil (4966.0 eV). For XANES the normalisation range was from 30-150 or 15-150 and for the EXAFS the range was from 150 to the end of the spectra for all samples. Titanium has a very low energy k-edge. At ESRF in Grenoble at SNBL, the spectral range lies from 4-70 keV so good data for titanium is very hard to obtain as explained above in section 2.5.7. During the insitu XANES was obtained for the samples. EXAFS was only obtained for the room temperature samples (ex-situ).

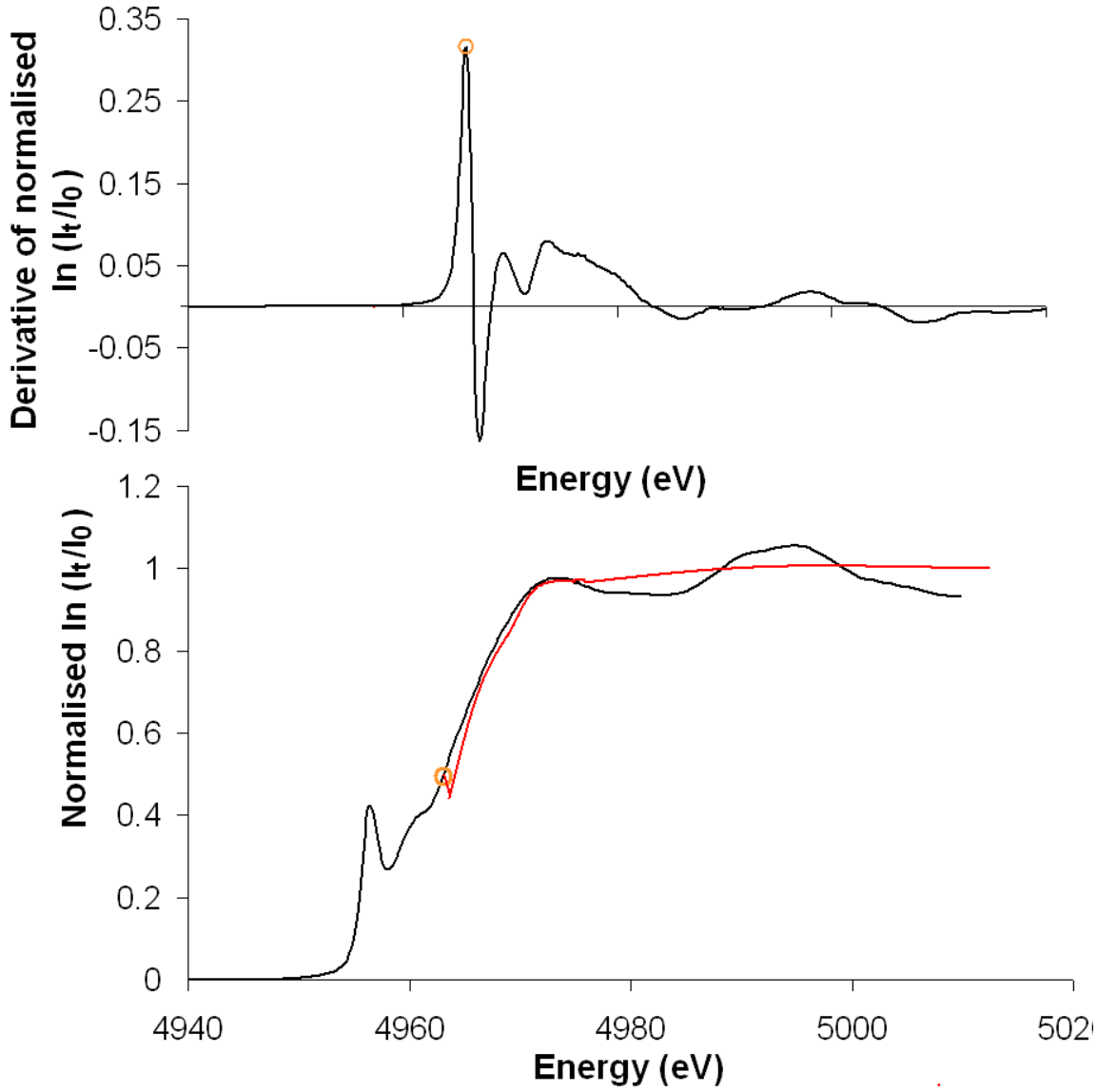

Figure 38: *XANES of normalised titanium calibration foil and its first derivative, where the red line is the background*

The Ti-foil model is shown in Figure 37 with its derivative. It was a necessity to find the correct E_0. The Ti-foil has a K-edge on 4966eV. The e-shift from Grenoble 07 was –0.2, and from MAX-lab it was an e-shift of 1.607.

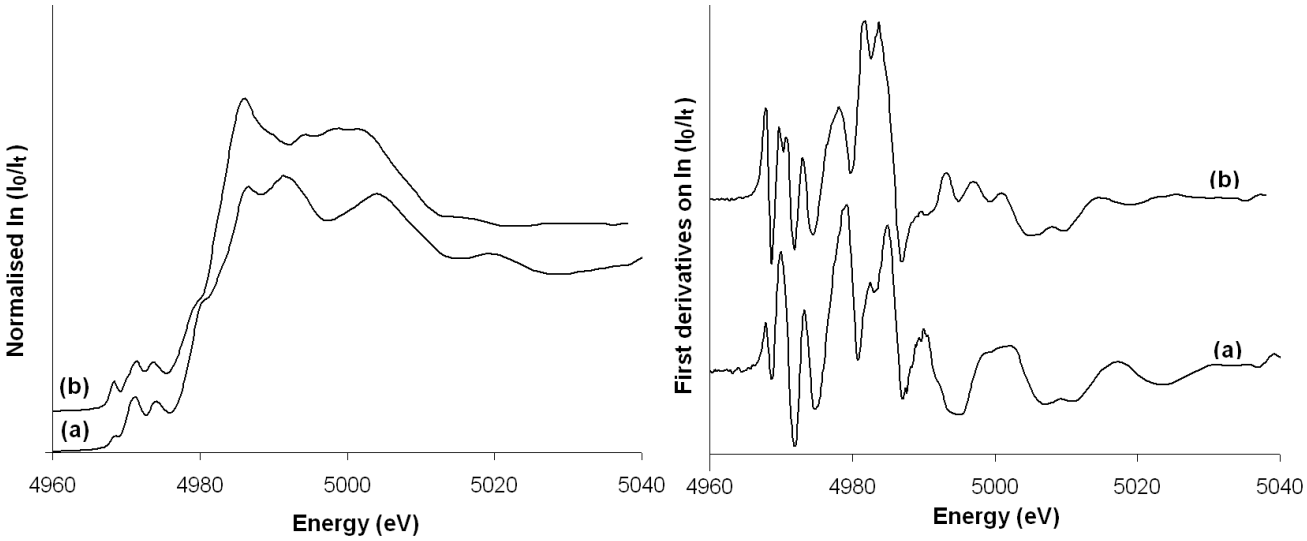

Figure 39: *The normalised and derivative XANES for the models anatase and rutile, (a) is rutile and (b) is anatase*

The models of anatase and rutile is shown in Figure 39, with the normalised XANES and the derivative, the synthesised sample TAPO-5/1 is shown in Figure 40, with the derivative and normalised XANES.

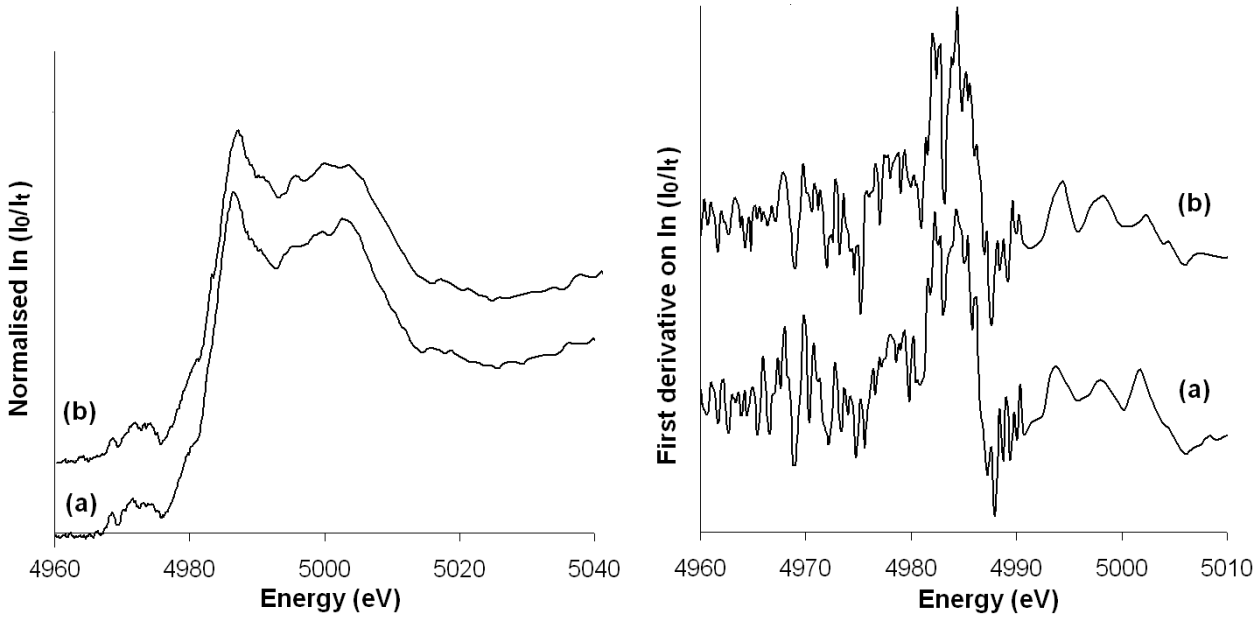

Figure 40: *The derivative and normalised XANES for the sample TAPO-5/1, (a) is the as-synthesised and (b) is the calcined sample*

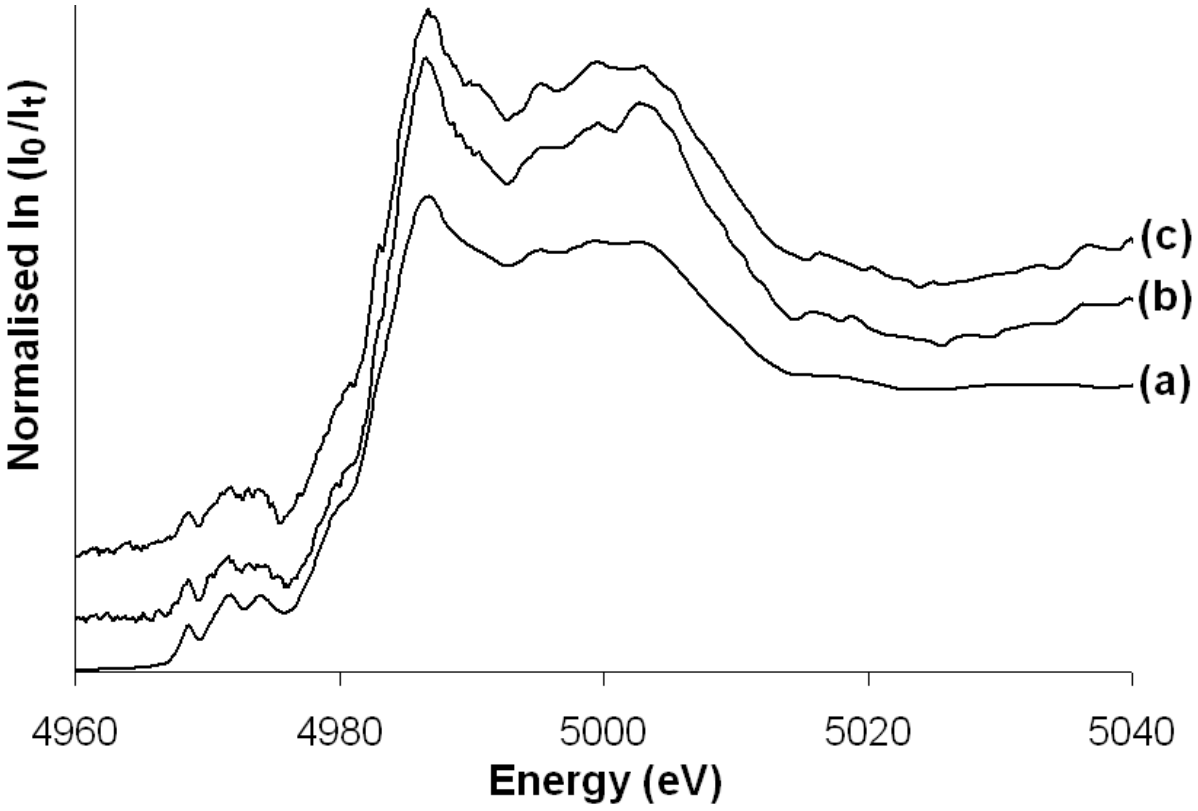

Figure 41: *Comparison of TAPO-5/1 with anatase model, where (a) is anatase, (b) is as-synthesised TAPO-5/1 and (c) is the calcined TAPO-5/1*

The TAPO-5/1 is very similar to the model of anatase, this can be seen in Figure 41 were it looks very much alike. The titanium source used in the synthesis was TiO_2. The reason for the similarity is that most likely the TiO_2 particles was not dissolved properly in the synthesis and incorporated in the framework of the TAPO-5/1. This can be seen from the BET results where the total surface area was $9.8 m^2/g$, which is very small for a microporous material. So this synthesis was not successful for incorporation. The difference in anatase and rutile is shown in Figure 39. A comparison was done of the as-synthesised and calcined sample of TAPO-5/1 with anatase. This comparison is shown in Figure 41, and it can be seen that the samples is more similar to anatase then rutile from Fig. 39.

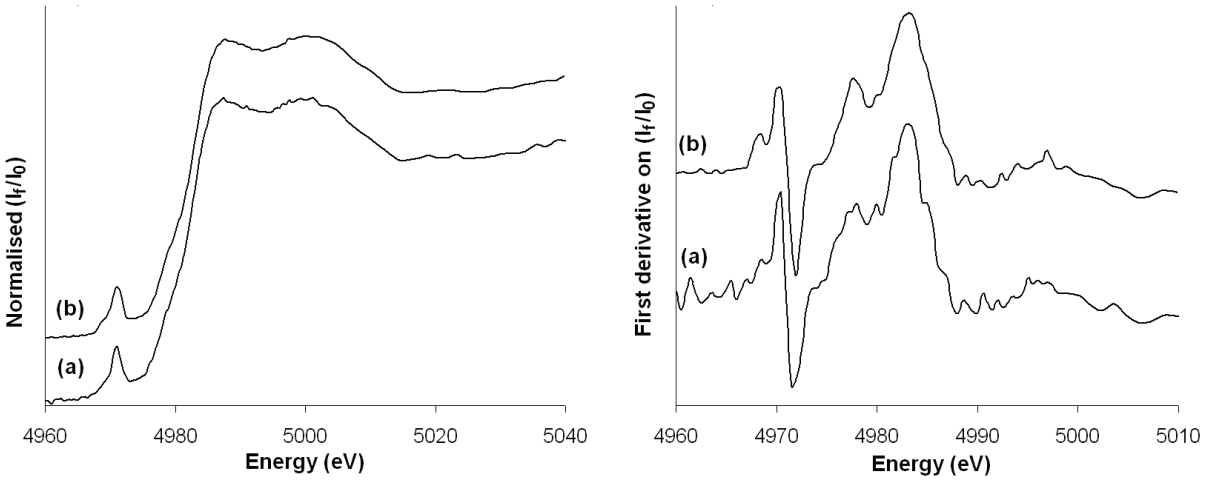

Figure 42: *Normalised and first derivative XANES of TAPO-5/2, (a) is the as-synthesised and (b) is the calcined sample*

Figure 42 shows the normalised XANES and first derivative of TAPO-5/2 obtained at MAX-lab. This is completely different from the TAPO-5/1 which was synthesised with TiO_2 as the titanium source. It is not similar to the anatase model as shown in Figure 41; this sample has only one pre-edge. From the theory written of the pre-edges of titanium, the coordination of most six coordinated titanium has multiple low intensity pre-edges. The TAPO-5/2 has a low intensity peak, but it is not a sharp peak as most of the 4- and 5- coordinated titanium compounds as seen in section 2.5.4 under the theory chapter. It can also be seen a small shoulder to the left of the pre-edge. Peak fitting was done to clarify the question of what kind of coordination number this sample has.

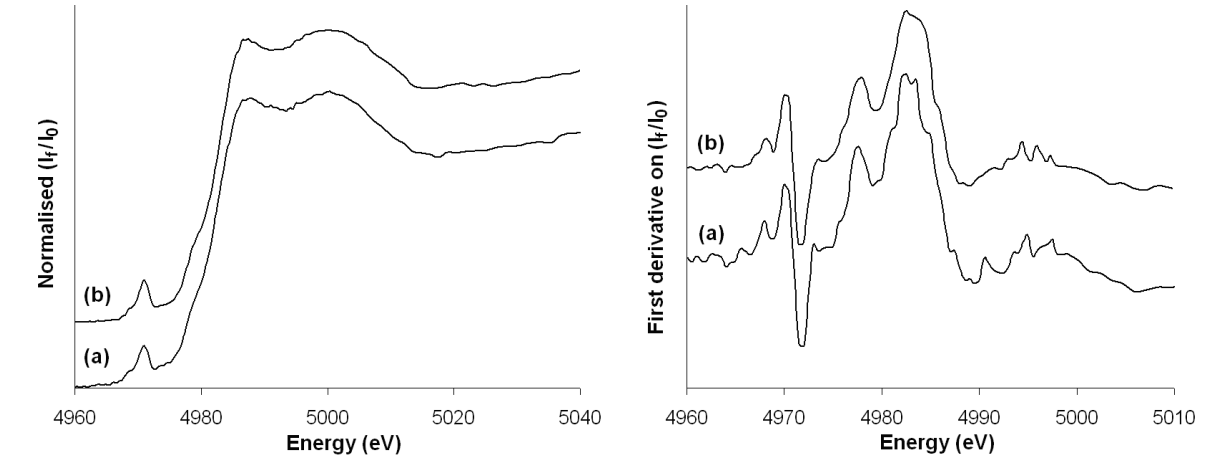

Figure 43: *Normalised and first derivative XANES of TAPSO-5/1, (a) is the as-synthesised and (b) is the calcined sample*

The normalised and first derivative of TAPSO-5/1 is shown in Figure 43. This TAPSO-5/1 is similar to TAPO-5/2 and not TAPO-5/1. Peak fitting was also done here as well to see what information the pre-edges could give considering the coordination state of the material.

3.8.1 Peak fitting in Athena

Yamamoto et.al and Farges et.al [44, 45] has written and done experiments about the pre-edges of titanium. From their and others work, they have concluded that the pre-edge area, intensity and position of the centroid, can be used as a guide to see what coordination number different samples has from the pre-edges. So therefore peak fitting has been executed on the samples TAPO-5/1, TAPO-5/2 and TAPSO-5/1 both as-synthesised and calcined, and the models anatase and rutile. Insitu peak-fitting analyses have been done on TAPO-5/2 and TAPSO-5/1, this will be discussed later in the thesis.

Peak fitting in room temperature

Peak fitting of TAPO-5/1 as-synthesised and calcined with the models anatase and rutile are displayed in Figure 44 below. The area under these pre-edges is shown in a bar graph in Figure 45. The peak fitting data of these models and the TAPO-5/1 is displayed in Table 7, with the r-factor and energy placement of the centroids.

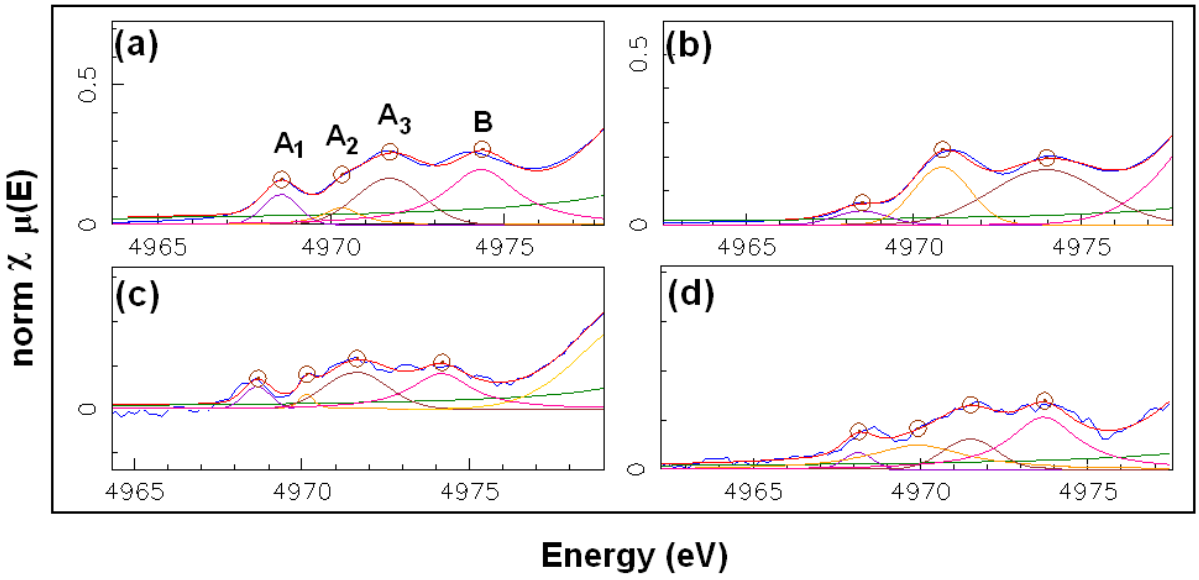

Figure 44: *Peak fitting in Athena of (a) anatase, (b) rutile, (c) TAPO-5/1 as-synthesised and (d) TAPO-5/1 calcined*

From Fig. 44 it can be seen that the as-synthesised and calcined TAPO-5/1 has very similar pre-edges of anatase and not rutile. As explained earlier with the different results of XRD and BET it can be interpreted that there are anatase particles in the sample, and therefore it is similar to the anatase model. It can also be seen that rutile does not have the A_2 peak as TAPO-5/1 and anatase model have. The naming of the pre-edge peaks are as mentioned before A_1, A_2, A_3 and B, as seen in this figure.

Table 7: *The peak fitting data with r-factor and area under the pre-edges, both Gaussian and Lorensian function were used. This data were obtained at ESRF, SNBL beamline BM1B*

Samples	A_1		A_2		A_3		B		R-factor
	Area	Centroid	Area	Centroid	Area	Centroid	Area	Centroid	
Anatase	0.14(4)	4969(1)	0.13(6)	4970(3)	0.4(2)	4971.7(7)	0.8(3)	4974.3(9)	0.00098
Rutile	0.08(2)	4968.4(9)	-	-	0.36(3)	4970.8(2)	0.7(1)	4973.9(6)	0.00029
TAPO-5/1 as-synth	0.05(2)	4969(1)	0.03(2)	4970(2)	0.20(8)	4971.6(8)	0.3(1)	4974(1)	0.0033
TAPO-5/1 calcined	0.04(2)	4968(2)	0.3(2)	4970(2)	0.13(3)	4971.5(8)	0.4 (2)	4973.7(7)	0.0012

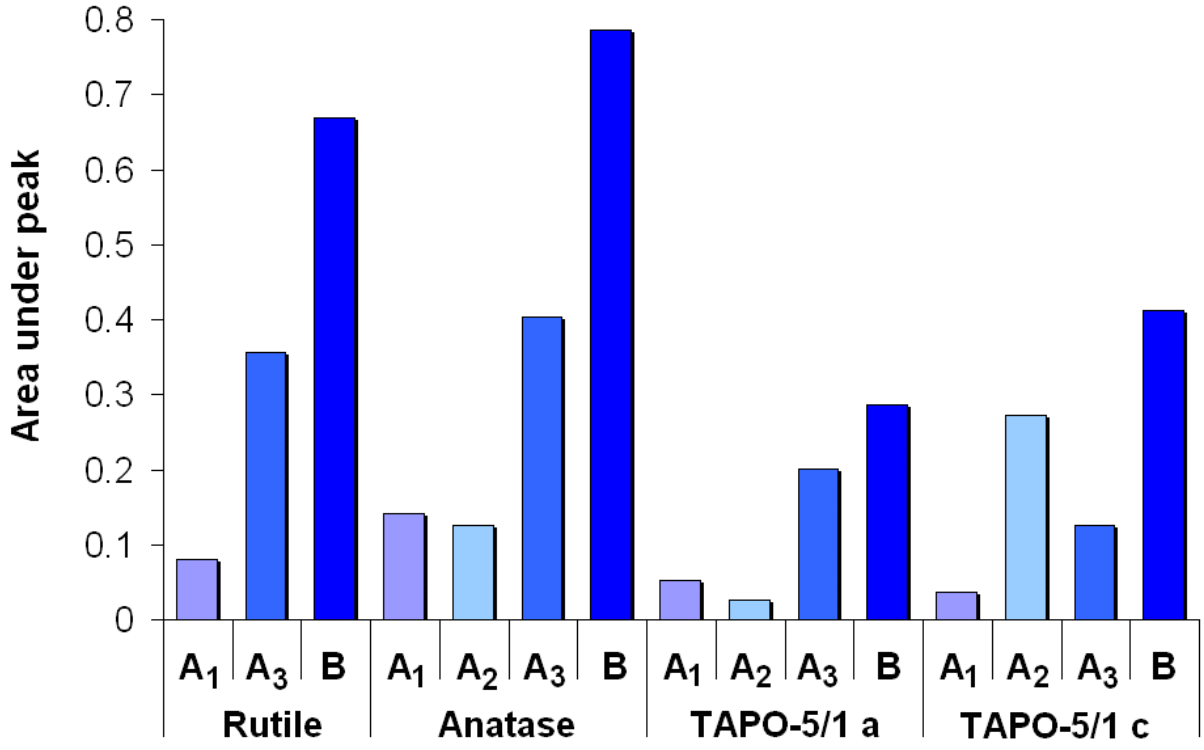

Figure 45: *Bar graph over the peak fitting of models anatase and rutile, and peak fitting of TAPO-5/1 where a stands for as-synthesised and c stands for calcined*

Figure 45 shows a bar graph of the peak fitting area of the TAPO-5/1 with models anatase and rutile. From this bar graph it can be seen that the TAPO-5/1 has the pre-edges A_1-A_3 and B, like anatase. Rutile has only A_1, A_3 and B, this substantiates the assumption that there is anatase particles in the TAPO-5/1. The TAPO-5/1 has lower intensity than the models; one

reason for this is that there was less titanium in the prepared samples than the models. More of the beam got absorbed by the other elements in the sample so the intensity was lower.

Peak fitting for TAPO-5/2 and TAPSO-5/1 were also done. Below in Figure 46, the peak fitting for the as-synthesised and the calcined samples is shown. In all of these peaks there can be seen a smaller peak at lower energy (to the left) of all the main peaks of the samples. An attempt was made to fit these smaller peaks as well, but this was not successful. A reason for this can be that the peaks are too small to be fitted, but a smaller shoulder can clearly be seen on all of the samples. This can also indicate that the samples are 6-coordinated, because the 4- and 5-coordinated samples had a sharp high intensity peak as shown previous in section 2.5.4. The as-synthesised were fitted with Lorensian function and the calcined were fitted with Gaussian function.

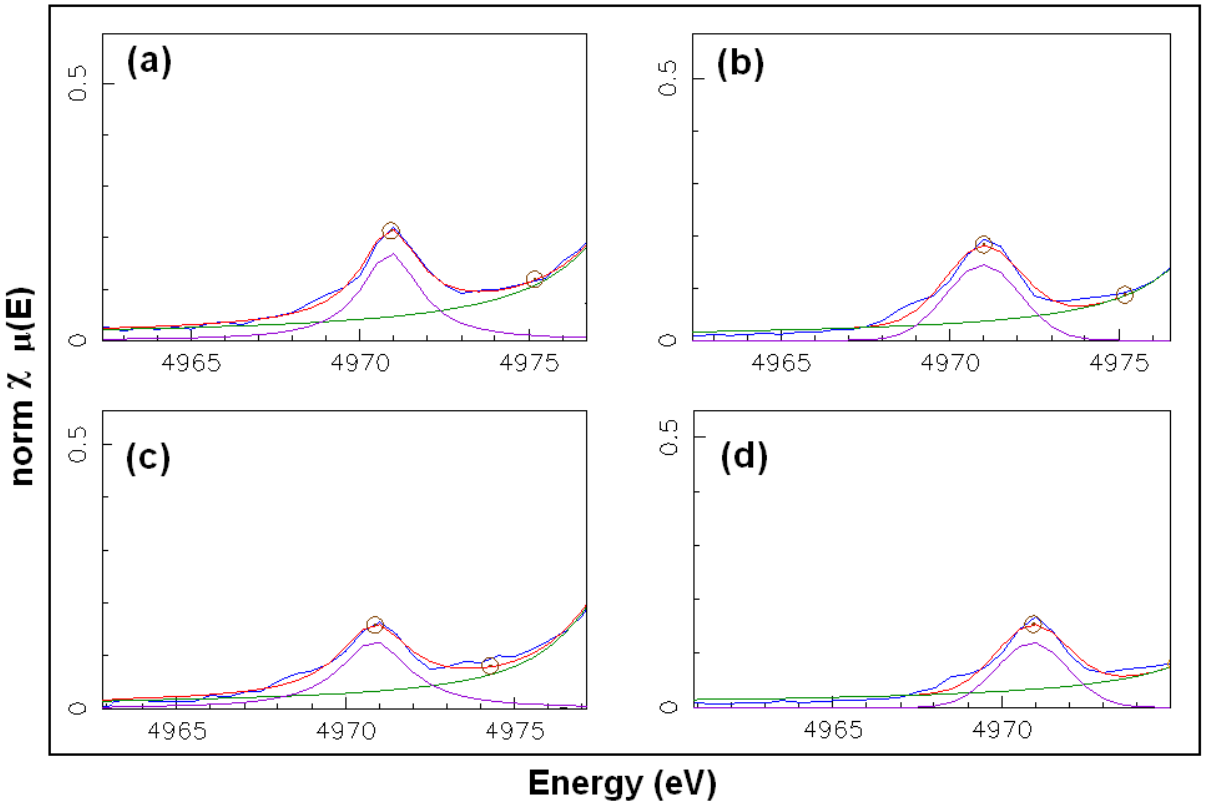

Figure 46: *Peak fitting of TAPO-5/2 (a) as-synthesised and (b) calcined, and TAPSO-5/1 (c) as-synthesised and (d) calcined*

Table 8 shows the peak fitting data for the TAPO-5/2 and TAPSO-5/1, the r-factor is not as low as the TAPO-5/1, anatase and rutile in table 7. Some of the problems with the fitting were the smaller peak, which did not want to be fitted. Another interesting detail was that the TAPO-5/2 and TAPSO-5/1 is similar to one another, and different from TAPO-5/1.

Table 8: *The peak fitting data for the as-synthesised and calcined TAPO-5/2 and TAPSO-5/1, the fitting range were (-20:5) relative to centroid of step function. This data were obtained at MAX-lab at beamline I811*

Samples:	TAPO-5/2 as-synthesised	TAPO-5/2 calcined	TAPSO-5/1 as-synthesised	TAPSO-5/1 calcined
R-factor	0.00183	0.00461	0.00588	0.00439
Area	0.56(9)	0.40(5)	0.5(1)	0.32(4)
Centroid	4970.9(3)	4971.0(5)	4970.9(8)	4970.9(4)
Function	Lorens	Gauss	Lorens	Gauss

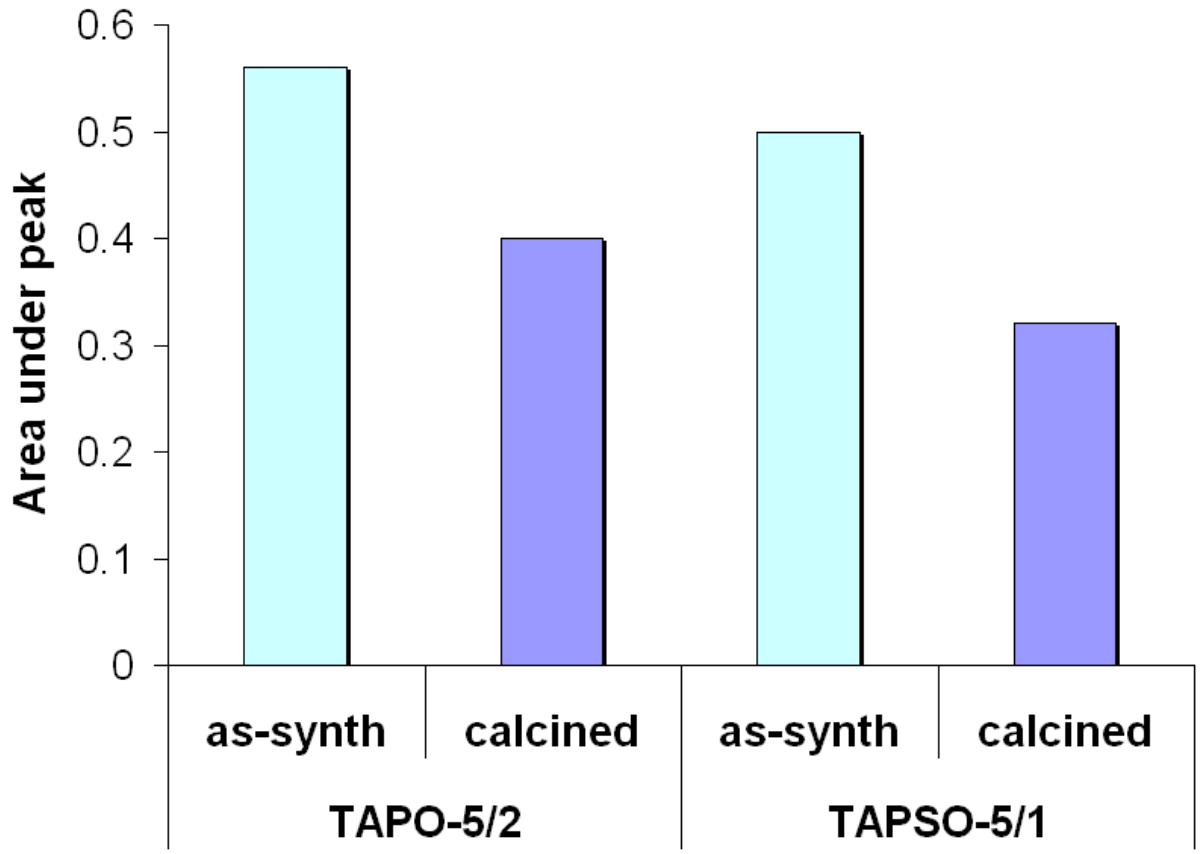

Figure 47: *Bar graph of the area under the pre-edge peaks of as-synthesised and calcined TAPO-5/2 and TAPSO-5/1*

Figure 47 shows a bar graph of the area from table 8. From this figure it can be seen that the area for the as-synthesised samples are larger then the calcined samples. It is likely at looking at different literature that this TAPO-5/2 and TAPSO-5/1 is six-coordinated just with looking at the area of the pre-edges. From a review article written by T.Yamamoto about pre-edges [45], has he come to a conclusion that the area Ti^{4+} of 4-, 5-, and 6-coordinated titanium decreases with increasing coordination number. From a plot in this article it is shown that the

four-coordinated titanium area lies from 0.8-1.4. Five-coordinated titanium area is lower 0.6-0.8, and the six-coordinated is very spread from 0.1-0.8 this is shown in Figure 48. From that figure it can be seen that the samples TAPO-5/1, TAPO-5/2 and TAPSO-5/1 lie around he six coordinated box. This gives a strong indication that these samples are 6-coordinated and a oxidation state of Ti^{4+}.

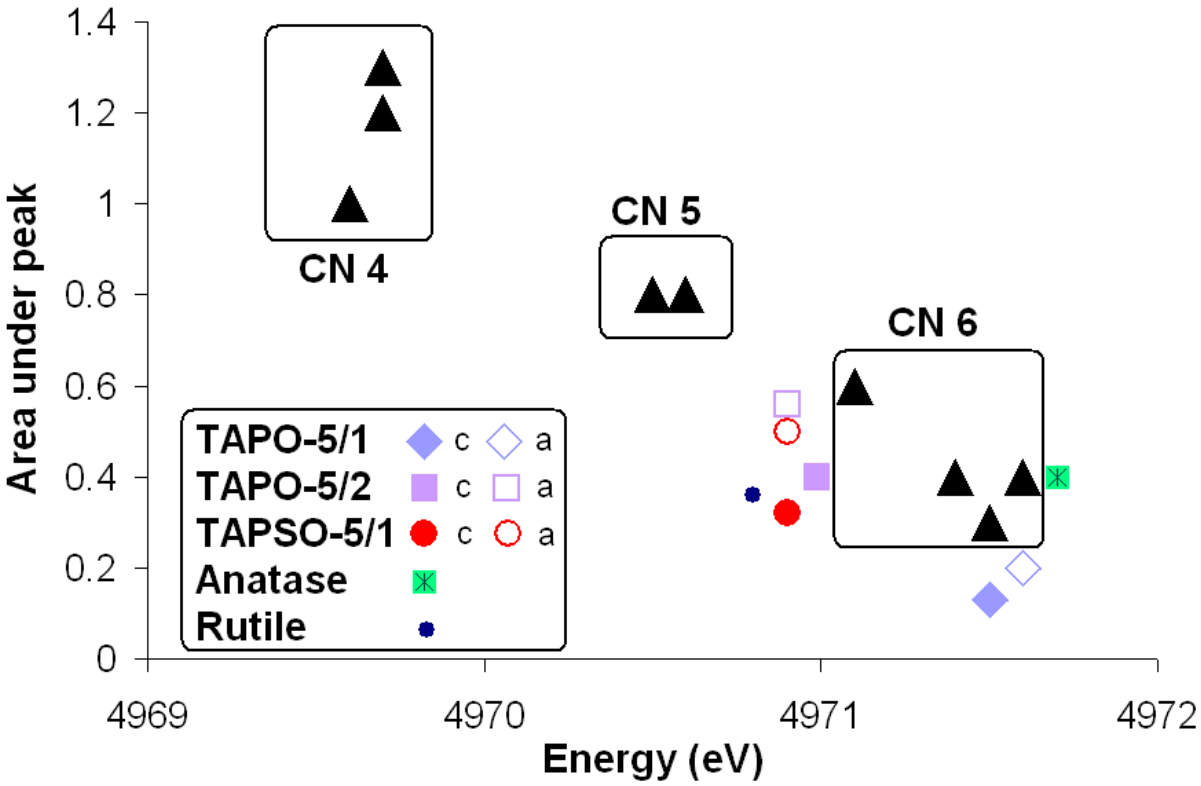

Figure 48: *Dependencies of pre-edge features on coordination number for Titanium. The framed boxes with different coordination numbers are taken from an article from Farges. et.al.[46]* **c** *means calcined and* **a** *means as-synthesised.*

Table 9 gives the data for the 4-, 5- and 6-coordinated titanium displayed in the framed boxes in Figure 48.

Table 9: *Energy position and area under peak for 4-, 5- and 6-coordinated Ti, values taken from Farges et.al.[45]*

Samples	Ti – Coordination	Position (eV)	Area
$Ni_{2.6}Ti_{0.7}O_4$	4	4969.7	1.2
$Ni_{2.4}Ti_{0.7}Si_{0.05}O_4$	4	4969.6	1
$K_6Ti_2O_7$	4	4969.7	1.3
$KNaTiO_3$	5	4970.6	0.8
$Rb_2Ti_4O_9$	5	4970.5	0.8
$BaTiOSi_2O_7$	5	4970.6	0.8
Rutile (article)	6	4971.6	0.4
Anatase (article)	6	4971.5	0.3
Neptunite	6	4971.1	0.6
Titanite	6	4971.4	0.4

What happens during calcination?

In calcination of the samples it can be seen that the area of the two pre-edges from Fig. 47, and 48 decreases from as-synthesised to calcined. There is no difference in the energy of the pre-edge peak, this stays put around the 6-coordinated box as seen in Fig 47. This will mean that no change happen in coordination number during calcination. Water and the template are burned off, so maybe the ligands are water and a rearrangement happens with the molecules. It can be a chemical shift which happens, which means a change in ligands (The chemical environment around titanium varies).

In situ of TAPO-5/2 and TAPSO-5/1 and peak fit in Athena

At MAX-lab in Sweden, two insitu's were obtained of TAPO-5/2 and TAPSO-5/1. The samples were pre-heated in helium to 150°C to remove water and other impurities. After the pre-treatment in helium, the samples were heated in a mixture of propene/O_2 (60% / 24%). This was done to see if it showed any oxidation and reduction properties. The samples were cooled down in a mixture of NO/O_2 (60% / 29%). Peak fitting in Athena were done to decide the area under the pre-edges of the different in-situs. To my knowledge no in-situ studies have previously been done on TAPO-5 or TAPSO-5 so there were some challenges with the analyses of the XANES and the interpretation of these analyses.

TAPO-5/2

The in-situ of TAPO-5/2 started with heating the sample to 150°C in helium to remove water and impurities. Then it was heated in a mixture of propene/O_2 (60% / 24%) to 331°C and finally cooled down to room temperature in a mixture of NO/O_2 (60% / 29%). Figure 49 shows the area under the pre-edges when the sample was heated and cooled down. It can be seen that the area increases when heated, and decreases when cooled.

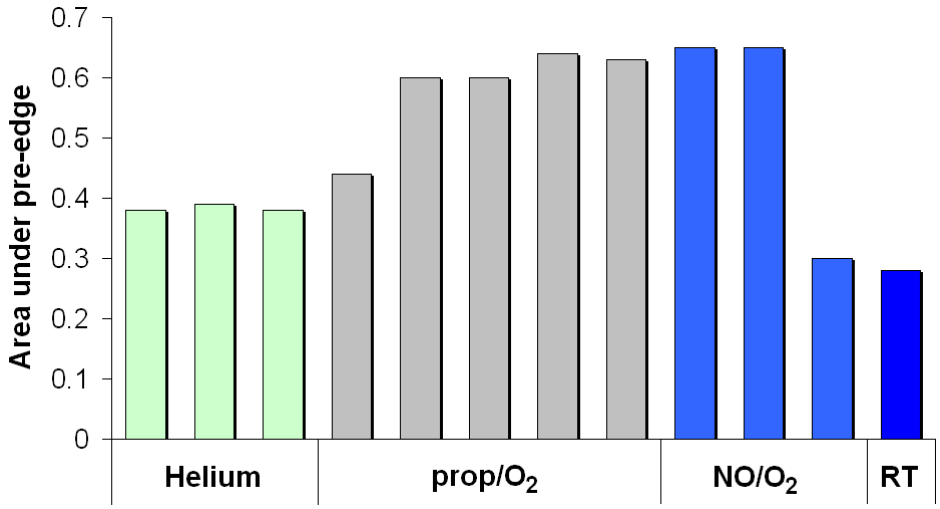

Figure 49: *Area under the pre-edges on sample TAPO-5/2, in-situ experiment*

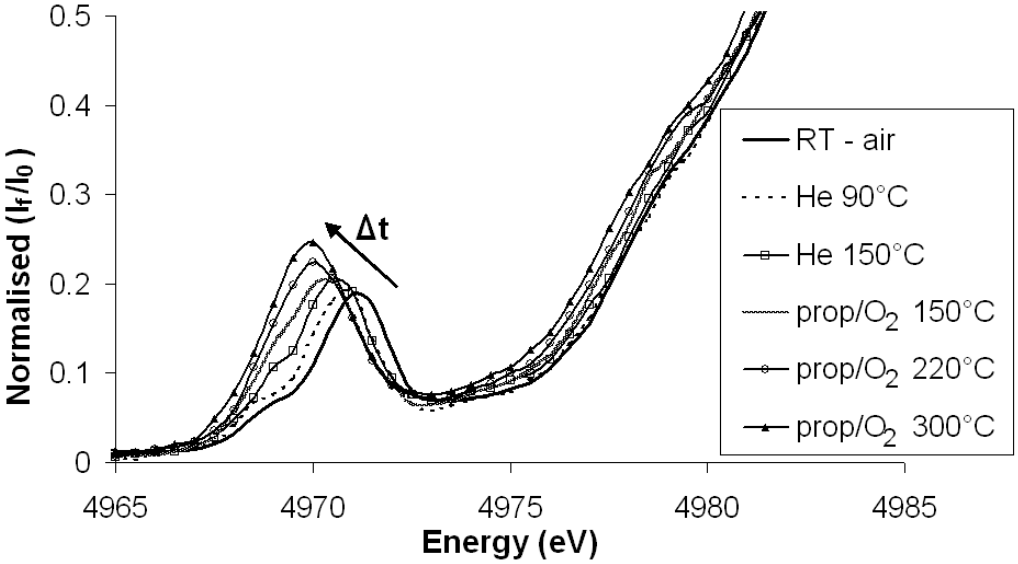

Figure 50: *The heating of the TAPO-5/2 in a mixture of propene and oxygen from room temperature to 300°C.*

From Figure 50 it can be seen that the pre-edge moves to the left and the area under the peak increases, when it was heated from room temperature to 300°C in a mixture of prop/O_2. Figure 51 shows the cooling NO/O_2 down process, where it can be seen that the area of the

pre-edge decreases and moves to the right. The edge also shows this similar trend in the same figures.

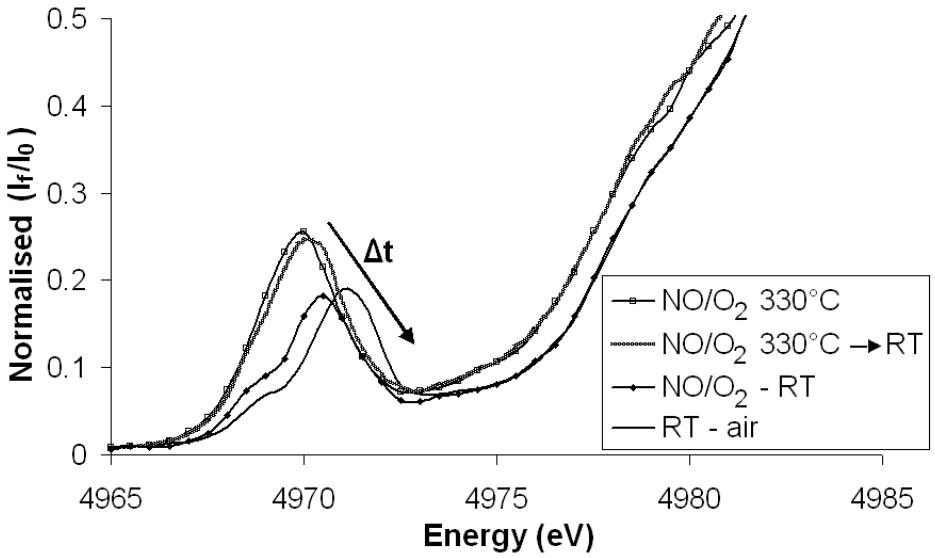

Figure 51: *The cooling in NO/O_2 of the TAPO-5/2 from 330°C to room temperature.*

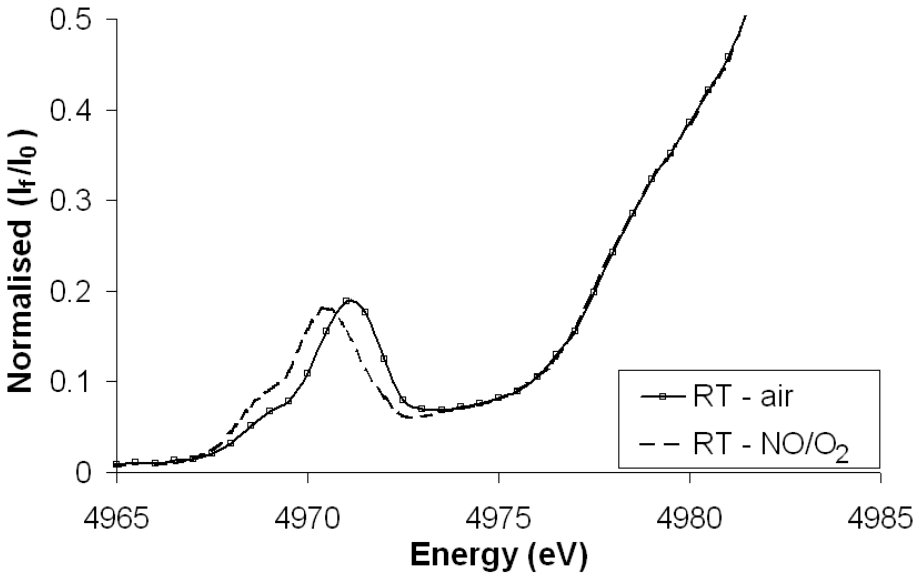

Figure 52: *Comparison of the two XANES spectra of the TAPO-5/2 in room temperature before and after the in-situ.*

A XANES comparison of the room temperature in air and room temperature after it was cooled down in NO/O_2 is shown in Figure 52, there is only a slight difference in the pre-edge but the edge is on the same place. From Figure 49 it can be seen that the area nearly is the same. Table 10 below gives an overview of the TAPO-5/2 in situ. Figure 53 shows how the pre-edge centroid moves during the insitu. When heated in helium it can be seen that the energy moves slightly to the right, but with further heating in the presence of propene/O_2 the energy goes left and decreases in energy (eV).

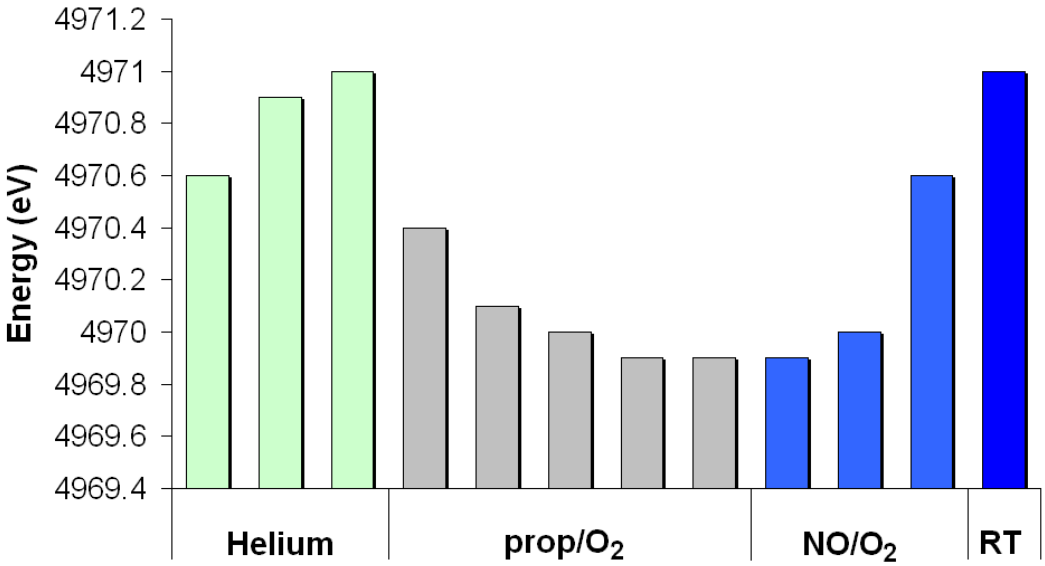

Figure 53: *The centroid movement for the insitu TAPO-5/2.*

Figure 54 below, gives a summary of the bar graphs and shows the area and the pre-edge centroid movement during heating and cooling. From this figure it can be seen that when it starts to heat it's around the coordination number 6 - box, with further heating it moves down to coordination number 4. There is an increase in area and a shift in energy to the lower range. During cooling it moves back again to the starting point in energy and area.

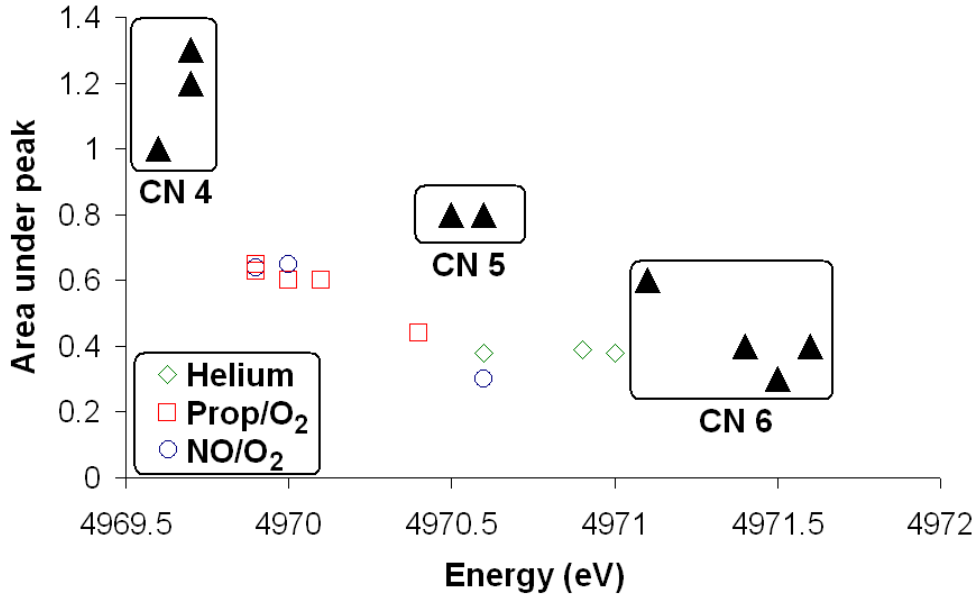

Figure 54: *Dependencies of pre-edge features on coordination number for Ti. The boxed 4- ,5- an 6- coordination is taken from Farges et.al which shows different coordination number for Ti^{4+} [45] and is shown in table 9 above. The rest is the insitu of TAPO-5/2, table 10 has the pre-edge area and the position of the insitu.*

Figure 55 displays the valence shift of the Ti^{4+} to Ti^{3+}; this figure shows the difference in the energy of the different valence states. Ti^{3+} is located at around 4967 eV and Ti^{4+} samples are located around 4969 eV.

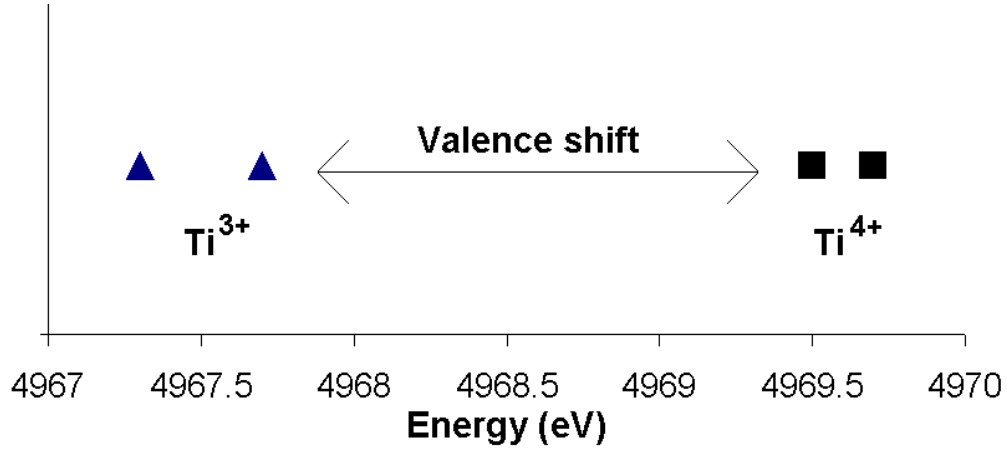

Figure 55: *Plot of Ti^{4+} and Ti^{3+}, which are located at different energies*

Table 10: *Overview of the TAPO-5/2 in-situ at Max-lab, the function of all the pre-edges was gaussian, where RT is room temperature.*

XANES	Temperature (°C)	Area	Centroid	R-fac
Helium	30	0.38(4)	4970.6 (5)	0.00388
Helium	90	0.39(8)	4970.9 (9)	0.00462
Helium	150	0.38(9)	4971 (1)	0.00226
Prop/O_2	150	0.44 (7)	4970.4 (8)	0.00113
Prop/O_2	185	0.60 (4)	4970.1 (3)	0.00186
Prop/O_2	220	0.60 (4)	4970.0 (3)	0.00134
Prop/O_2	250	0.64 (4)	4969.9 (4)	0.00141
Prop/O_2	300	0.63 (6)	4969.9 (4)	0.00143
NO/O_2	330	0.65 (8)	4969.9 (6)	0.00228
NO/O_2	330→ RT	0.65 (6)	4970.0 (5)	0.0022
NO/O_2	RT	0.30 (3)	4970.6 (5)	0.00249
RT-air	RT	0.28 (9)	4971 (2)	0.00153

From the bar graphs (Fig. 49, 53) and the figures that shows the in-situ (Fig. 50, 51, 52) it can be seen that the pre-edge moves to the right during heating and back left again in energy when cooled. With the comparison of different coordination number of Ti^{4+} compounds in Fig. 54 it

can be fair to say that the coordination number changes during this insitu. It goes from CN 6 to CN 4 when the sample is heated, and back again to CN 6 when cooled. The edge energy also changes during the insitu, but if the edge-energy is compared with the different valence state energy of the Ti^{3+} and Ti^{4+} in Fig. 55, it can be seen that there is not a total change in oxidation state. But since the edge moves back and forth can it be said that it occurs a partial reduction and re-oxidation in the valence state of TAPO-5/2.

TAPSO-5/1

The in-situ of TAPSO-5/2 had the same procedure as TAPO-5/2. Water and impurities was removed with pre-heating in helium to 150°C. Then it was heated in a mixture of propene/O_2 (60% / 24%) to about 500°C and then cooled down to room temperature in a mixture of NO/O_2 (60% / 29%). The areas under the pre-edges when heated and cooled are displayed in a bar graph in Figure 55. It can be seen that the area increases when heated, and decreases when cooled. Figure 57, 58 and 59 shows the heating in propene/O_2, cooling in NO/O_2 and comparison of the two room temperatures respectively.

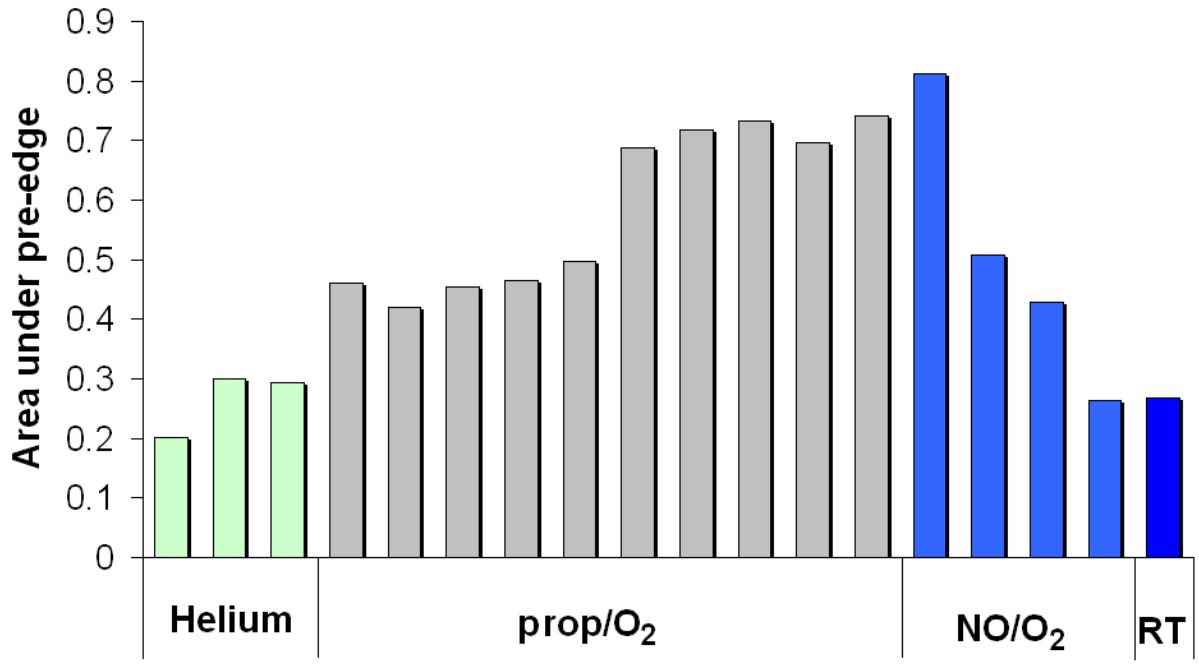

Figure 56: *Area of the pre-edges of TAPSO-5/1 during the in-situ*

The TAPSO-5/1 shows an increase in the pre-edge area from 0.2 to 0.7 during heating in propene/O_2 to 500°C, and a decrease from 0.8 to 0.2 in normalised area as shown in Figure 56. The room temperature in air and the cooled down XANES in NO/O_2, shows the same area even though it is a bit displaced in the XANES spectra shown in Figure 59.

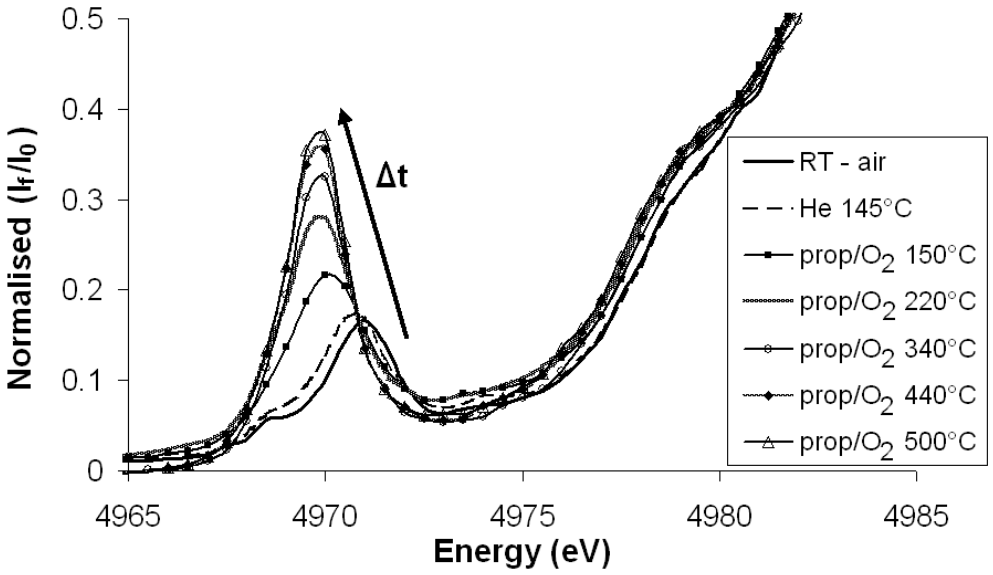

Figure 57: *Heating in propene/O_2 of the TAPSO-5/1, from room temperature to 500°C.*

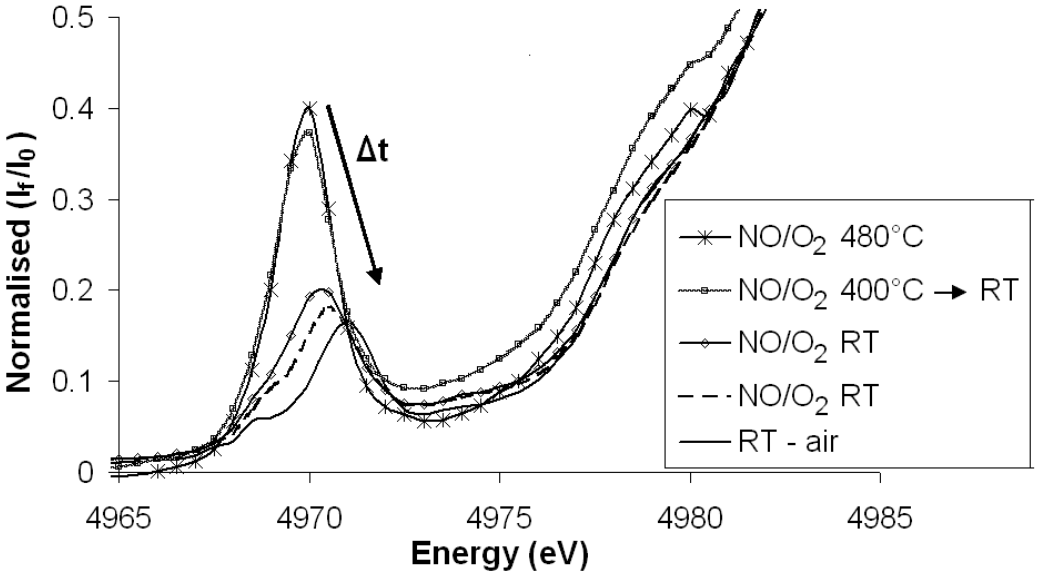

Figure 58: *Cooling in NO/O_2 of the TAPSO-5/1 from 500°C to room temperature.*

The heating in prop/O_2 went to 500ºC, and it can be seen that the area under the pre-edge increases considerably and it moves to the left which is shown in Figure 57. The cooling shows the same tendency, that during cooling the area decreases and it moves slightly to the right which is shown in Figure 58.

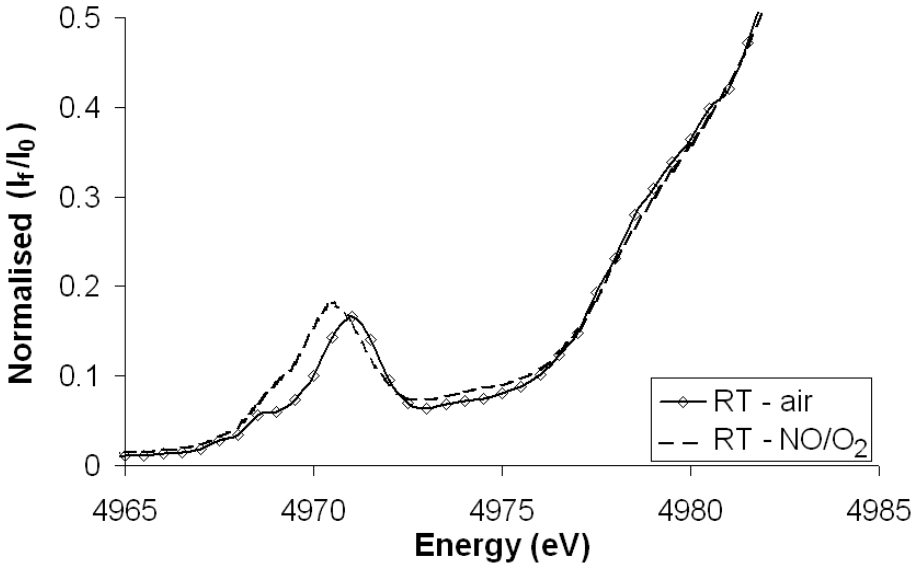

Figure 59: *Comparison of the two room temperature of the TAPSO-5/1, before and after the in-situ.*

The comparison of the pre-edge in room temperature before and after the in-situ is shown in Figure 59 there it just a slightly difference but the area is approximately the same, from table 11 it can be seen that those values are 0.26 (RT NO/O_2) and 0.27 (RT-air). The movement in the pre-edge is also illustrated in Figure 60, where it is plotted how the pre-edges moves during the in situ. The energy moves to lower energy (eV), during heating and then it moves back again when cooled. It is the same results for these edges as it was for TAPO-5/2. The edge energy goes right when heated and goes back left again when cooled. This indicates a partial reduction and re-oxidation happens.

Table 11: *Overview of the in-situ of TAPSO-5/1 obtained at Max-lab, all pre-edges was Gaussian, where RT is room temperature.*

XANES	Temperature (°C)	Area	Centroid	R-fac
Helium	50	0.20 (6)	4971 (2)	0.00198
Helium	90	0.3 (1)	4971 (2)	0.00111
Helium	145	0.29 (4)	4970.8 (7)	0.00232
Prop/O_2	150	0.46 (3)	4970.0 (5)	0.0009
Prop/O_2	180	0.42 (3)	4969.9 (5)	0.0007
Prop/O_2	220	0.45 (2)	4969.8 (4)	0.00111
Prop/O_2	260	0.47 (3)	4969.8 (3)	0.00097
Prop/O_2	300	0.50 (3)	4969.9 (2)	0.00087
Prop/O_2	340	0.69 (5)	4969.8 (2)	0.00345
Prop/O_2	370	0.72 (6)	4969.8 (2)	0.00411
Prop/O_2	400	0.73 (6)	4969.8 (3)	0.00659
Prop/O_2	440	0.70 (5)	4969.8 (3)	0.0073
Prop/O_2	500	0.74 (6)	4969.8 (3)	0.00513
NO/O_2	480	0.81 (6)	4969.9 (3)	0.00659
NO/O_2	400 → RT	0.51 (3)	4969.9 (3)	0.00094
NO/O_2	RT	0.43 (3)	4970.2 (5)	0.00251
NO/O_2	RT	0.26 (6)	4971 (1)	0.00116
RT-air	RT	0.27 (6)	4971 (1)	0.00243

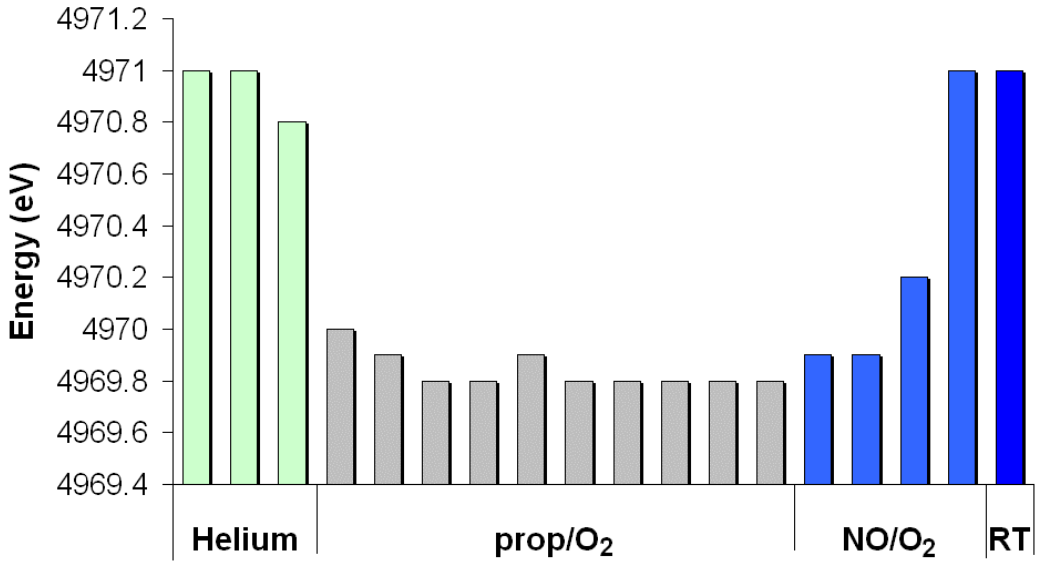

Figure 60: *shows how the TAPSO-5/1 insitu moves in energy with the centroid peak.*

Figure 61 below display the same result as the bar graphs. Only here it is compared to Ti^{4+} with different coordination number for titanium. It can be seen from the TAPSO-5/1 insitu that the sample starts at 6 CN and then during heating in prop/O_2 the centroid peak moves to the left and increases in area. During the heating it goes from 6 coordinated to the box with coordination number 4, there is also a significant increase in the area during this heating. This also is a trend for titanium with coordination number 4. Then when it is cooled down it goes back to the 6-coordinated number. Even though the area of the insitu is smaller then the ones plotted form literature.

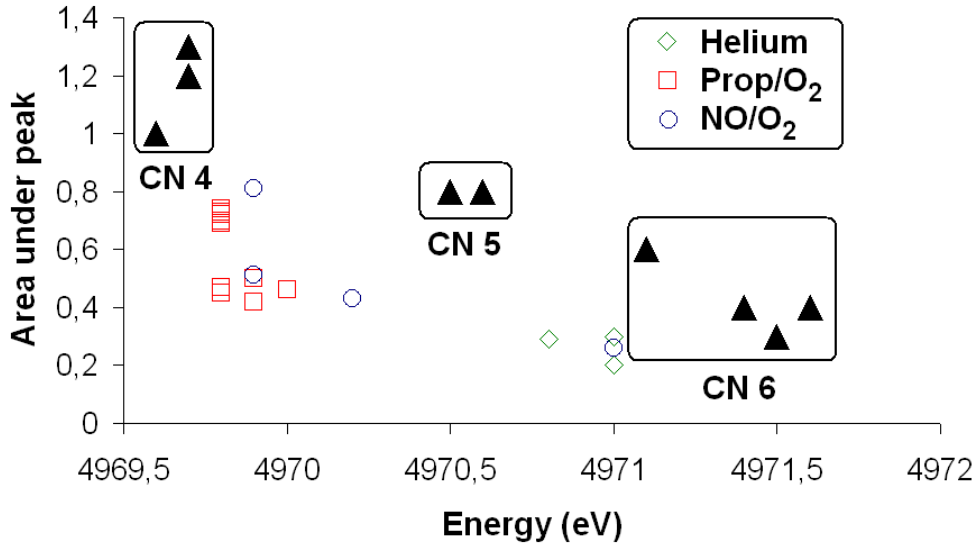

Figure 61: *Dependencies of pre-edge features on coordination number for Ti. The boxed 4- ,5- an 6- coordination is taken from Farges et.al [45] and is shown in table 9 above. The rest is the insitu of TAPSO-5/1, table 11 has the pre-edge area and the position of the insitu.*

From Fig. 61 it gives an indication that the coordination number changes for the sample during the insitu from CN 6 to CN 4. This insitu behaves the same way as the TAPO-5/2. A change in coordination number happens. When it's heated the coordination number goes from 6 to 4 and back again when cooled, but it is still in the same range as Ti^{4+}. From this insitu as well it can also be seen a change in the edge of the XANES in Fig. 57 and 58 when it was heated and cooled. From the change in the edge it can be concluded that a partial oxidation and re-oxidation occurred here as well.

Summary of the two insitu-studies

From the peak fitting and plotting of the pre-edges in the two insitus (TAPO-5/2 and TAPSO-5/1) it can be concluded that during the insitus it occurs a change in coordination number. When heated in propene/O_2 a decrease in CN happens from 6 to 4, the when it cools in NO/O_2 the CN increases from 4 to 6. There is a rearrangement in neighbours of titanium. Maybe there is more water in the samples which disappears during the heating in propene, and when it cools down it absorbs more water. Or something completely different happens, it is not good to know. From my knowledge, no insitu studies have occurred on TAPO-5 or TAPSO-5. It can also be said that a partial reduction and re-oxidation happens for the oxidation state. The edge moves sligthly in energy to the left (reduces) when heated and goes back again when cooled down (re-oxidises).

3.9 EXAFS analyses

Analysis of the samples and models were done in *EXCURV98*. Some difficulty occurred during the analyses of the EXAFS data, most of the problem happened with the AFAC.

3.9.1 Difficulties with the AFAC

AFAC is the amplitude reduction factor ($S_i(k)$) from the EXAFS equation. It is important to have a correct AFAC in the EXAFS analyses. To obtain a correct AFAC will say to refine a model with known multiplicity, and then transfer it to the sample which is analysed. Then the sample has a correct AFAC and the process of further refinements with multiplicity (N), Debye-Waller ($2\sigma^2$), radial distances (R) and E_F can continue.

Some troubles occurred with the AFAC during the EXAFS analyses. For titanium, the refinements of the models give a better fit with a low AFAC, between 0.4-0.6 [61]. Most papers that write about XAS analyses of titanium do not give any information about the AFAC. The AFAC was refined for each model, and the two models used were anatase and rutile, where the AFAC for anatase originally was used. The problem came when the AFAC for anatase was transferred to the different samples in *EXCURV98*. The multiplicity for the samples went haywire, they wanted to be N= 20 or more for each shell. When the AFAC was set to 1 the multiplicities behaved. So the way to resolve this problem was to either fix the AFAC to 1, or fix the different multiplicities for the different shells.

The solution used in this thesis was to fix the AFAC to 1 for both the models and samples. Different k-weighting were used to see which gave the best fit, the k-weighting varied between k^2 and k^3. To give the best optimal fit number of shells varied for different samples to see what was best for that sample.With search in literature most articles do not include AFAC for the refinements of titanium samples. This is probably because of the problem with the AFAC.

3.9.2 EXCURVE

The chi and the FT curve of anatase are shown in Figure 62 and the values of distances and multiplicity of anatase is given in table 12 below.

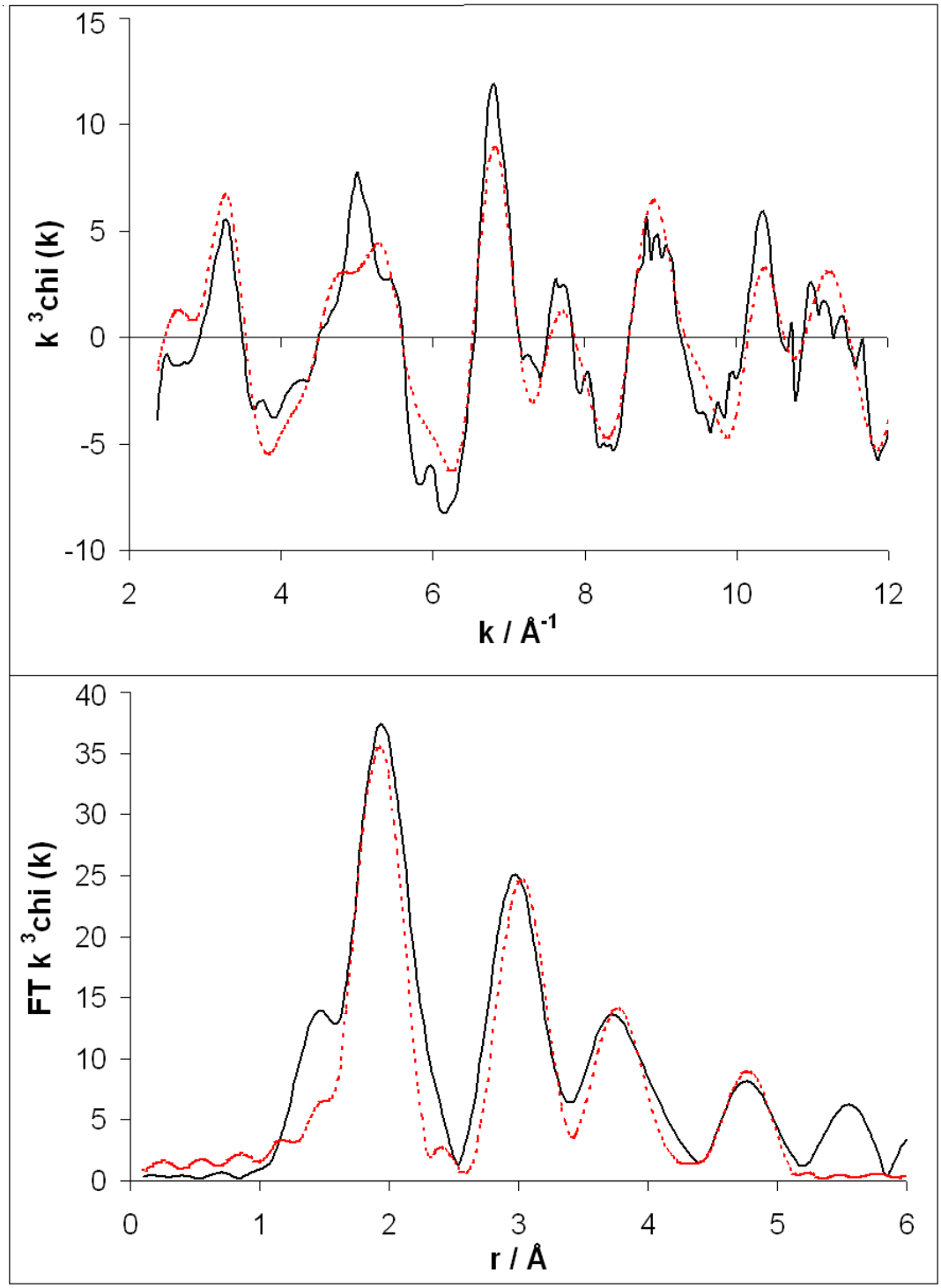

Figure 62: *Anatase model, the k^3 weighted chi curve and the Fourier Transform curve. Where the experimental (-) and theoretical (---) is shown, and where the afac is 0.4746*

Table 12: *The refined AFAC value and fixed AFAC value for Anatase, [a]The fixed multiplicities and crystallographic distances are taken from an article written of A.Weibel, R. Bouchet et.al [62]. [b]These shells are impossible to separate so therefore the multiplicity is added together*

Sample (Anatase) TiO_2	shell	N XRD[a]	RD (Å) XRD[a]	N EXAFS	RD (Å)	Debye-waller $2\sigma^2$ ($Å^2$)	R (%)	E_F
AFAC	Ti-O	4	1.934	6[b]	1.956(7)	0.006(1)	44.94	1.5(7)
= 0.4746	Ti-O	2	1.979	-	-	-		
	Ti…Ti	4	3.039	4	3.043(8)	0.006(2)		
	Ti…Ti	4	3.785	4	3.85(2)	0.001(5)		
	Ti…O	8	3.856	8	3.93(2)	0.001[c]		
	Ti…O	8	4.250	16[b]	4.77(2)	0.008(5)		
	Ti…O	8	4.271	-	-	-		
AFAC	Ti-O	4	1.934	6[b]	1.97(1)	0.023(3)	62.99	1.4(9)
= 1	Ti-O	2	1.979	-	-	-		
	Ti…Ti	4	3.039	4	3.05(1)	0.016(3)		
	Ti…Ti	4	3.785	4	3.85(2)	0.009(5)		
	Ti…O	8	3.856	8	3.94(2)	0.004(5)		

Table 12 displays the parameters from the least squares EXAFS analysis fore one model compound used for analysis of the Ti K-edge data. The EXAFS refinements give information about multiplicity (N). Bonding distances (R) and thermal vibration (Debye Waller factor $2\sigma^2$) as mentioned previously. The E_F is the refined correction of Fermi energy in vacuum the standard deviation for samples and models is calculated I *EXCURV98*.

The AFAC was refined for the models, and for anatase it became 0.4746 and for rutile it became 0.5331. The models had a better fit with a low afac, but the TAPO-5's and the TAPSO-5 needed a higher afac to get a decent fit. The models with the refined afac are displayed in Figure 62 and 64, and the fixed afac is shown in Figure 63 and 65. This comparison shows that it really should be a lower afac for anatase and rutile. For anatase the

fit is 44.94 % for the refined afac, and for the fixed afac value the fit is 62.99 %. The rutile model had a 49.97 % and 68.25 % fit for refined and fixed afac respectively.

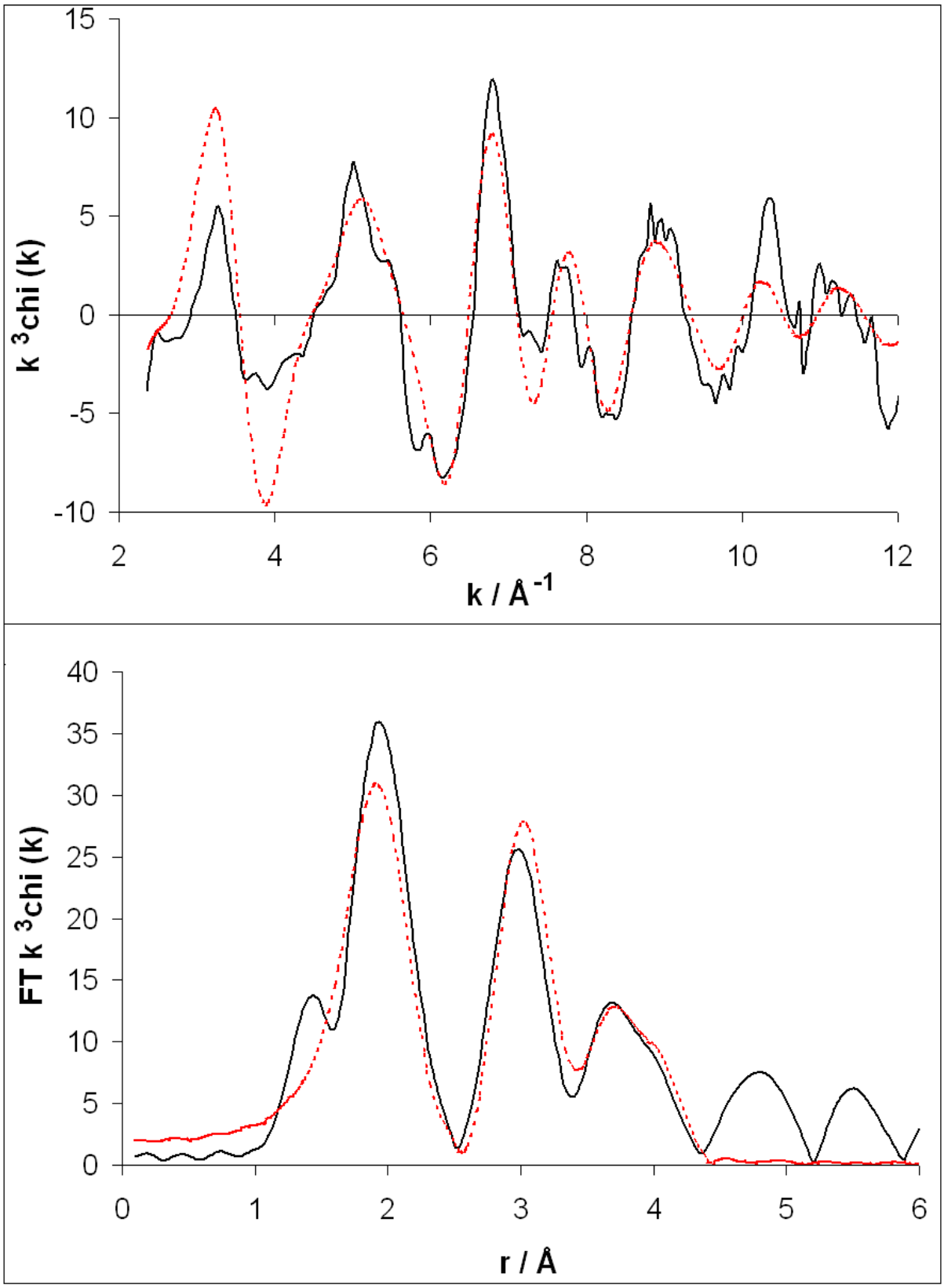

Figure 63: *Anatase model, the k^3 weighted chi curve and the Fourier Transform curve. The experimental (-) and theoretical (---), where the afac is 1.00*

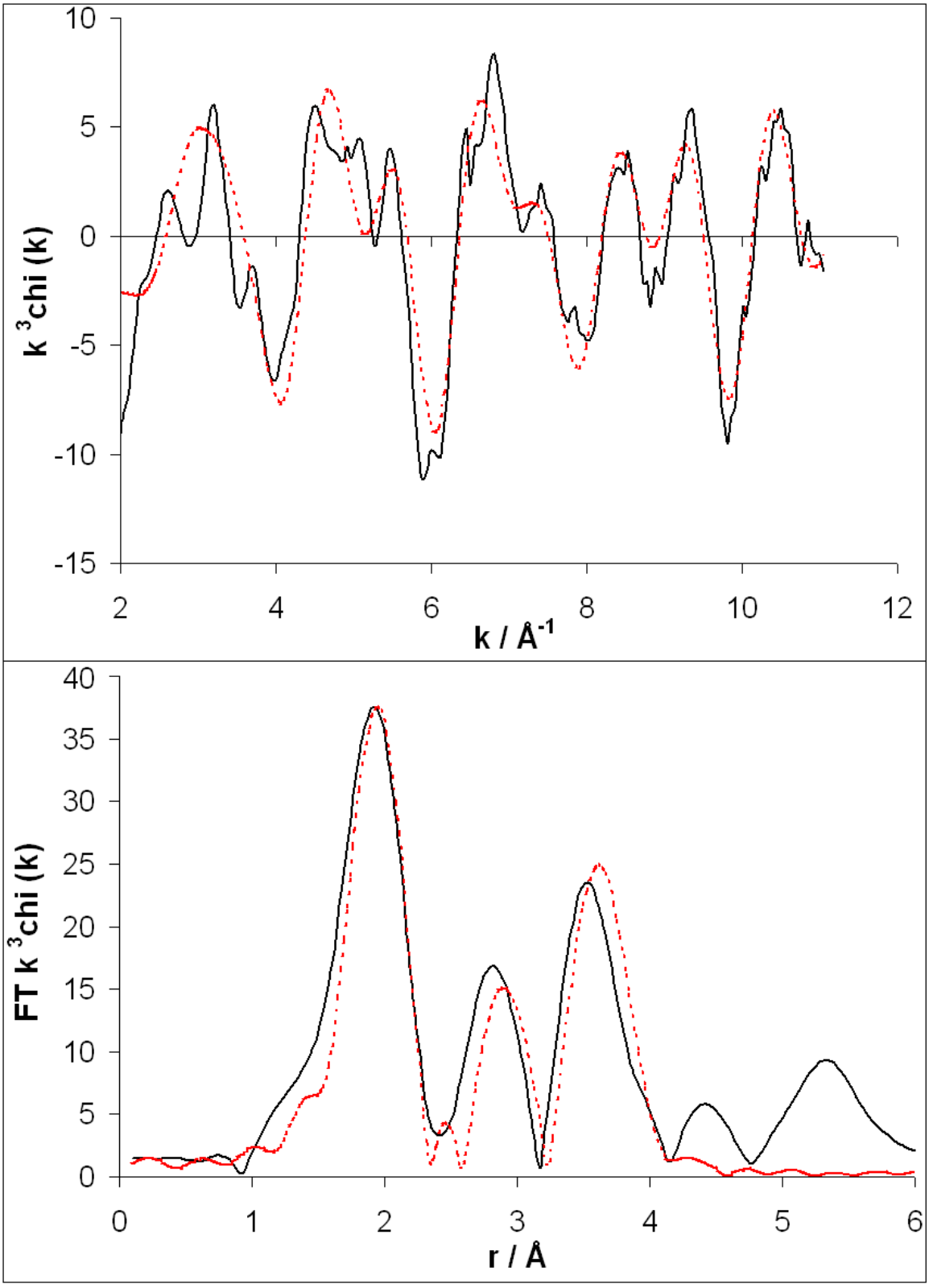

Figure 64: *Rutile model, the k^3 weighted chi curve and the Fourier Transform curve. The experimental (-) and the theoretical (--) is shown, where the afac is 0.5331*

The chi curve and the Fourier transform of the rutile model with afac 0.5331 is given in Figure 64, and the multiplicity and bond lengths of rutile is given in table 13, for both the refined afac and for the fixed afac.

Table 13: *The refined AFAC value and fixed AFAC valur for Rutile [a]The fixed multiplicities and crystallographic distances are taken from an article written of D.M Pickup et.al [63].*

Sample (Rutile) TiO_2	Shell	N XRD[a]	RD (Å) XRD[a]	N EXAFS	RD (Å)	Debye-Waller $2\sigma^2$ ($Å^2$)	R (%)	E_F
AFAC	Ti-O	6	~1.959	6	1.98(1)	0.006(2)	49.97	-2(1)
= 0.5331	Ti…Ti	2	~2.959	2	2.98(2)	0.006(5)		
	Ti…Ti	8	~3.569	8	3.61(1)	0.010(3)		
AFAC	Ti-O	6	~1.959	6	1.98(2)	0.039(6)	68.25	2(1)
= 1.00	Ti…Ti	2	~2.959	2	2.98(2)	0.016(5)		
	Ti…Ti	8	~3.569	8	3.59(1)	0.01(3)		

From this table 13 it can be seen the difference both in R-fit has increased from the refined AFAC from nearly 50% to 70% fit, when the afac was fixed to 1. The rutile model with the fixed afac is given in figure 65.

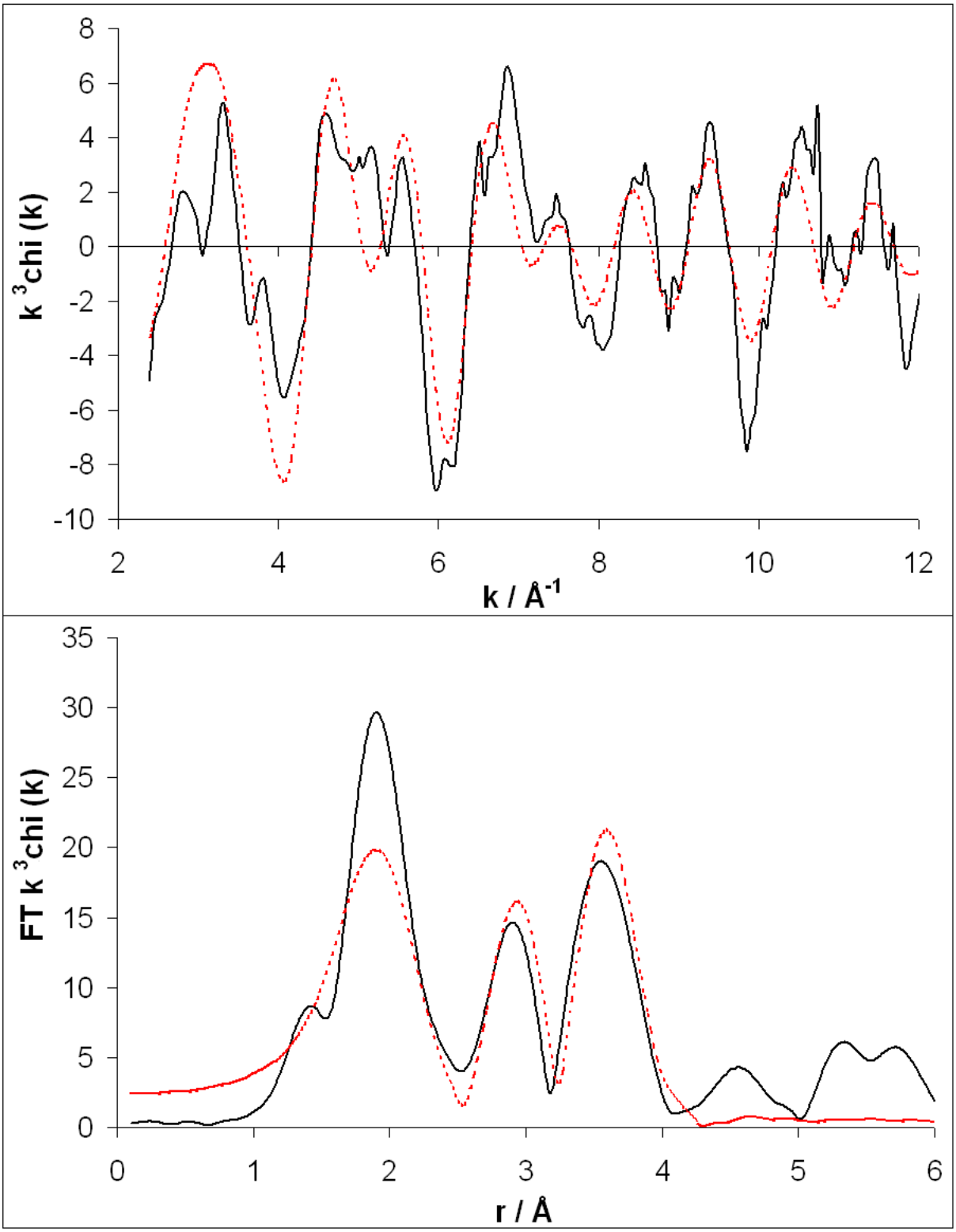

Figure 65: *Rutile model, the k^3 weighted chi curve and the Fourier Transform curve. The experimental (-) and the theoretical (--), where the afac is fixed to 1.00*

Table 14: *Bond lengths and multiplicity all the samples; TAPO-5/1, TAPO-5/2 and TAPSO-5/1, both calcined and as-synthesised. The AFAC is fixed to 1.00 for all of them.* [a] *is* k^2 *weighting and* [b] *is* k^3 *weighting*

Sample		Shell	RD (Å)	N (EXAFS)	Debye-Waller $2\sigma^2$ (Å^2)	R %	E_F
TAPO-5/1	As-synth[a]	Ti-O	1.97(2)	6(1)	0.001(5)	63.86	-2(1)
		Ti…Al	2.85(4)	3(1)	0.001(1)		
	Calcined[a]	Ti-O	1.99(1)	5.4(8)	0.001 (4)	53,49	-3.0(9)
		Ti…Al	2.86(3)	4(2)	0.003 (10)		
		Ti…P	3.69(2)	6(2)	0.0010 (8)		
TAPO-5/2	As-synth[b]	Ti-O	2.02(2)	5(1)	0.019(9)	60.78	-2(1)
	Calcined[a]	Ti-O	2.03(1)	3.1(3)	0.013(3)	32.86	-5.3(5)
		Ti…Al	2.92(2)	1.0(4)	0.003(9)		
TAPSO-5/1	As-synth[b]	Ti-O	2.01(1)	3.9(7)	0.009(5)	49.54	-5(1)
		Ti…Al	2.87(2)	1.4(4)	0.0010(9)		
	Calcined[b]	Ti-O	1.99(1)	3.5(7)	0.007(5)	49.96	-4(1)
		Ti…Al	2.87(2)	1.5(5)	0.0010(1)		

Table 14 shows the bond lengths and multiplicity for the samples. The AFAC was set to 1 since the fit were better for the samples, but this can lead to uncertainties in the multiplicity, bond lengths and the Debye-Waller factor. The weighting was also altered for some samples to k^2 and not k^3 to also get a better fit. From the previous XANES analyses it is shown that the coordination number is 6 for the samples. From the EXAFS analyses that are shown in Table 14 can it be seen that the Ti-O shell for the calcined TAPO-5/2 and for TAPSO-5/1 as-synthesised and calcined the multiplicity is around 3-4. The data differs from one another, this are not good. An explanation for the difference in multiplicity can be that under the oxygen peak there is two oxygen shells and not only one. The peak is very broad and it is a possibility that only one shell was fitted. For anatase the oxygen shell is two shells with coordination number 2 and 4, so this can happen here as well. From the XANES analyses it is shown from

the plot of intensity and energy that the samples are 6-coordinated. It is very difficult to fit two shells under the same peak so therefore in these analyses it is assumed there are two oxygen shells under the same peak, since from XANES analyses the coordination is 6.

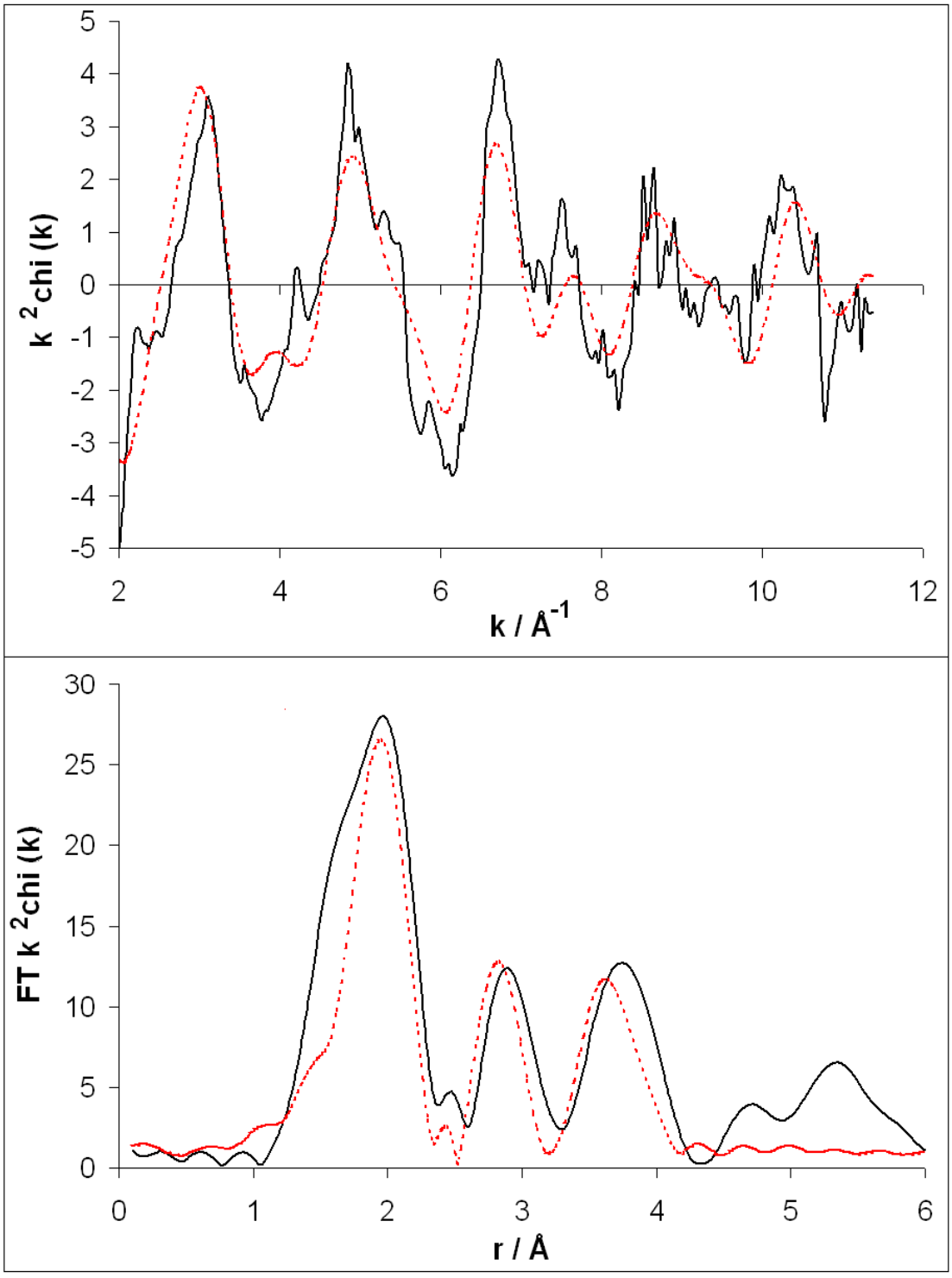

Figure 66: *Calcined TAPO-5/1. The k^2 weighted chi curve and the Foruier Transform curve. The experimental (-) and theoretical (--), afac is fixed to 1.00*

The k^2 weighted chi curve and the Fourier transformed of the calcined TAPO-5/1 sample is shown in Figure 66, the afac was set to 1, which lead to a better multiplicity than for k^3 weighting and a low afac (0.4746). The multiplicity and bond lengths of the TAPO-5/1 calcined and as-synthesised is given in table 14. From Fourier filtration it was determined that the calcined in Figure 66 and as-synthesised in Figure 67 had aluminium as the second shell and the phosphorus as the third shell. Because of bad fit, the third shell was not refined for the *EXCURV98* analysis.

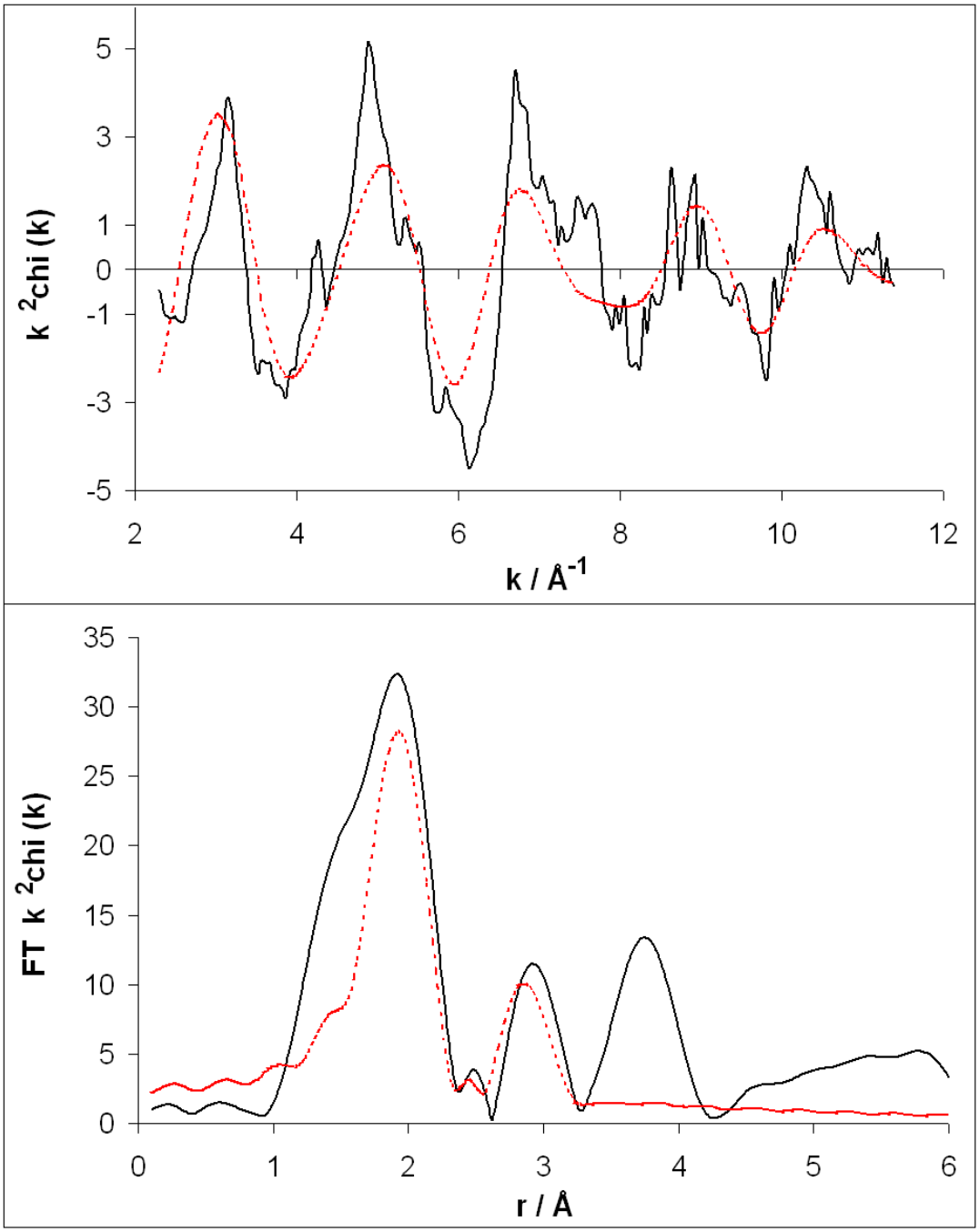

Figure 67: *k^2 weighted chi and Fourier Transformed of as-synthesised sample TAPO-5/1, the experimental (-) and theoretical (--). The AFAC is fixed to 1.00*

The k^2 - weighted chi curve and the Fourier transformed of the calcined sample TAPO-5/2 is shown in Figure 68, it was also done Fourier filtration on this sample. From that result the best fit for the second shell was aluminium and for the third shell was phosphorus. The calcined TAPO-5/2 sample had a best fit with k^2-weighting and two shells, the parameters are shown in table 14 above.

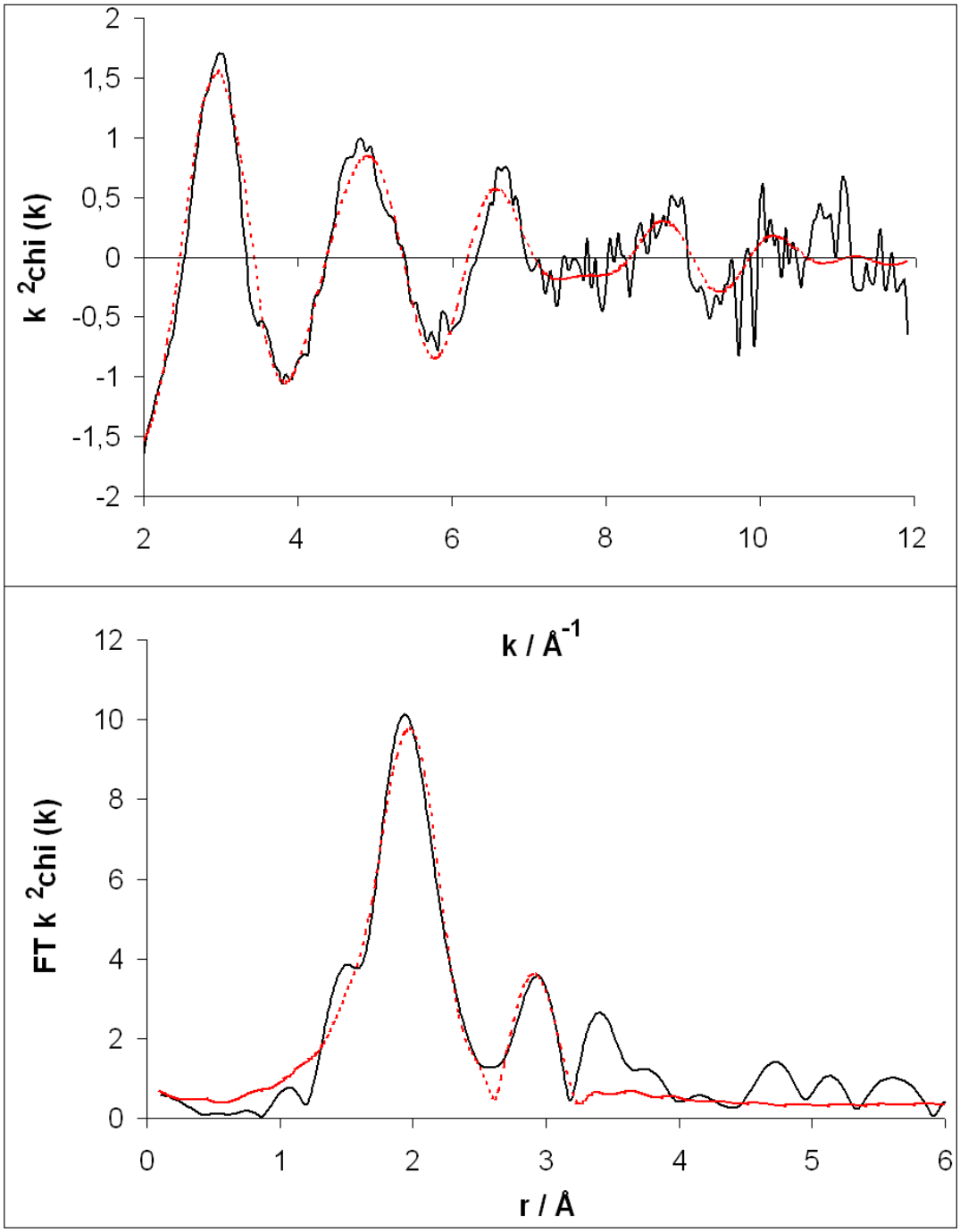

Figure 68: *k^2 weighted chi and Fourier Transformed of calcined sample TAPO-5/2, the experimental (-) and theoretical (--). The AFAC is fixed to 1.00*

The as-synthesised TAPO-5/2 is shown in Figure 69; this sample obtained a better fit with k^3 weighting and one shell. The multiplicity didn't want to cooperate if it was more than one shell. The parameters and values are shown in table 14. It did not have the best fit; this is also probably for the huge glitches as seen in the figure below. In fear to remove too much information in *k*-space it needed to be like this, it was truncated and deglitched carefully.

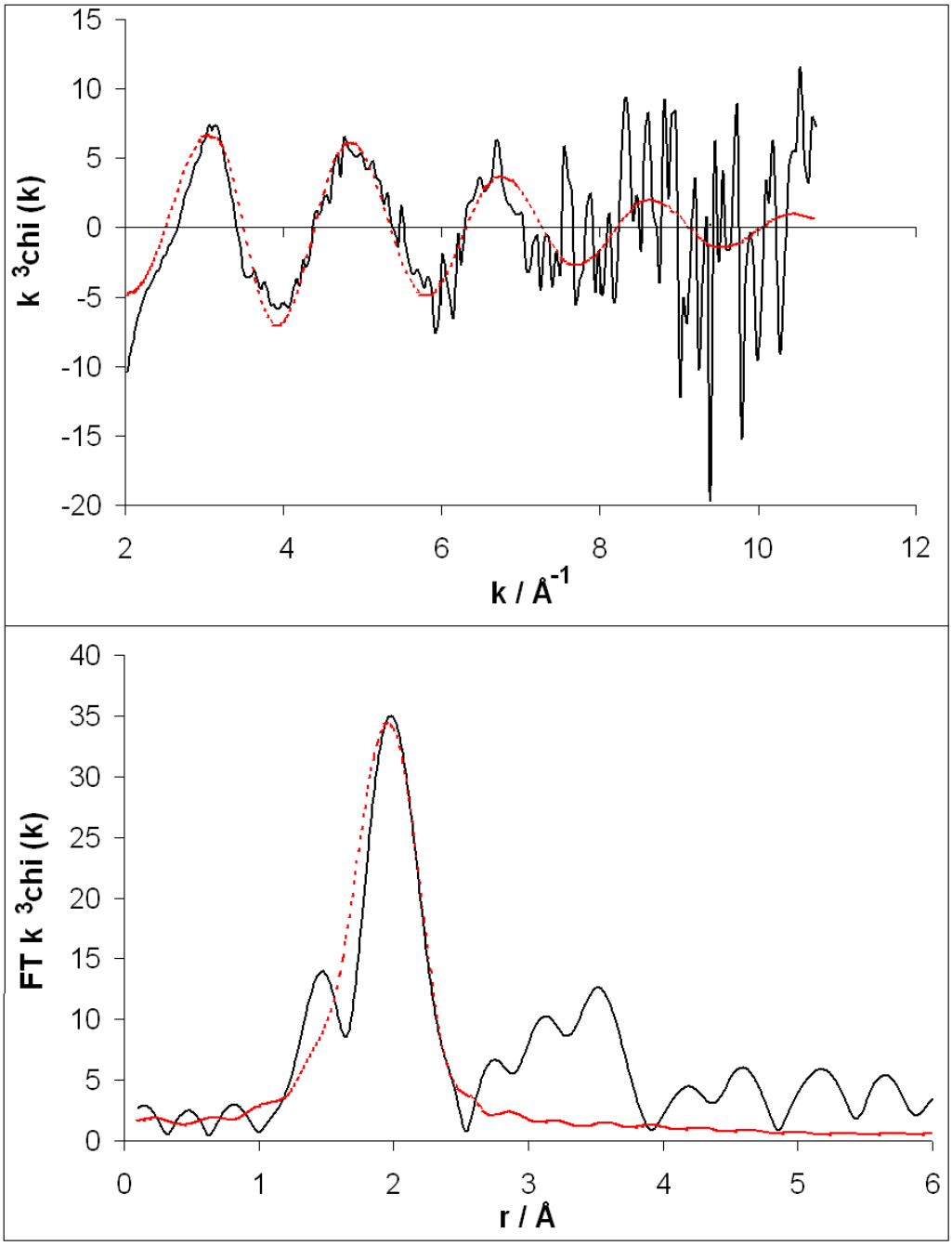

Figure 69: *k^3 weighted chi and Fourier Transformed of as-synthesised sample TAPO-5/2, the experimental (-) and theoretical (--). The AFAC is fixed to 1.00*

The calcined and as-synthesised sample of TAPSO-5/1 is shown in Figure 70 and 71 respectively. The calcined TAPSO-5/1 had the best fit with k^3-weighting, and from Fourier

filtration it showed that the second shell was aluminium and the third shell was most likely to be phosphorus. The parameters for the as-synthesised and calcined TAPSO-5/1 is shown in table 12 above.

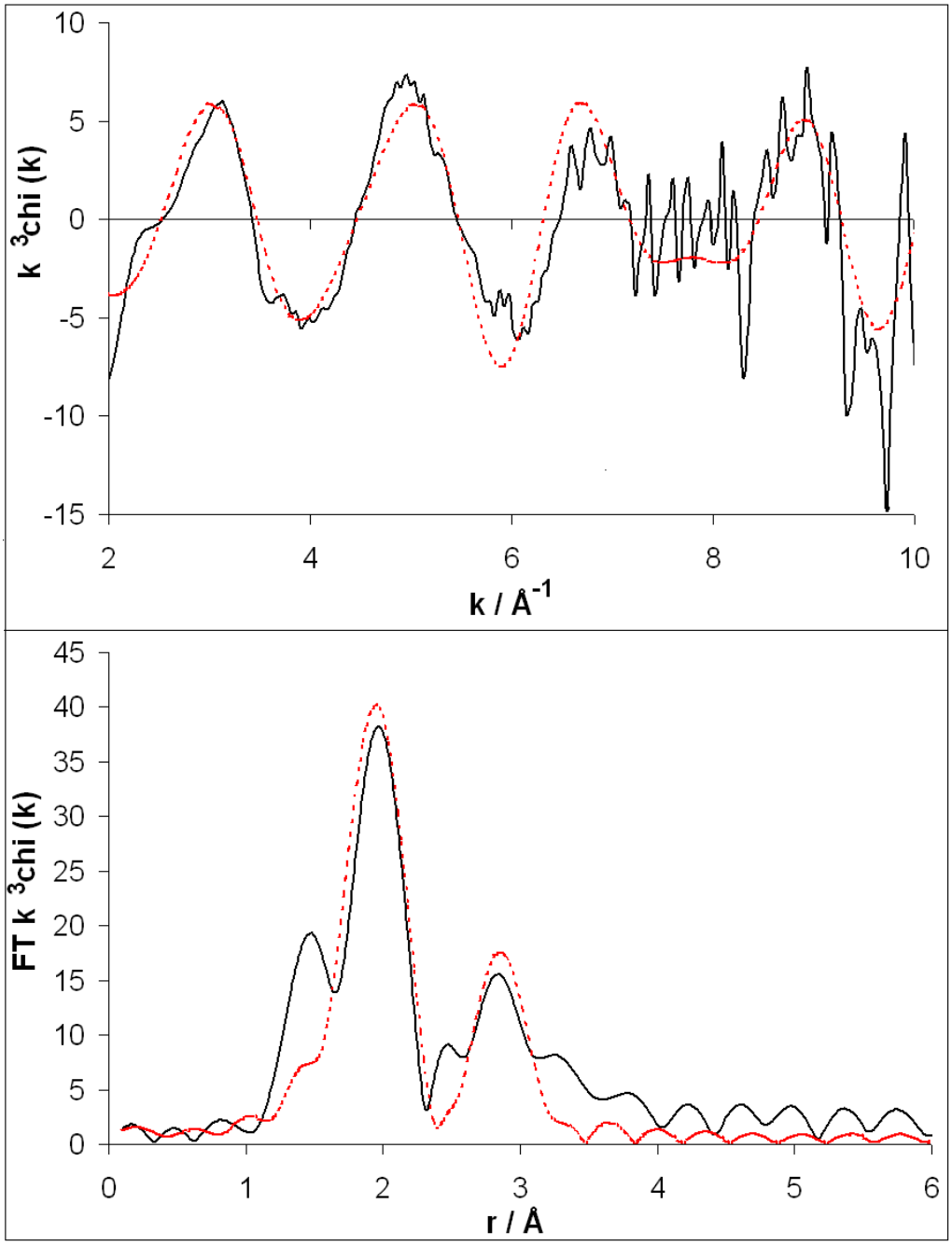

Figure 70: *k^3 weighted chi and Fourier Transformed of calcined sample TAPSO-5/1, the experimental (-) and theoretical (--). The AFAC is fixed to 1.00*

The k^3 weighted chi curve and FT curve of the as-synthesised TAPSO-5/1 had the best fit with k^3 weighting and two shells. From Fourier filtration the third shell would most likely been phosphorus.

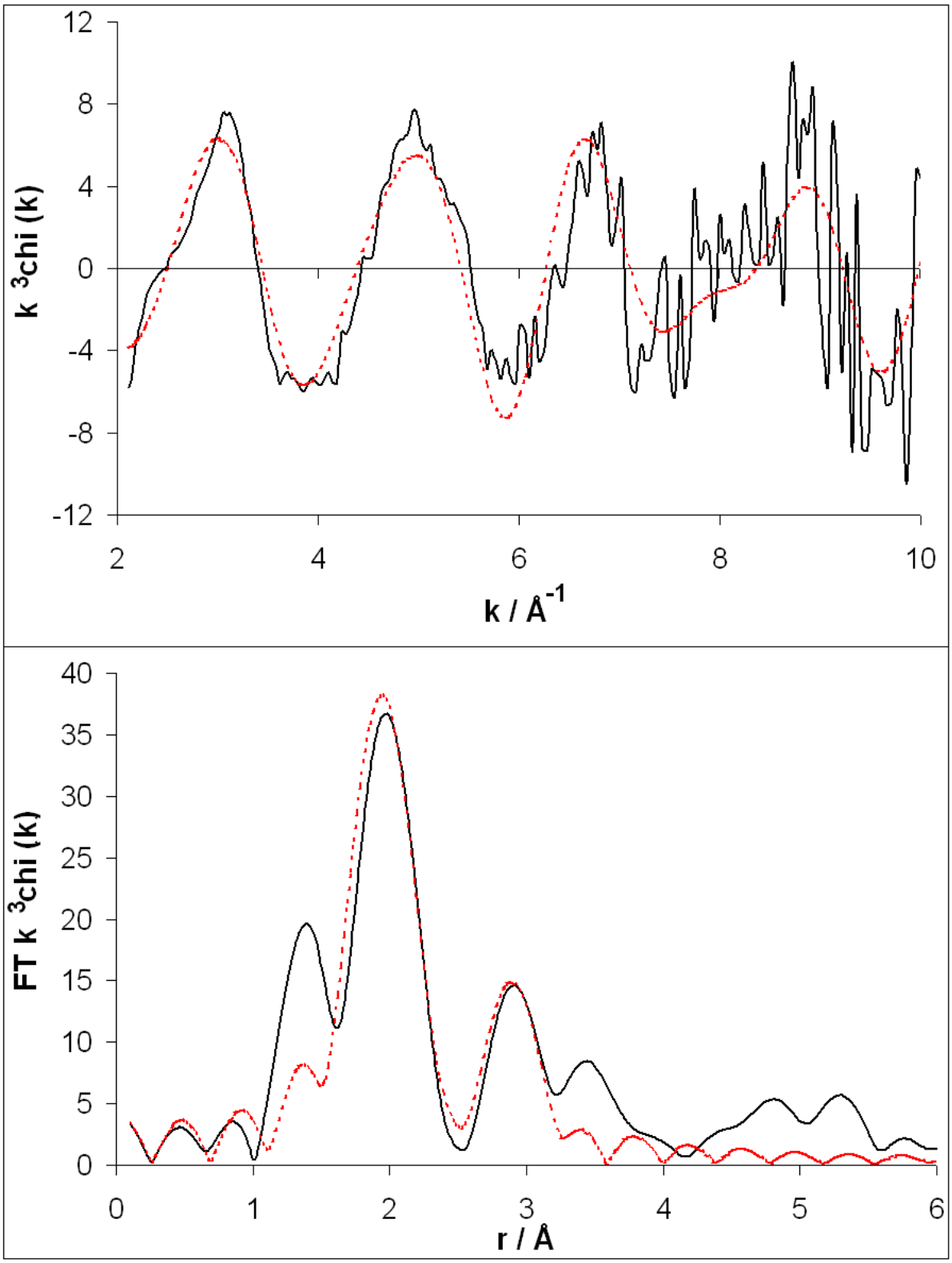

Figure 71: *k^3 weighted chi and Fourier Transformed of as-synthesised sample TAPSO-5/1, the experimental (-) and theoretical (--). The AFAC is fixed to 1.00*

3.9.3 Fourier Filtering of the different TAPO-5 and TAPSO-5

Fourier filtering were done on the samples of the as-synthesised and calcined TAPO-5/1, TAPO-5/2 and TAPSO-5/1 during the EXAFS analyses in *EXCURV98*. The figures of only the as-synthesised samples are shown in this thesis. Fourier filtering was done to give an indication of which element belonged to which peak in the FT-spectra. The fit for each shell tried for different element is shown in different tables below. The filtering method was also used to see where the titanium metal would be incorporated in the framework. A suggestion of where titanium would place itself is shown in section 2.1. According to the Löwenstein rule it has to be alternating Al-O-P bonds and not Al-O-Al.

TAPO-5/1

Figure 72 and 73 below shows the Fourier filtering of the two different peaks after the huge oxygen peak in the FT-spectra. The R min and R max are a bit displaced from the FT spectra and the Fourier filtering, but the peaks were still filtered. Table 15 shows the best fit for each element tried fitted for the different peaks on the as-synthesised and calcined sample.

It can be seen for the as-synthesised that the best fit for the shell after the oxygen peak is phosphorus with 25.9% fit and aluminium with 29.5% fit. It is same for the calcined sample with a fit of 12.21% for phosphorus and 12.78% for aluminium. This can then indicate that the titanium replaces the aluminium, but when this filtering was transferred to the samples aluminium gave the better overall fit for the shell after Ti-O. So from that result it can be concluded that most likely titanium substitute phosphorus in the $AlPO_4$-5 structure. The whole refinements for calcined and as-synthesised TAPO-5/1 with the FT-spectrum are shown in Fig. 66 and 67 respectively.

Table 15: *Best fit factor for the refined shells of TAPO-5/1 as-synthesised and calcined*

Sample	Shells	Δ R 2.21-3 Å	Δ R 3-4 Å
TAPO-5/1 as-synthesised		R-Fit (%)	R-Fit (%)
	Aluminium	29.5	29.5
	Phosphorus	25.9	25.9
	Titanium	33.3	33.3
	Oxygen	43.5	43.5
Sample	Shells	Δ R 2.21-3.1Å	Δ R 3-4 Å
TAPO-5/1 calcined		R-Fit (%)	R-Fit (%)
	Aluminium	12.78	46.64
	Phosphorus	12.21	39.54
	Titanium	35.46	19.08
	Oxygen	33.90	56.66

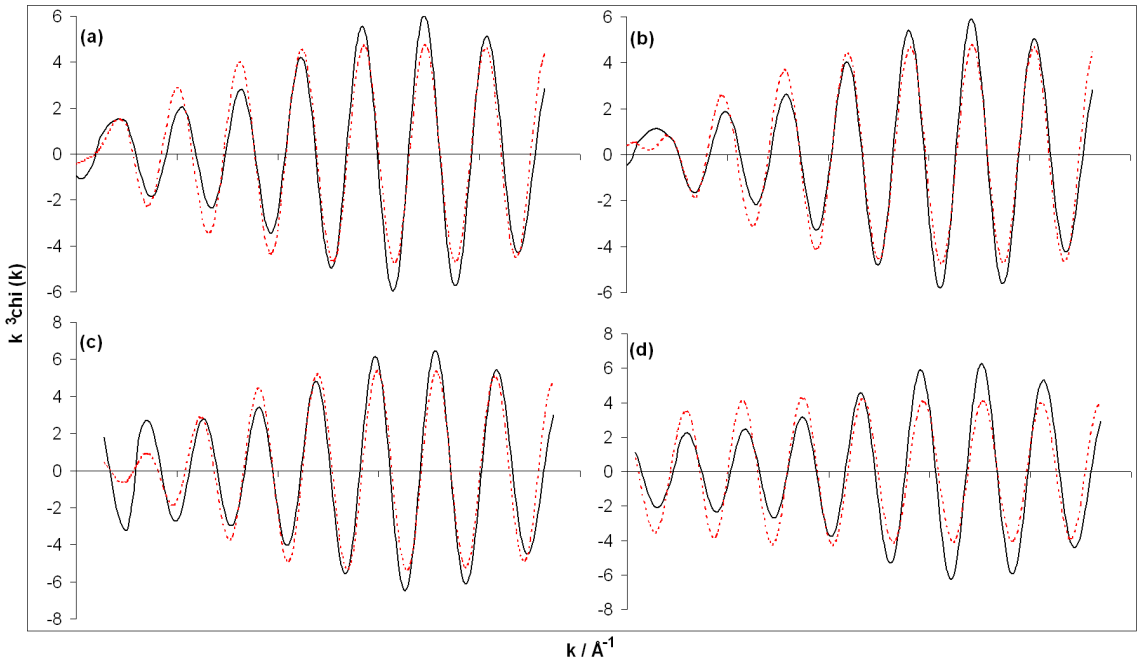

Figure 72: *The refined Fourier filtration of TAPO-5/1 as-synthesised, k^3 weighted peak 2. (a) is aluminium, (b) is phosphorus, (c) is titanium and (d) is oxygen, with the experimental (-), and theoretical (--). The k-space ($Å^{-1}$) was from 2-12 $Å^{-1}$, the FF boundaries was r min 2.21Å and r max 3.0 Å and an afac of 1.*

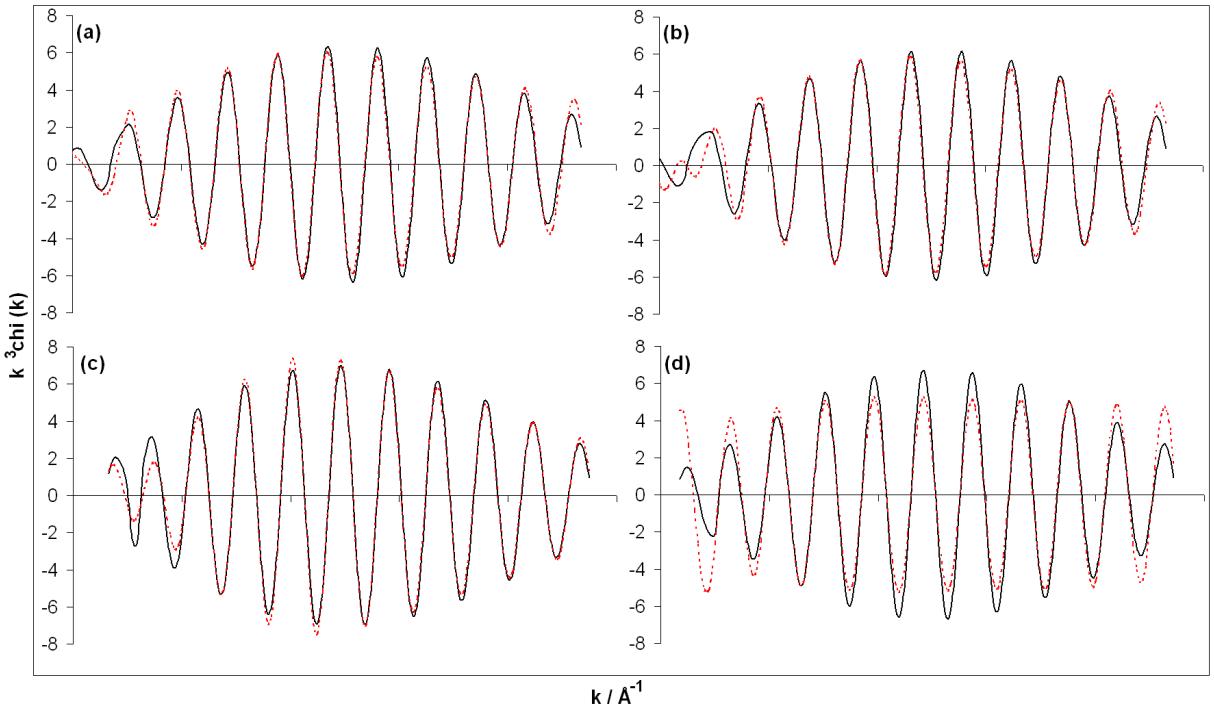

Figure 73: *The refined Fourier filtration of TAPO-5/1 as-synthesised, k^3 weighted peak 3. (a) is aluminium, (b) is phosphorus, (c) is titanium and (d) is oxygen, with the experimental (-), and theoretical (--). The k-space ($Å^{-1}$) was from 2-12 Å-1, the FF boundaries was r min 3.0Å and r max 4.0 Å and an afac of 1.*

TAPO-5/2

Figure 74 and 75 shows the Fourier filtering of the as-synthesised sample of TAPO-5/2 of the two shells after the Ti-O shell. The best fit for the different element tried is shown in table 16. It can be seen from that table the as-synthesised sample prefers phosphorus slightly over aluminium with 14.3% and 14.9% respectively. For the calcined the shell after Ti-O prefers aluminium over phosphorus. When the whole sample was refined with the different shells in *EXCURV98* aluminium was the preferred element. This indicates that titanium also has substituted phosphorus in the incorporation of the framework. This can be seen in Fig. 68 and 69 which shows the whole EXAFS refinements for the whole sample, as-synthesised and calcined.

Table 16: *best fit factor for the Fourier filtering of TAPO-5/2 as-synthesised and calcined*

Sample	Shells	Δ R 2.6-3.1 Å	Δ R 3.1-3.7 Å
TAPO-5/2 as-synthesised		R-Fit (%)	R-Fit (%)
	Aluminium	14.9	29.6
	Phosphorus	14.3	17.2
	Titanium	26.3	21.9
	Oxygen	28.9	26.7
Sample	Shells	Δ R 2.4-2.9 Å	Δ R 2.9-3.4 Å
TAPO-5/2 calcined		R-Fit (%)	R-Fit (%)
	Aluminium	17.65	15.18
	Phosphorus	22.14	17.63
	Titanium	30.08	31.89
	Oxygen	23.32	30.88

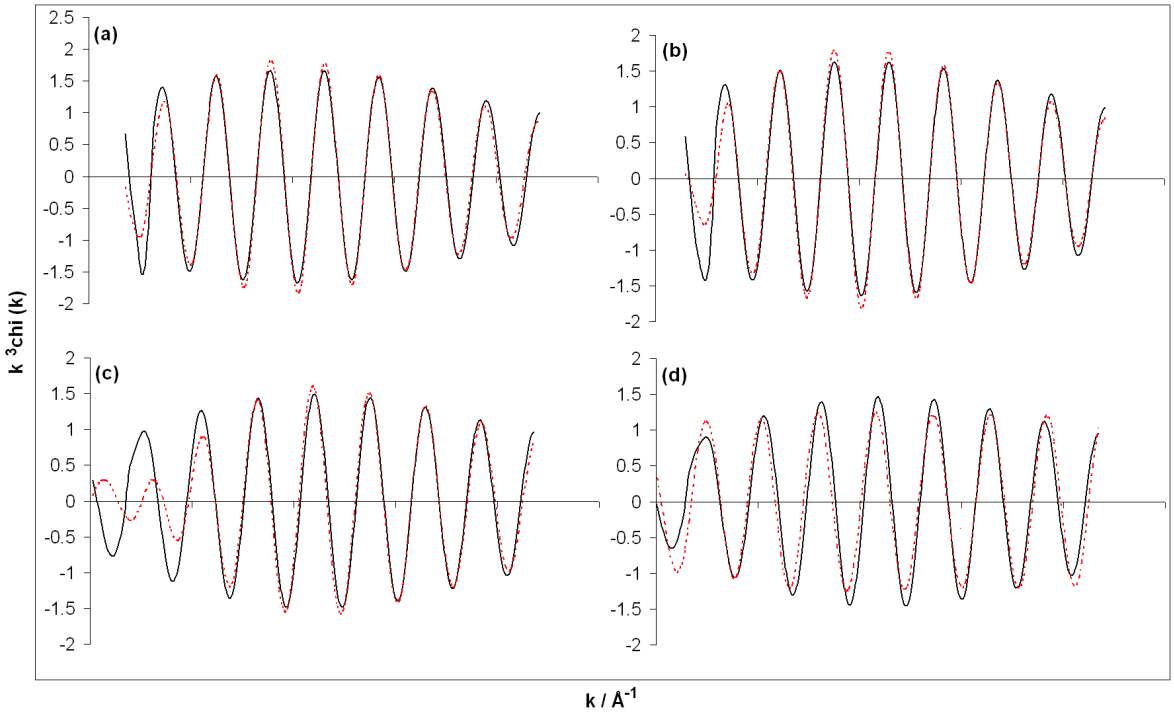

Figure 74: *The refined Fourier filtration of TAPO-5/2 as-synthesised, k^3 weighted peak 2. (a) is aluminium, (b) is phosphorus, (c) is titanium and (d) is oxygen, with the experimental (-), and theoretical (--).The k-space ($Å^{-1}$) was from 2-12 $Å^{-1}$, the FF boundaries was r min 2.6Å and r max 3.1 Å and an afac of 1.*

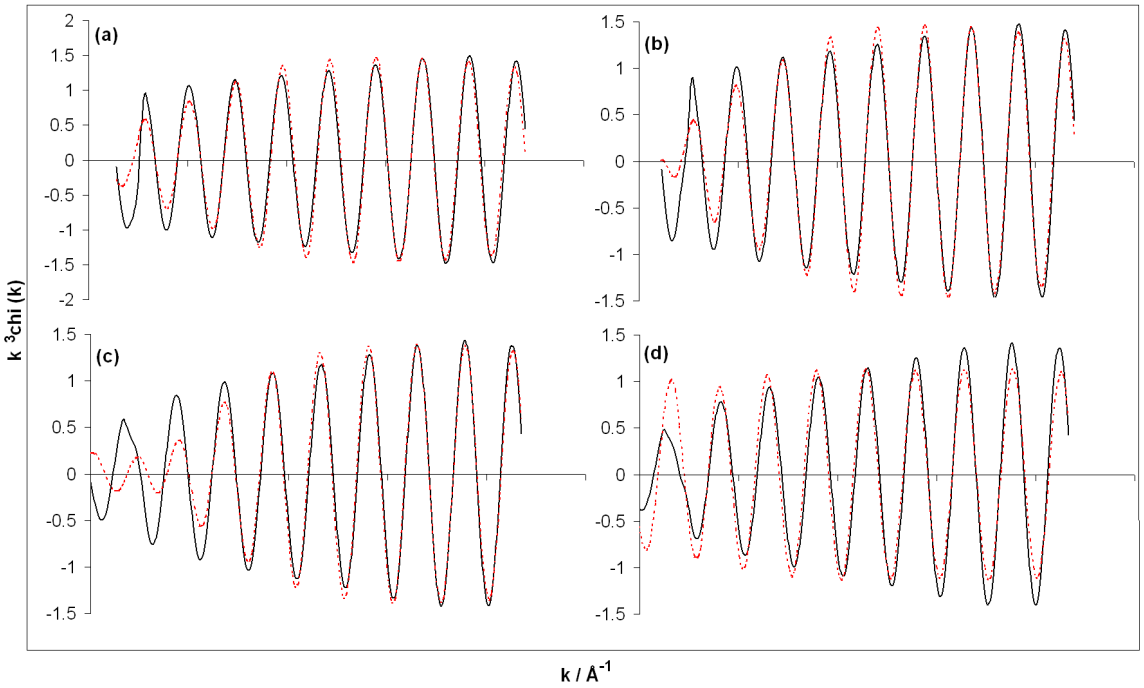

Figure 75: *The refined Fourier filtration of TAPO-5/2 as-synthesised, k^3 weighted peak 3. (a) is aluminium, (b) is phosphorus, (c) is titanium and (d) is oxygen, with the experimental (-), and theoretical (--). The k-space ($Å^{-1}$) was from 2-12 $Å^{-1}$, the FF boundaries was r min 3.1 Å and r max 3.7 Å and an afac of 1.*

TAPSO-5/1

The Fourier filtering data of the calcined and as-synthesised samples are displayed in Table 17 below and the as-synthesised samples are shown in figure 76 and 77. For the shell after Ti-O the as-synthesised sample prefers aluminium and for the calcined it prefers titanium. This is a very interesting result. A reason for this can be that maybe it forms titaniumoxide in the sample, but nothing indicates that this have happened, except for the Fourier filtering. When the whole refinements for the total EXAFS took place aluminium was preferred as the shell after Ti-O. This concludes that titanium substitute's phosphorus in the framework and the second peak in the FT spectra in Fig. 70 and 71 is aluminium.

Table 17: *best fit factor for the Fourier filtration of TAPSO-5/1 as-synthesised and calcined*

Sample	Shells	Δ R 2.3-2.9 Å	Δ R 2.9-3.6 Å
TAPSO-5/1 as-synthesised		R-Fit (%)	R-Fit (%)
	Aluminium	9.7	24.5
	Phosphorus	11.3	17.7
	Titanium	17.1	18
	Silicon	24.3	20.7
Sample	Shells	Δ R 2.4-3 Å	Δ R 2.9-3.5 Å
TAPSO-5/1 calcined		R-Fit (%)	R-Fit (%)
	Aluminium	23.24	19.1
	Phosphorus	17.52	13.12
	Titanium	10.04	16.32
	Silicon	20.59	15.56

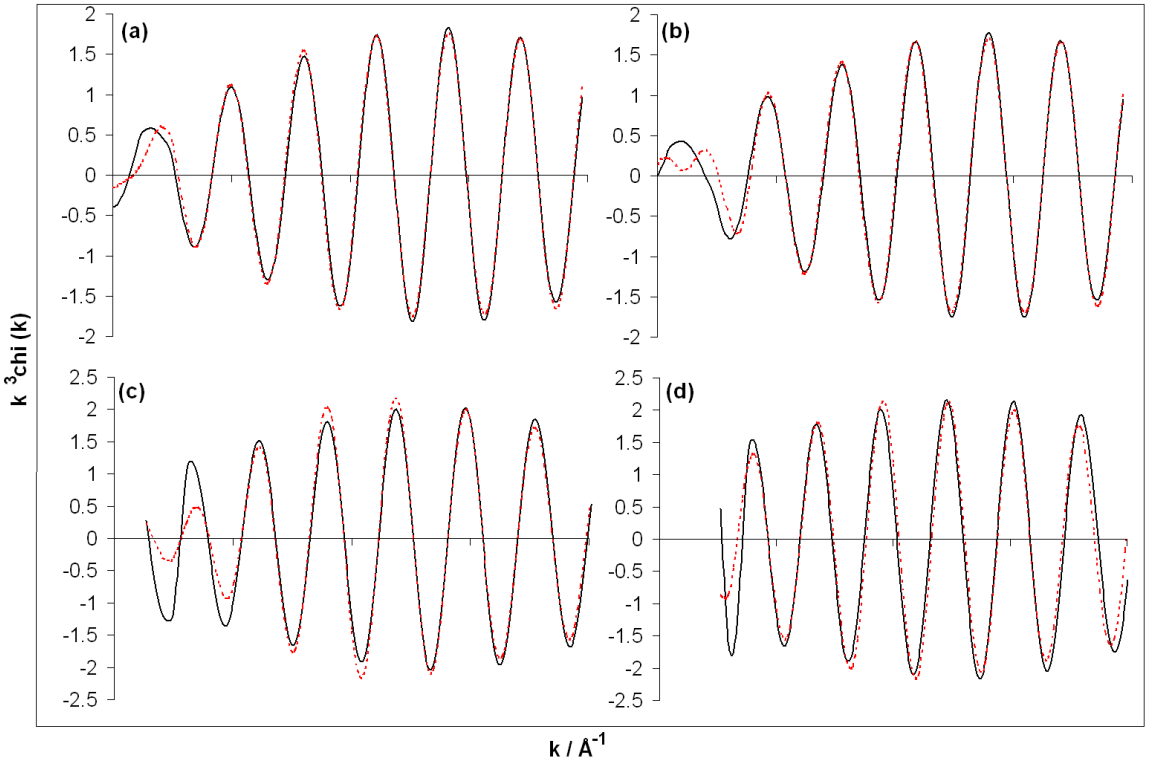

Figure 76: *The refined Fourier filtration of TAPSO-5/1 as-synthesised, k^3 weighted peak 2. (a) is aluminium, (b) is phosphorus, (c) is titanium and (d) is silicon. The k $Å^{-1}$ was from 2-10 $Å^{-1}$, with the experimental (-), and theoretical (--). The FF boundaries was r min 2.3 Å and r max 2.9 Å and an afac of 1.*

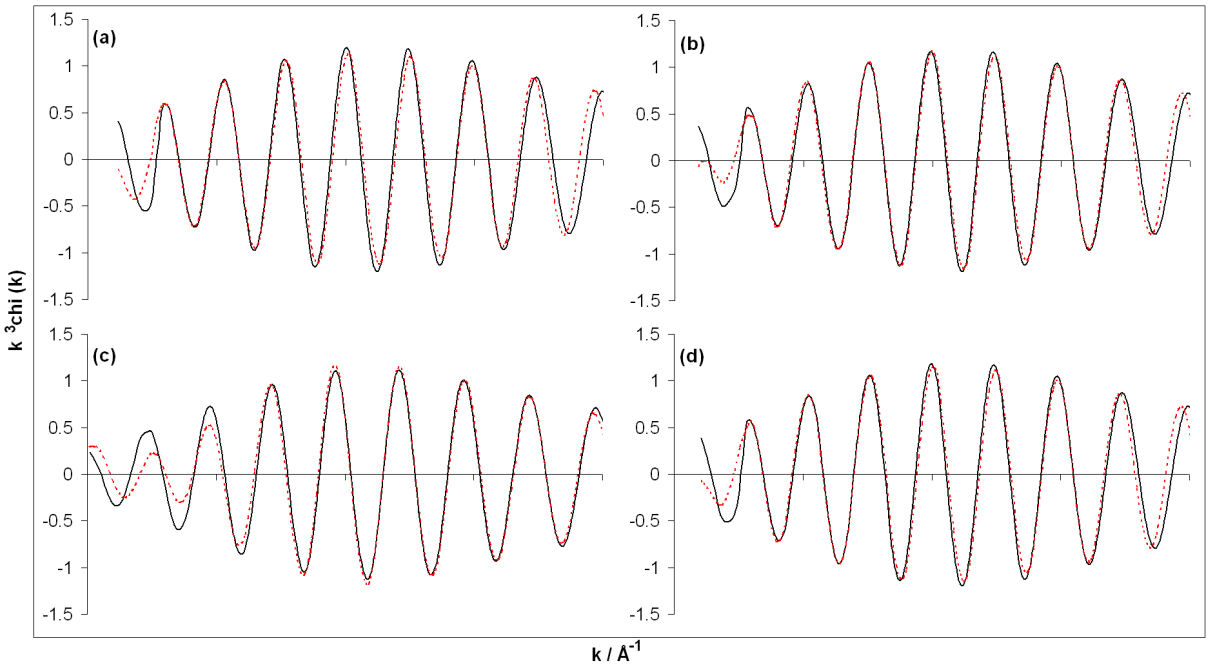

Figure 77: *The refined Fourier filtration of TAPSO-5/1 as-synthesised, k^3 weighted peak 3. (a) is aluminium, (b) is phosphorus, (c) is titanium and (d) is silicon. The k $Å^{-1}$ was from 2-10 $Å^{-1}$, with the experimental (-), and theoretical (--). The FF boundaries was r min 2.9 Å and r max 3.6 Å and an afac of 1.*

3.10 Temperature Programmed Reduction (TPR)

TPR-data was obtained of different TAPO-5 and TAPSO-5 to see the reducibility of different TAPO-5's and TAPSO-5's in hydrogen.

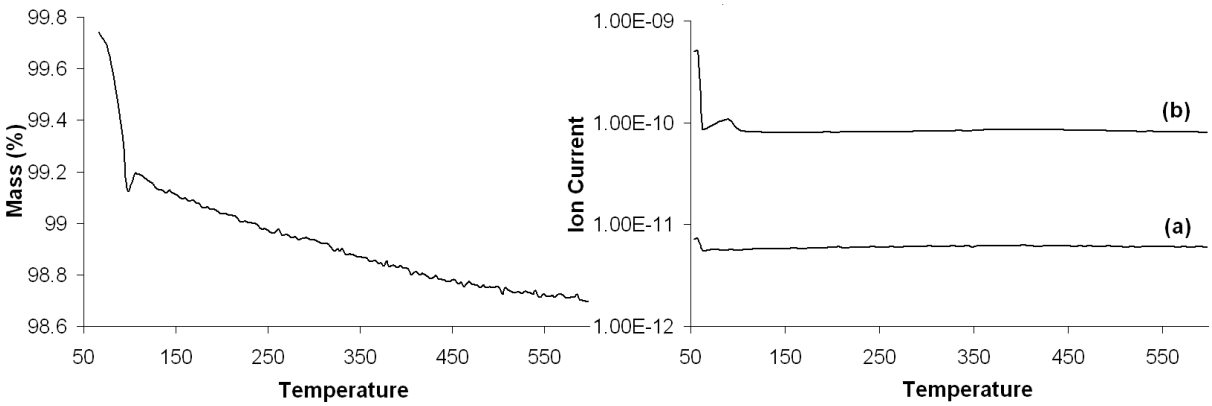

Figure 78: *TPR of TAPO-5/1 with mass-spec where (a) hydrogen (H_2) and (b) is water (H_2O)*

The TPR of TAPO-5/1 is shown in Figure 78. At 100°C water evaporates (b) there is just a straight line on H_2, this gives an indication that no reduction happens when it comes to oxidation state.

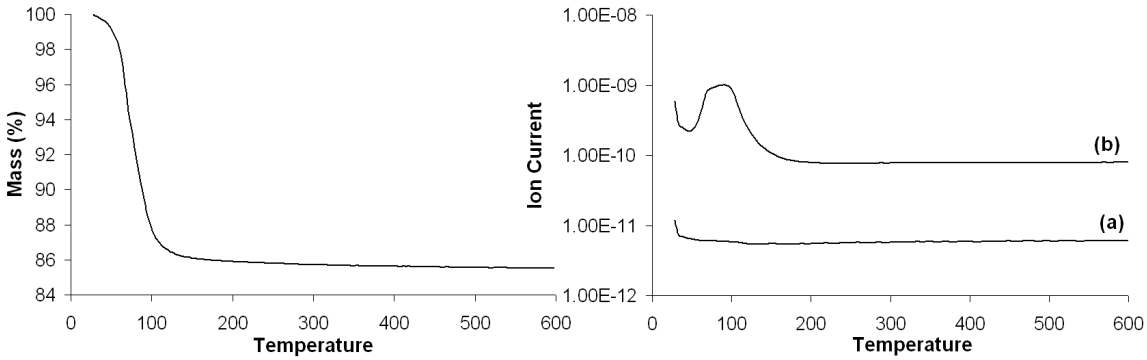

Figure 79: *TPR spectra with mass-spec of TAPSO-5/1 where (a) hydrogen (H_2) and (b) is water (H_2O)*

From Figure 79 it is shown a TPR of TAPSO-5/1. The only change here is at around 100°C which disappears. The ion-current of hydrogen does not show anything at all. This indicates that no reduction happens here; only water disappears and is burned off.

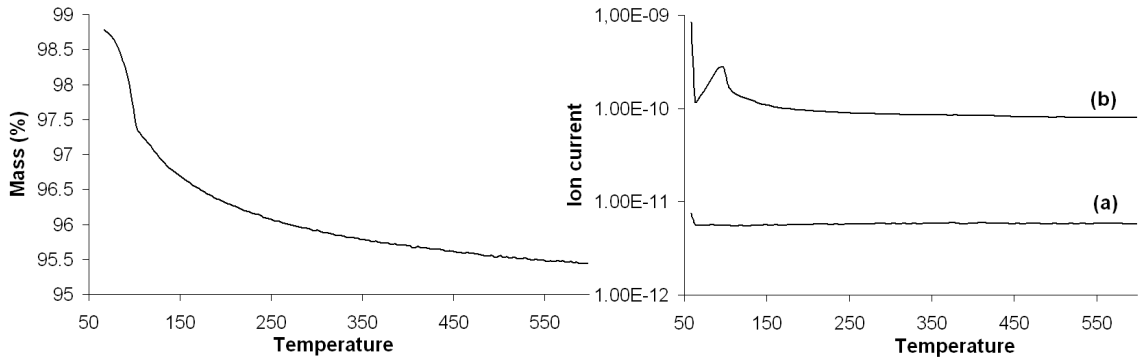

Figure 80: *TPR spectra with mass-spec of TAPO-5 Ti^{3+}, (a) is H_2 and (b) is water*

Figure 80 displays the TPR of TAPO-5 Ti^{3+} with 4 hours of crystallisation time. From this spectrum it can be seen that water disappears at around 100°C and nothing happens with hydrogen as the other TPR's.

From these TPR experiments it can be concluded that there is no reduction in hydrogen. But from the analyses from the insitu's it can be seen that the major change was the coordination number. There were as well some changes in the edge of the XANES so a partial reduction probably occurred in the valence state. But no change happened for the TPR results in hydrogen.

4 Conclusions

- The best template for titanium substituted $AlPO_4$-5 is TEA, since that gave the best X-ray diffractograms with the best crystalline phases. The crystallisation time did not have that much influence, but 4 hours gave just as good crystalline material as a crystallisation time of 48 hours.

- The titanium source had some importance in the syntheses. The two most successful sources were titanium(IV)butoxide and titanium(IV)isopropoxide. These two titanium sources gave very crystalline diffractograms. The Ti^{3+} source gave also a crystalline phase, but since this was not tested with XAS or ICP-MS it can not be certain how much or any titanium was incorporated in the framework.

- TiO_2 as titanium source gave a phase of anatase particles that clogged the pores; this was probably because it did not dissolve properly during the synthesis. A solution could probably be fixed with other parameters for the synthesis such as crystallisation time and template. But this was not further investigated because other and better titanium sources were available, so this titanium source was not used anymore other than the first synthesis.

- The XAS data collection obtained better spectra with fluorescence for the k-edge of titanium than transmission. The synchrotron source at MAX-lab was better at handling the titanium and gave better spectra then at ESRF. This was because the beamline I811 at MAX-lab had the energy range of 2.3 – 20 keV.

- From the XANES and EXAFS analyses it can be concluded that from two of the syntheses (TAPO-5/ and TAPSO-5/1) there were successful incorporation of titanium in the framework of the $AlPO_4$-5.

- From the EXAFS analyses it can be concluded that the TAPO-5/1, TAPO-5/2 and TAPSO-5/2 had a multiplicity of oxygen at around 6, and the next neighbour shell was aluminium.

- The two successful insitu's from MAX-lab showed with XANES analyses what happened during heating in propene/O_2 and cooling in NO/O_2 for TAPO-5/2 and TAPSO-5/1. The

titanium decreased in coordination number from 6 to 4 during heating and increased when it cooled down (from 4 to 6). From the plot it still looked like the valence state was primarily Ti^{4+}.

- There was also a change in the edge energy during the two insitu's. The energy shifted to the left when heated (reduced) and went right (re-oxidised) when it cooled down. From the slight change in the edge energy it can be concluded that there happened a partial reduction and re-oxidation.

- From the TPR experiments obtained the mass-spec data show no reducibility in hydrogen. The only change was water and that disappeared at 100°C as expected.

5 Future Work

- In this thesis the main focus was to see if titanium was incorporated and how the structure behaved during insitu in propene and NO. There was actually a meaning to do catalysis measurements of the samples, but there was no time for that.

- Future work would be to take FT-IR of the samples to investigate if there are any acid sites in the samples. This is smart to do because the samples showed a partial reduction, when looking at the edge of the XANES. This edge moved back and fourth so it is an indication of a partial reduction and re-oxidation.

- There were done syntheses with a trivalent titanium source; both a TAPSO-5 and TAPO-5 were made. The diffractograms of these four syntheses showed a crystalline phase of the AFI structure. It would be very interesting to see if the titanium is incorporated in the framework of the $AlPO_4$-5. This can be done with XAS experiments. It would be interesting to see if the titanium still were trivalent or if it has oxidised to Ti^{4+}. And how this TAPO-5/Ti^{3+} would behave during an insitu if it still was trivalent.

- Catalysis measurements would also be of interest. This is to see if the samples have any catalytic reactivity. The samples had major changes in the insitu's of propene and NO, it would be logic to test the material for reducibility of NO_x.

6 References

[1] Materials research laboratory, University of California, Santa Barbara.
URL adress: http://www.mrl.ucsb.edu/mrl/centralfacilities/xray/xray-basics/index.html
Downloaded: 2008-07-03

[2] Boon K. Teo, "*Exafs: princples and data anlysis"*, Springer-Verlag, (1986)

[3] N. Herron and David R.Corbin, *"Inclusion chemistry with zeolites: Nanoscale materials by design",* Kluwer academic publishers, (1995), ISBN: 0-7923-3606-2

[4] J.Rouqureol et.al, *Pure & applied Chemistry*, vol 66, no.8, p. 1739-1758 (1994)

[5] Alan Dyer, "*An introduction to zeolite molecular sieves"*, John Wiley & sons Ltd, (1988), ISBN: 0-471-91981-0

[6] K.Byrappa, M.Yoshimura, "*Handbook of hydrothermal technology – A technology for crystal growth and material processing"*, Chapter 6; Hydrothermal synthesis and growth of zeolites, William Andrew Publishing / Noyes, (2001)

[7] Stephen T. Wilson, Brent M. Lok, Celeste A. Messina, Thomas R. Cannan and Edith M. Flanigen, "Aluminophopshate molecular sieves: a new class of microporous crystalline inorganic solids", *Journal of American Chemical Society*, vol. 104, no.4, p.1146-1147 (1982)

[8] R.Sozstak, "*Molecular Sieves – principles of synthesis and identification"*, Van Norstrand Reinhold, (1989), ISBN: 0-442-28023-8

[9] Sang-Ok Lee, Robert Raja, Kenneth D.M Harris, John Meurig Thomas, Brian F. G. Johnson and Gopinathan Sankar, "Mechanistic insights into the conversion of cyclohexene to adipic acid by H_2O_2 in the presence of a TAPO-5 catalyst" *Angewandte Chemie International Edition*, vol.42, iss.13, p.1520-1523 (2003)

[10] J.C Bailar, H.J. Emeleus, Sir Ronald Nyholm and A.F Trotman-Dickenson, *Comprehensive Inorganic Chemistry vol. 3*, Pergamon press (1973)

[11] The University of Sheffield, WebElements Ltd, UK, copyright 1993-2009,
Downloaded: 2009-27-03. URL: http://www.webelements.com/titanium/compounds.html

[12] U.S Geological Survey, page last mod: 2009-11-02, downloaded: 2009-27-03
URL:http://minerals.usgs.gov/minerals/pubs/commodity/titanium/

[13] M. Kitano, K. Tsujimaru, M.Anpo, "Hydrogen production using highly active titaniumoxide based photocatlysts", *Topics in Catalysis*, vol.49, p.4-17 (2008)

[14] M.Anpo, H. Yamashita, M. Matsvoka et.al, "Design and development of titanium and vanadium photocatalysts incorporated within zeolite cavities and their photocatalytic reactivities", *Journal of Industrial and Engineering Chemistry*, vol.6, no.2, p. 59-71 (2000)

[15] Nina Hammer, "Au-TiO2 catalysts supported on carbon nanostructures for CO removal reactions", *Doctoral thesis at NTNU 2008:269*

[16] Nan-Yu Topsøe, Mark Anstrom, J.A Dumesic,"Raman, FTIR and theoretical evidence for dynamic structural rearrangements of vanadia/titania DeNOx catalysts", *Catalysis letter*, vol.76, no.1-2 p.11-20 (2001)

[17] Oliver Kröcher and Martin Elsener, "Chemical deactivation of V_2O_5/WO_3-TiO_2 SCR catalysts by additives and impurities from fuels, lubrication oils, and urea solution: I Catalytic studies", *Applied Catalysis B: Environmental*, vol.77, p.215-227 (2007)

[18] P.H. Mutin, A. F. Popa, A. Vioux, G. Delahay and B. Coq, "Nonhydrolytic vanadia-titania xerogels: synthesis and characterisation and behaviour in the selective catalytic reduction of NO by NH3", *Applied Catalysis B: Environmental*, vol. 69, p. 49-57 (2006)

[19] J.F. Brazdil, A. M. Ebner and F.A.P. Cavalcanti, "Rutile vanadium antimonates: A new class of catalysts for the selective reduction of NO with ammonia", *Applied Catalysis A: General*, vol.165, p. 51-55 (1997)

[20] J.L.G. Fierro, "*Metal oxides chemistry and applications",* CRC Taylor & Francis, (2006)

[21] Clive Whiston, "*X-ray methods – analytical chemistry by open learning*", John Wiley & Sons, ISBN: 0 471 91387 1

[22] Hans C. Ohanian, "*Principles of physics*", W.W. Norton & Company, ISBN: 0-393-95773-X, chap. 28

[23] Mark T. Weller, "*Inorganic Materials Chemistry*", Oxford University press, (1994)

[24] The International Centre for Diffraction Data, downloaded: 2009-27-04
URL:http://www.icdd.com/

[25] Lytle F. W."The EXAFS family tree: a personal history of the development of extended x-ray absorption fine structure", *Journal of Synchrotron radiation*, vol.6, p.123-134 (1999)

[26] Sayers, Lytle, Stern, "New technique for investigating noncrystalline structures: Fourier analysis of the extended X-ray absorption fine structure", *Physical Review Letters*, vol. 27 p.

[27] Martin J. Fay, Andrew Proctor, Douglas P. Hoffmann and David M. Hercules, "Unravelling EXAFS spectroscopy", *Analytical chemistry*, vol.60 no.21, (1988)

[28] Farideh Jalilehvand, University of Calgary Downloaded: 2008-07-03
URL: http://www.chem.ucalgary.ca/research/groups/faridehj/

[29] National Synchrotron Light Source, Brookhaven national laboratory, downloaded; 2009-23-04, *"History of synchrotron"*, URL: http://www.nsls.bnl.gov/about/history/

[30] Diamond Light Source Ltd. (2009), downloaded: 2009-26-04, *"what is a synchrotron",*

URL:http://www.diamond.ac.uk/AboutDiamond/Diamondstep-by step/WhatIsASynchrotron.htm

[31] Lightsources.org, copyright (2006), downloaded: 2009-24-04
URL:http://www.lightsources.org/cms/?pid=1001362

[32] Matthew Neville, *"Fundamentals of XAFS"*, Consortium for advanced Radiation sources, University of Chicago, Chicago, IL. Last mod: 2004-22-07, downloaded: 2008-27-02
URL: http://cars9.uchicago.edu/xafs/xas_fun/xas_fundamentals.pdf

[33] Hyun Chul Choi et.al, "Characterization of the structures of size – selected TiO_2 Nanoparticles Using X-ray Absorption Spectroscopy", *Applied Spectroscopy*, vol.58, no.5, p. 598-602 (2004)

[34] Marcos Fernandez Garcia, "XANES analysis of catalytic systems under reaction conditions", *Catalysis Reviews*, vol.44, iss.1, p.59-121 (2002)

[35] P. Atkins, T. Overton, J. Rourke, M.Weller and F.Armstrong, *Shriver & Atkins Inorganic Chemistry 4th edition*, OXFORD University press, (2006)

[36] D. Trong On, S. Kaliaguine, L. Bonneviot, "Titanium Boralites with MFI structure Characterised using XRD, XANES, IR and UV-Visible techniques: Effect of hydrogen peroxide on the preparation ", *Journal of Catalysis* , vol. 157, Iss.1, p 235-243, (1995),

[37] G.Antonioli, D.Bersani, P.P Lottici, I.Manzini, G.Gnappi and A. Montenero, "Local order in sol-gel derived glassy TiO_2", *Nuclear Instruments and Methods in Physics Research section B*, vol. 97, p.198-201, (1995)

[38] Z.Y. Wu, G. Ouvrand, P. Gressier and C. R. Natoli, "Ti and O K edges for titanium oxides by multiple scattering calculations: comparison to XAS and EELS spectra" *Physical Review B*, vol. 55, no.16, p10382-10391 (1997)

[39] V. Luca, S. Djajanti and R. F. Howe, *Journal of Physical Chemistry B*, vol.102, p.10650 (1998)

[40] David M. Pickup et.al, J. *Mater Sci: Mater Med* vol.19 p.1681-1685 (2008)

[41] L. A Grunes, "Study of the K-edges of 3d transition metals in pure and oxide form by x-ray absorption spectroscopy", *Physical Review B*, vol.27, no.4, p 2111-2131 (1983)

[42] M.A. Kahn, A.Kotani and J.C Parlebas,"Electronic structure and core level photoemission spectra in TiO_2 compounds", *Journal of Physics: Condensed Matter*, vol.3, no.12, p.1763-1772 (1991)

[43] J.C Parlebas, M.A.Kahn, T.Uozumi, K.Okada and A. Kotani, "Theory of many-body effects in valence, core-level and isochromat spectroscopies along the 3d transition metal

series of oxides", *"Journal of Electron Spectroscopy and related phenomenon"*, vol.71, Iss. 2, p.117-139 (1995)

[44] T. Yamamoto, "Assignment of pre-edge peaks in K-edge x-ray absorption spectra of 3d transition metal compounds: electric dipole or quadrapole?", *X-ray Spectrometry*, vol 37, p. 572-584, (2008)

[45] François Farges, Gordon E. Brown and John J. Rehr, "Coordination chemistry of Ti(IV) in silicate glasses and melts: I. XAFS study of titanium coordination in oxide model compounds", *Geochimica et Cosmochimica Acta, Elsevier*, vol.60 p. 3023-3038 (1996)

[46] G. A. Waychunas, "Synchrotron radiation XANES spectroscopy of Ti in minerals: Effects of Ti bonding distances, Ti valence, and site geometry on absorption edge structure", *American Mineralogist,* Vol. 72, p. 89-101 (1987)

[47] D.C Koningsberger, B.L. Mojet, G.E. van Dorssen and D.E. Ramaker, "XAFS spectroscopy; fundamentals principles and data analysis", *Topics in analysis*, Vol.10, p.143-155, (2000)

[48] B. Ravel and M. Neville, "ATHENA, ARTEMIS, HEPHAESTUS: data analysis for X-ray absorption spectroscopy using IFEFFIT", *journal of Synchrotron Radiation* (2005), number 12, p. 537-541.

[49] B.Ravel, *Athena: a users guide XAS data processing and manipulation*, copyright 2001-2008, URL address: http://cars9.uchicago.edu/~ravel/software/doc/Athena/html/index.html

[50] N.Binsted, *EXCURV98*, CCLRC, Daresbury Laboratory computer program, Warrington UK, (1998)

[51] European Synchrotron Radiation Facility (ESRF), last mod. 2009, downoloaded: 2009-14-05, URL: http://esrf.eu/UsersAndScience/Experiments/CRG/BM01/bm01b

[52] MAX-lab, last mod: 2009-02-10, downloaded: 2009-14-05,
URL: http://www.maxlab.lu.se/beamline/index.html

[53] Ruth E. Wolf, Ph.D, USGS/Central Region/Crustal Imaging & Characterization Team, U.S Geological Survey, March 2005, page last mod: 2009-12-04, downloaded: 2009-01-05
URL:http://minerals.cr.usgs.gov/icpms/intro.html

[54] Skoog, West, Holler and Crouch, "*Fundamentals of analytical chemistry 8th edition"*, Thomson Learning, Brooks/Cole (2004)

[55] S. Brunauer, P.H. Emmett and E. Teller, "Adsorption of Gases in Multimolecular Layers", *Journal of the American Chemical Society*, vol. 60, p. 309-319, (1938)

[56] V.S Ramachandran and James J. Beaudoin, *Handbook of analytical techniques in concrete science and tecnology*, William Andrew Publlishing / Noyes (2001). Chapter 7, chapter 4

[57] S. Besselman, C. Freitag, O. Hinrichsen and M. Muhler, "Temperature-programmed reduction and oxidation experiments with V_2O_5/TiO_2 catalysts", *Physical Chemistry Chemical Physics*, vol.3, p.4633-4638, (2001)

[58] Bo-Ya Hsu, Soofin Cheng, Jin-Ming Chen, "Synthesis and catalytic properties of Ti-Substituted SAPO molecular sieves", *Journal of molecular Catalysis A:Chemical*, , no 149, p. 7-23 (1999)

[59] N. Ulagappan and V. Krishnasamy, "Titanium Substitution in Silicon-free Molecular Sieves: Anatase-free $TAPO_4$-5 and $TAPO_4$-11 Synthesis and Characterisation for Hydroxylation of Phenol", *Journal of Chemical Society Chemical communication*, vol.3, p. 373-374 (1995)

[60] Lansuelo Montes, Mark E. Davis, Brendan Murray, Mysore Narayana, "Isolated Redox Centres within Microporous Environments 2.Vanadium-containing aluminophosphate molecular sieve five ", *Journal of Physical Chemistry,* vol.94 Iss. 16, p.6431-6435 (1990)

[61] M.P Feth, A. Weber, R. Merkle, U. Reinöhl, H. Beragnolli, "EXAFS and X-ray diffraction studies n sol-gel prepared zirconium titanium oxides", *Journal of Non-Crystalline Solids*, vol. 298, p. 43-52 (2002)

[62] A.Weibel, R. Bouchet et.al. "Local Atomic and electronic structure in nanocrystalline Sn-doped anatase TiO_2", *ChemPhysChem*, 7, p.2377-2383 (2006)

[63] D.M Pickup, G. Mountjoy et.al, "In situ EXAFS and XANES measurements of the change in Ti coordination during the calcination of a $(TiO_2)_{0.18}(SiO_2)_{0.82}$ aerogel", *Journal of Physics: Condensed Matter*, Vol. 12, no.47 p.9751-9760, (2000)

7 Appendix 1

The syntheses of the non-crystalline TAPO-5, with DCHA and TEAOH as the template source are shown in Table 18 below.

Table 18: *Overview of what added in the syntheses for TAPO-5 with different templates*

Chemicals	Quantity g	Quantity added g (24h)	Quantity added g (48 h)	Quantity added g (48 h)
H_3PO_4	11.5 g	11.5 g	11.54 g	11.54 g
H_2O	27.024 g	27.06 g	27.33 g	27.05 g
$TiOSO_4$	1.5994 g	1.590 g	1.594 g	-
Titanium(IV)isopropoxide	1.42g	-	-	1.47 g
Al_2O_3	7.065 g	7.062 g	7.065 g	7.055 g
TEAOH	21.04 g	21.04 g	21.01 g	-
DCHA	9.77g	-	-	9.76 g

Both of the syntheses were made with modification of the synthesis of Bo-Ya Hsu et.al. The synthesis with the DCHA as template source used titanium(IV)isopropoxide as the titanium source. The distilled water and phosphoric acid was stirred together, then the titanium source was added. This was stirred for 1 hour before adding the pseudobohemite, this was then stirred until a homogenous mixture was obtained. After the template was added, the DCHA made a yellow phase on top of the mixture before poured in a autoclave. The crystallisation time was 48 hours at 200°C. The molar ratio was Al: P: 0.05 Ti : 0.5 TEA :15 H_2O.

The two other syntheses with TEAOH as template source were made in the same way. The titanium source for these two syntheses was $TiOSO_4$. The water and phosphoric acid was stirred together then the $TiOSO_4$ was added and stirred until the titanium salt was dissolved. Then the pseudobohemite was added and stirred until it was dissolved. The template source was added in the end of the synthesis. Then the solution was poured into two Teflon coated autoclaves. The crystallisation time for these two syntheses was 24 and 48 hours. The molar ratio was Al : P : 0.1Ti : 0.5 TEAOH : 15 H_2O.